AALTO UNIVERSITY

School of Electrical Engineering

Electrochemical Measurement of Dopamine with Diamond-like Carbon/Pt Composite Electrodes

Tommi Palomäki

Thesis submitted for examination for the degree of Master of Science in Technology,
Espoo 02.09.2013.

Thesis supervisor and advisor:

Prof. Tomi Laurila

Aalto-yliopisto
Sähkötekniikan korkeakoulu

AALTO YLIOPISTO
SÄHKÖTEKNIIKAN KORKEAKOULU

Diplomityön tiivistelmä

Tekijä: Tommi Palomäki

Työn nimi: Dopamiinin sähkökemiallinen mittaaminen timantinkaltaisella hiili/platina yhdistelmäelektrodilla

Päivämäärä: 02.09.2013 Kieli: Englanti Sivumäärä: 10 + 88

Sähkötekniikan korkeakoulu
Professuuri: Mikrosysteemitekniikka S-113

Työn ohjaaja ja valvoja: Prof. Tomi Laurila

Dopamiini on yksi tärkeimmistä välittäjäaineista keskushermostossa. Se toimii esimerkiksi ihmisen käyttäytymiseen liittyvien sekä kognitiivisten ja motoristen toimintojen välittäjänä. Lisäksi dopamiinin tiedetään vaikuttavan useisiin neurologisiin sairauksiin, kuten skitsofreniaan ja Parkinsonin tautiin. Dopamiinin vaikutusmekanismeja ei kuitenkaan tunneta tarkasti ja niiden ymmärtämiseksi on tärkeää kehittää riittävän herkkä anturi, joka soveltuisi myös elimistössä suoritettaviin mittauksiin. Näissä sovelluksissa mittauselektrodi on avainasemassa.

Sähkökemiallisia menetelmiä on käytetty laajalti dopamiinin mittauksessa, koska dopamiini on sähkökemiallisesti aktiivinen kationi elimistössä. Erityisesti syklistä voltammetriaa (SV) on käytetty laajalti välittäjäaineiden mittaamiseen, sillä se on selektiivinen ja nopea menetelmä äkillisten pitoisuusmuutoksien mittaamiseen aivoissa.

Hiilen allotroopit soveltuvat usein jaloja metalleja paremmin biologisien molekyylien sähkökemialliseen mittaamiseen ja niitä onkin käytetty paljon näissä sovelluksissa. Erityisesti timantinkaltaisella hiilellä (DLC) on laaja vesi-ikkuna, matala taustavirta ja se on sähkökemiallisesti hyvin inertti, mikä tekee siitä kiinnostavan elektrodimateriaalin. Lisäksi sen ominaisuuksia voidaan laajasti muuttaa säätämällä hiilen sp^2/sp^3 –suhdetta sekä seostamalla.

Tässä työssä valmistettiin yhdistelmäelektrodeja, joissa sähköisesti aktiivisen platinasubstraatin pinnalle päällystettiin inertti DLC-kerros. Elektrodeja käytettiin dopamiinin mittaamiseen SV:llä. Havaitsemisrajaksi saatiin 10 µM, mikä oli parempi kuin platinan tai DLC:n havaitsemisrajat erikseen. DLC-pinnoitteen ansiosta elektrodit olivat inerttejä, niillä oli laaja vesi-ikkuna ja alhainen taustavirta. DLC-kerroksen alta paikallisesti paljastunut Pt taas tarjosi hapetus-pelkistysreaktioille katalyyttisen alustan. Yhteenvetona voidaan todeta, että passiivisen DLC:n yhdistäminen aktiiviseen platinaan paransi elektrodin kykyä havaita dopamiinia.

Avainsanat: dopamiini, syklinen voltammetria, timantinkaltainen hiili, elektrodi, sähkökemiallinen mittaus

AALTO UNIVERSITY
SCHOOL OF ELECTRICAL ENGINEERING

Abstract of the Master's Thesis

Author: Tommi Palomäki

Name of Thesis: Electrochemical Measurement of Dopamine with Diamond-like Carbon/Pt Composite Electrodes

Date: 02.09.2013 Language: English Number of Pages: 10+88

School of Electrical Engineering
Professorship: Microsystems Technology S-113

Supervisor and Instructor: Prof. Tomi Laurila

Dopamine (DA) is an important neurotransmitter in the central nervous system. It conveys cognitive, behavioral and motor functions, and it is involved in several neurological disorders, such as schizophrenia and Parkinson's disease that affect millions of people worldwide. Although DA is implicated in so many functions, the precise mechanisms by which it mediates these effects are largely unknown. Thus, the development of a sensitive sensor for DA measurement in living systems would greatly contribute to understanding the specific role of DA and the functions it imparts. The electrode material is a key factor determining the feasibility of these kinds of sensors.

DA occurs as an electroactive cation in the brain and it can thus be detected directly by electrochemical methods. Cyclic voltammetry (CV) has been widely used to detect neurotransmitters, because it combines good selectivity and high temporal resolution to detect small, transient fluctuations in the concentrations of analytes in the brain.

Carbon allotropes have several advantages and are often superior to noble metals in electrochemical measurement of biological molecules. Especially, diamond-like carbon (DLC) has many attractive properties as an electrochemical sensor. It is chemically inert, has a low background current and a wide potential window. Its electrochemical properties can be tailored widely by adjusting its sp^2/sp^3 ratio and doping.

In this work, the electrochemical properties and performance of DLC/Pt composite electrodes in DA detection were investigated. Pt wires exhibiting good electron transfer kinetics were coated with thin layers of inert DLC. These electrodes were used to measure DA using CV. DLC showed a wide potential window and a low background current. The partly uncovered Pt underneath the DLC layer provided the necessary catalytic sites for the redox reactions to occur. The DA detection limit was 10 µM, which is better than that of DLC or Pt separately. The enhanced detection is expected to result from the combination of the active Pt with the passive DLC thin film material.

Keywords: dopamine, cyclic voltammetry, diamond-like carbon, electrode, electrochemical measurement

Preface

I would like to thank professors Mervi Paulasto-Kröckel and Tomi Laurila for granting me the opportunity to write my Master's Thesis at the EILB laboratory in Aalto University. I am grateful to my supervisor, professor Tomi Laurila, for showing interest and enthusiasm toward my work and for all the useful feedback I received.

Several people have contributed to this work and they deserve to be mentioned here. Professor Jari Koskinen prepared the DLC coatings. Emilia Berg introduced me to CV measurements and provided a lot of useful information on this subject. Antti Rautiainen helped with the sample preparation and Sami Sainio made the electrochemical measurements with the Si substrate and took the SEM images.

I would also like to thank Noora and Mikael for the peer support, as well as all the friends who brought my thoughts away from work. Life is good!

I am very grateful to my family and Eunyoung for all their love and support. You are the best!

Espoo, September 2nd 2013

Tommi Palomäki

Table of Contents

Abbreviations and Symbols

Abbreviations

AA	**Ascorbic acid**
a-C	**Amorphous carbon**
ADHD	**Attention-deficit hyperactivity disorder**
BDD	**Boron-doped diamond**
CNS	**Central nervous system**
CNT	**Carbon nanotube**
CV	**Cyclic voltammetry**
DA	**Dopamine**
DAC	**Dopaminechrome**
DAQ	**Dopamine ortho-quinone**
DBS	**Deep-brain stimulation**
DLC	**Diamond-like carbon**
DOS	**Density of states**
DPV	**Differential pulse voltammetry**
EC / ECE	**E = Heterogeneous electron transfer**
	C = Homogeneous chemical reaction
EDL	**Electric Double Layer**
fMRI	**Functional magnetic resonance imaging**
FSCV	**Fast-scan cyclic voltammetry**
GC	**Glassy carbon**
HOPG	**Highly-oriented pyrolytic graphite**
IHP	**Inner Helmholtz plane**
LDAC	**Leucodopaminechrome**
NMR	**Nuclear magnetic resonance**
OHP	**Outer Helmholtz plane**
PECVD	**Plasma-enhanced physical vapor deposition**
PET	**Positron emission tomography**
PNS	**Peripheral nervous system**
SCE	**Saturated calomel electrode**

SHE	**Standard hydrogen electrode**
SEM	**Scanning electron microscopy**
ta-C	**Tetrahedral amorphous carbon**
TEM	**Transmission electron microscopy**
UA	**Uric acid**
UME	**Ultramicroelectrode**
XRR	**X-ray reflectivity**

Symbols

Subscript a and c denote anodic (oxidation) and cathodic (reduction), respectively.

A	a) Area (cm^2)
	b) Pre-exponential frequency factor
a_j	Activity of species j
c_j	Concentration of species j (M)
c_j^*	Bulk concentration of species j (M)
c_0	Standard concentration (1 mol dm^{-3})
C_d	Double-layer capacitance (F cm^{-2})
D	Diffusion coefficient (cm^2 s^{-1})
E_C	Voltage across the EDL (V)
E_0	Standard potential (V)
E^0	a) Electromotive force (V)
	b) Equilibrium potential (V)
E_f^0	Formal potential (V)
E_i	Initial potential (V)
E_λ	Switching potential (V)
E_p	Peak potential (V)
ΔE_p	Peak potential separation (V)
F	Faraday constant (9.64853×10^4 C)
G	Gibbs free energy (kJ, kJ mol^{-1})
$G^\ddagger$	Gibbs free energy of activation (kJ mol^{-1})

$G_0^{\ddagger}$	Gibbs free energy of activation at equilibrium potential (kJ mol^{-1})
i	Current (A)
i_l	Limiting current (A)
i_0	Exchange current (A)
i_p	Peak current (A)
$I_{p\ ox}$	Peak oxidation current (background-subtracted) (A)
j	a) Current density (A cm^{-2})
	b) Flux (net mass transfer rate) (mol m^{-2} s^{-1})
j_0	Exchange current density (A cm^{-2})
k^0	Standard heterogeneous electrochemical rate constant (cm s^{-1})
k	Heterogeneous electrochemical rate constant (cm s^{-1})
m_T	Mass transfer coefficient (cm s^{-1})
n	Amount of substance (mol)
R	Universal gas constant (8.31447 J mol^{-1} K^{-1})
R_S	Solution resistance (ohm)
μ_j	Chemical potential of species j
μ_j^0	Standard chemical potential of species j
$\bar{\mu_j}$	Electrochemical potential of species j
v	a) Rate of reaction
	b) Scan rate (V s^{-1})
T	Temperature (K)
t	Time (s)
Z_j	Charge number on species j
α	Transfer coefficient
β	Transfer coefficient
γ_j	Activity coefficient of species j
η	Overpotential (V)
λ	Reorganization energy for electron transfer (eV)
ϕ	Potential (V)

1. Introduction

Dopamine (DA) is one of the most important neurotransmitters in the brain, affecting cognitive, behavioral and motor functions. Dopamine is also involved in neuronal plasticity, learning, memory, brain reward system and attention span, although the precise mechanisms by which it mediates these effects is largely unknown owing to the complexity of DA systems. [1-3]

Interest in dopamine is further stimulated by its involvement in several neurological diseases such as schizophrenia, Parkinson's disease, attention-deficit hyperactivity disorder, obsessive compulsive disorder, Tourette's syndrome and drug addiction. [1, 4-6] Parkinson's disease alone affects 6.3 million people worldwide and epilepsy approximately 50 million. [7, 8]

Since DA is crucially implicated in so many physiological, behavioral and pathological functions, the development of a sensitive and selective sensor for its measurement in living systems would greatly contribute to the understanding of these conditions and the specific role of dopamine in them.

Dopamine is an electroactive molecule, which permits its detection and measurement with electrochemical methods. Nonetheless, the measurement of DA in the brain poses several challenges. Dopamine is present at very low concentrations and it is surrounded by several interfering compounds. The major interferents, ascorbic acid and uric acid, occur at concentrations 10^3-10^6 times higher than that of dopamine and have a similar electrochemical response that overlaps with the DA signal. Furthermore, the release of dopamine in the chemical communication of the brain occurs in rapid transients on a sub-second timescale. [3, 9]

Some of these challenges can be overcome with the use of cyclic voltammetry (CV), which combines very good selectivity and high temporal resolution [2, 3]. This method's strength lies in the qualitative evaluation of electrochemical systems and has been used extensively for DA detection [2, 10, 11]. CV has been successfully coupled with carbon fiber electrodes for the in vivo measurement of dopamine since the work of Adams in the late 1970's [11-13].

More recently, the discovery of new carbon materials, most notably graphene, carbon nanotubes and boron-doped diamond, have sparked considerable research in carbon-based electrochemical sensors. Carbon electrodes are inexpensive, relatively inert and are often better suited for the electrochemical measurement of biological molecules than the commonly used noble metals. The different carbon materials and allotropes offer distinct electrochemical properties compared to the conventional graphitic electrodes, such as carbon fiber, and allow new applications in analytical electrochemistry. [14]

Diamond-like carbon (DLC) has many attractive properties for sensing dopamine. It is chemically inert, shows a wide potential range, a low background current and it is

biocompatible. [15-17] Furthermore, the properties of DLC can be modified by adjusting the ratio of sp^2/sp^3 hybridization and doping so that a wide range of electrochemical properties can be obtained. [18, 19]

The aim of this work is to evaluate the electrochemical properties of DLC electrodes and their performance in the detection of dopamine. Only a few articles have reported the use of doped DLC electrodes in the electrochemical measurement of DA. However, no measurements of DA using undoped DLC electrodes were found in literature. The theoretical part of this work reviews the electrochemical properties of dopamine and DLC, and explains the thermodynamics, electrode kinetics and mass transfer governing the electrochemical response of electrodes using cyclic voltammetry. In the experimental part, DLC/Pt composite electrodes are used for the detection of dopamine using cyclic voltammetry and the results are reported and discussed.

2. Communication in the Brain

The nervous system transmits signals in the body and coordinates actions. It is composed of two main divisions, the central nervous system (CNS) and the peripheral nervous system (PNS). The CNS comprises the brain and the spinal cord. The PNS consists of the nerves that connect the CNS to every other part of the body. At the cellular level the signals are transmitted by neurons, also known as nerve cells. [1]

A neuron consists of the soma, the axon and the dendrites. The inside of the neuron is separated from the outside by a neuronal membrane. The soma is the central part of the neuron and contains the nucleus and a number of organelles in a potassium-rich fluid called the cytosol. Everything contained inside the cell membrane including the organelles and excluding the nucleus is referred to as the cytoplasm. [1, 9]

The axon is highly specialized in the transfer of information in the nervous system. Axons project from the soma and may extend from less than a millimeter to over a meter. They are usually branched and have a terminal at the end of each branch. The axon terminal is where the axon comes into contact with the dendrite or soma of another neuron. This point of contact is called the synapse where information is passed from one neuron to another. The axon terminal and synapse are depicted in Figure 1. Synapses contain numerous synaptic vesicles that contain neurotransmitters. [1] The information to be transferred is encoded in the form of action potentials with a certain frequency and pattern. Action potentials are caused by the work of ion channels and pumps that change the ionic concentration of the cytosol. As a result, the neuronal membrane depolarizes generating an action potential. The action potentials propagate through the axons and dendrites to pass information in the body. [1, 9]

Dendrites are branched projections from the soma that collectively form the dendritic tree of the neuron. They are covered with thousands of synapses and have many specialized protein molecules called receptors that detect the neurotransmitters in the synapse. [1]

The synapse has two sides, the presynaptic side, which is generally the axon terminal, and the postsynaptic side, which is the dendrite or soma of another neuron. The space between the presynaptic and postsynaptic membranes is the synaptic cleft which is 20-50 nm wide. There are two types of synapses, electrical synapses that allow the direct transfer of ionic current from one neuron to the next and chemical synapses that form the majority of synapses in the brain. [1]

In chemical synapses, the information traveling down the axon in the form of an electric signal is converted in the axon terminal into a chemical signal that crosses the synaptic cleft. The chemical signal is mediated by neurotransmitters that are stored and released in the synaptic vesicles in axon terminals. The transfer of information across the synaptic cleft is called synaptic transmission. The release of neurotransmitters is

triggered by the action potential. The depolarization of the terminal membrane causes an influx of Ca^{2+} ions in the cytoplasm that in turn signals the synaptic vesicles to release the neurotransmitters. The membrane of the vesicle fuses with the presynaptic membrane allowing the release of its content in the synaptic cleft. This process is called exocytosis. [1, 9]

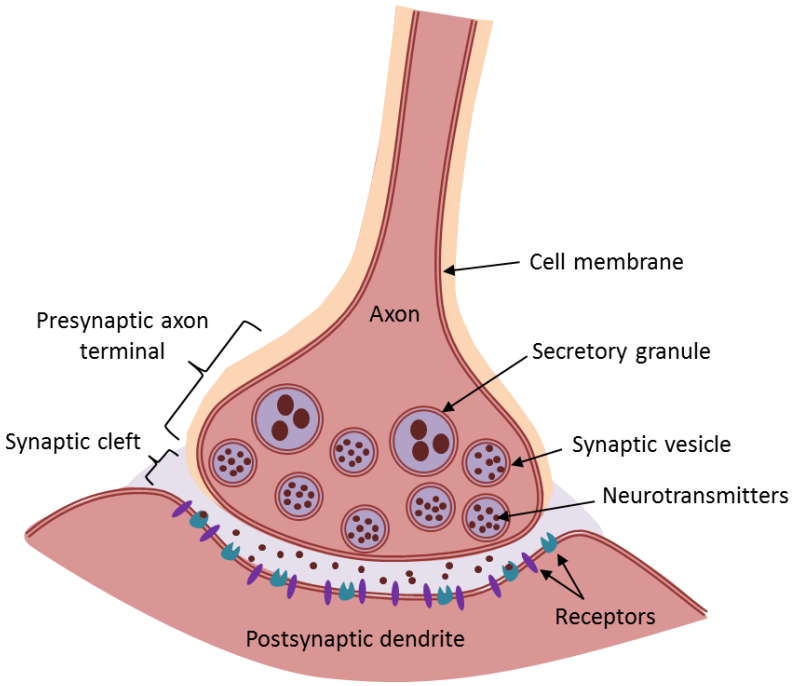

Figure 1. The axon terminal and the synapse.

Depending on the type of protein receptor that is activated by the neurotransmitter, the postsynaptic response can be quite varied. Although there are over a hundred different neurotransmitter receptors, they can be classified into two major types. Transmitter-gated ion channel receptors cause excitatory or inhibitory potentials depending on the type of neurotransmitter that is bound to them. G-protein-coupled receptors have slower, longer-lasting and much more diverse actions. They can activate enzymes that regulate cellular metabolism or ion channel function. A class of G-protein-coupled receptors known as autoreceptors, situated on presynaptic terminals, can inhibit neurotransmitter release or its synthesis to regulate neurotransmitter concentration in the synaptic cleft. [1]

2.1 Neurotransmitters

Most neurotransmitters can be divided into one of three chemical categories which are amino acids, amines and peptides (Table 1). The amino acid and amine neurotransmitters are small organic molecules containing at least one nitrogen atom and they are stored in and released from synaptic vesicles in the axon terminals. Peptide

neurotransmitters are large molecules formed by amino acids. They are stored in and released from secretory granules that are also found in axon terminals. [1]

Table 1: Electrochemical properties of neurotransmitters.

Chemical group	Neurotransmitter	Electroactivity	Charge (pH 7.4)	Oxidation potential in vivo vs Ag/AgCl (V)	Reference
Amino Acids	GABA	no	0		[3]
	Glutamate	no	–		[3]
	Glycine	no			[3]
Amines	Dopamine	yes	+	+0.2	[3]
	Acetylcholine	no	+		[3]
	Epinephrine	yes	+	+0.2	[3]
	Norepinephrine	yes	+	+0.2	[3]
	Histamine	no			[3]
	Serotonin	yes	+	+0.35	[3]
Peptides	Various	no			[1]
Other	Ascorbic acid	yes	–	+0.2	[3]
	Uric acid	yes	–	+0.3	[3]

2.1.1 Electrochemical Properties of Neurotransmitters

Neurotransmitter can be divided in three categories in regard to their electrochemical detection. The first category comprises electrochemically active neurotransmitters that can be detected directly by electrochemical methods as they undergo redox reactions at the surface of electrodes. These compounds include the catecholamines (dopamine, epinephrine and norepinephrine) and many of their metabolites such as DOPAC or L-DOPA. Electroactive neurotransmitters also include the tryptophan derivatives serotonin and melatonin, and histamine and adenosine. Other electroactive substances in the brain such as ascorbic acid and uric acid are also detectable by electrochemical methods and might interfere with the measurement of dopamine because of their higher concentration and similar oxidation potential. [3]

The second group of neurotransmitters consists of compounds that cannot be directly detected by electrochemical methods, because they are not inherently electroactive. An enzymatic reaction that catalyzes the neurotransmitter oxidation is typically used to form an electroactive species that can be consequently detected by electrochemical methods. Neurotransmitters in this category consist of glutamate and GABA among others. Other compounds such as glucose and lactate, that play an important role in energy production in the brain, have also been detected with this indirect approach. [3]

The neurotransmitters in the third group cannot be detected with electrochemical methods. The most notable neurotransmitters in this category are some of the amino

acid transmitters such as glycine and many neuroactive peptides. These compounds are usually measured by microdialysis and subsequent analysis methods. [3]

The electrochemical properties of the most common neurotransmitters are recapitulated in Table 1.

2.1.2 Measurement of Neurotransmitters

The measurement of neurotransmitters presents several challenges. The chosen method needs to be sufficiently sensitive so that it can detect the neurotransmitter in the physiological range. A high time resolution is needed to observe the fluctuations of these substances. Also, sufficient selectivity is needed to measure unequivocally the response caused by a particular neurotransmitter. [3] Long-term stability is also a concern as it tends to decrease over longer periods of time most probably as a result of adsorption of oxidation products. [2]

The measurement of neurotransmitters aims at understanding the mechanisms that control neurotransmitter concentrations, the interaction between neurotransmitters and receptors and the messages they convey as well as their role in specific behaviors. [3]

In order to investigate the correlations between neurotransmitter fluctuations and specific behavior, in vivo measurements need to be made in behaving animals. The lack of ways to observe neurotransmitter actions in real time has been a major impediment in understanding chemical communication in the brain. Neuronal action potentials underlying behavioral actions occur on a millisecond timescale and the fluctuations in neurotransmitter concentrations that transmit the signals are likely to change on the same timescale. Electrochemical approaches are well suited for this purpose, because they allow for high time resolution. For instance, fast scan cyclic voltammetry (FSCV) coupled with carbon-fiber microelectrodes can be used to sense dopamine levels in vivo, such as in animal brains. [3]

2.2 Dopamine

Dopamine (3,4-dihydroxyphenethylamine) is one of the most important neurotransmitters in the brain, affecting cognitive, behavioral and motor functions. Dopamine belongs to the catecholamine family of neurotransmitters and it is abundant in the central nervous system. [1, 2] Catecholamines derive from the amino acid tyrosine and include DA, epinephrine and norepinephrine. Catecholamines contain a ring-shaped chemical structure called a catechol with the molecular formula $C_6H_4(OH)_2$ and an amine functional group. In physiological conditions in the brain tissue and body fluids, dopamine occurs as large organic cations [2, 3, 14, 20, 21].

Dopamine is involved in neuronal plasticity, learning, memory and attention span, although the precise mechanisms by which DA mediates these effects is largely unknown owing to the complexity of DA systems. [2, 6] Dopamine has also a central

role in the brain reward system. It is believed to be involved in the mediation of pleasure and incentive salience i.e. motivational behavior towards reward-predicting stimuli. [1, 3] For this reason, dopamine is important in the study of drug addiction. For example amphetamine and cocaine block dopamine uptake and prolong its actions in the synaptic cleft, which could be the cause of the stimulant effect of these drugs. Since dopamine is also involved in reinforcing adaptive behavior, drugs that affect dopaminergic pathways reinforce drug-seeking behavior i.e. addiction. [1]

Interest in DA is further stimulated by its involvement, directly and indirectly, in several neurological diseases such as schizophrenia [1, 5], Parkinson's disease [1, 4, 5], attention-deficit hyperactivity disorder (ADHD) [1], obsessive compulsive disorder and Tourette's syndrome [6]. Low levels or practically complete depletion of dopamine in the central nervous system has been associated as a major cause of Parkinson's disease. In Parkinson's disease the dopaminergic neurons in the brain slowly degenerate and eventually die. One strategy for treating this disease is the administration of the DA precursor L-DOPA to increase dopamine synthesis in the remaining neurons. This alleviates some of the disease's symptoms and motor functions can be restored. However this treatment does not stop the progress of Parkinson's disease [1] and has multiple side effects such as nausea and vomiting. Chronic administration of L-DOPA can result in more adverse effects, for example problems in motor control, dyskinesia and psychotic reactions. [4, 5]

Since dopamine is crucially implicated in so many physiological, behavioral and pathological functions, the development of a sensitive and selective sensor for the measurement of dopamine in living systems would greatly contribute to the understanding of these conditions and the specific role of dopamine in them.

2.2.1 Oxidation of Dopamine

Catecholamine neurotransmitters, including dopamine, epinephrine and norepinephrine can be detected with electrochemical methods, because their oxidation potential, +0.2 V, is well within oxidation potential limits for carbon and metal electrodes. [3]

Several mechanisms have been proposed for the electrochemical oxidation of dopamine such as EC [21], ECC [22], ECE [23, 24], and ECECEE [25], where E denotes an electrochemical reaction and C a chemical reaction. While there is unanimity that the first step in DA oxidation involves a two-electron transfer accompanied with deprotonation, there is discrepancy about the order of deprotonation, whether the two-electron transfer occurs in one or two separate steps as well as the subsequent reactions in DA oxidation.

The first step in the suggested electrochemical mechanisms is the two-electron oxidation of DA into dopamine ortho-quinone (DAQ). Two mechanisms have been proposed for the consecutive chemical reaction of DAQ, the formation of leucodopaminechrome (LDAC) by intramolecular cyclization or the deprotonation of the amine group to produce an aminochrome. The intramolecular cyclization is inhibited in high acidic solution (< pH 5) [22, 25]. In the ECE and ECECEE mechanisms LDAC

is further oxidized in a two-electron transfer to dopaminechrome (DAC) [23, 25]. Li et al. and Wen et al. have proposed that DAC and aminochrome can undergo polymerization reactions on the electrode surface covering it with a melanin-like polymer that leads to gradual loss of electrode activity because it inhibits electron transfer reactions [22, 25].

Li et al. observed two oxidation peaks and two reduction peaks in a CV scanned with an Au electrode in PBS (pH 7.4) containing 2.0 mM DA at a scan rate of 20 mV/s. They concluded that the peaks correspond to the redox reactions of DA into DAQ and of LDAC into DAC. [25] It remains unclear if the authors considered the possibility of two consecutive one-electron transfers or the effect of DA adsorption on the electrode surface.

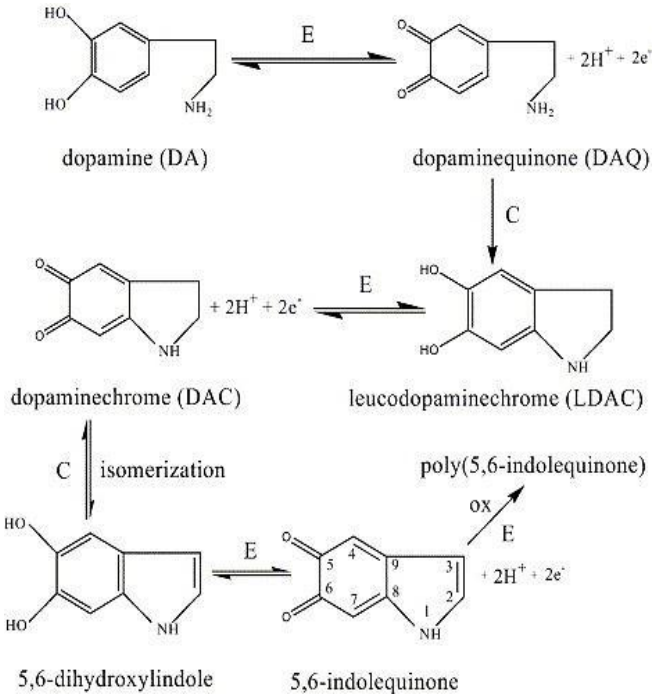

Figure 2. Dopamine oxidation pathway (ECECEE) proposed by Li et al. E denotes an electrochemical reaction while C a chemical one. [25]

Although it is widely accepted that dopamine is a cation at physiological pH, many studies on dopamine oxidation present a reaction pathway where DA is neutral and the positive charge of the amine group is omitted. Also, most publications on DA oxidation do not seem to question the mechanism of the first two-electron transfer step. Nevertheless, Corona-Avendano et al., Wang et al., Wen et al., Doménech et al. claim that the two-electron transfer occurs in two consecutive one-electron transfers and that dopamine forms an intermediate semiquinone after the first electron transfer. [21, 22, 24, 26, 27]

Some studies have tried to elucidate the deprotonation path of dopamine using acidity constants (pK_a) [21, 26, 28]. The acidity constant is a measure of the acidity of a

compound i.e. the capacity to donate a proton to a common base. Kiss et al. have proposed acidity constant values of 8.89, 10.41 and 13.1 for dopamine [28], whereas Sanchez-Rivera et al. have proposed values of 9.05, 10.58 and 12.07 [29]. Corona-Avendano et al. attributes the differences in acidity constants in literature to the diversity of experimental conditions employed to evaluate these constants [26].

A predominance zone diagram, shown in Figure 3, can be constructed from the pK_a values. In each of the four pH regions a different protonated form of dopamine predominates. At physiological pH, below pK_{a1}, the fully protonated form of DA predominates, which is widely accepted in literature [3, 14, 21, 22, 25, 28, 30]. Schüsler-Van Hees et al. have reported that at pH 7.85, the protonated form of DA is predominant at a percentage of 84.0 [31].

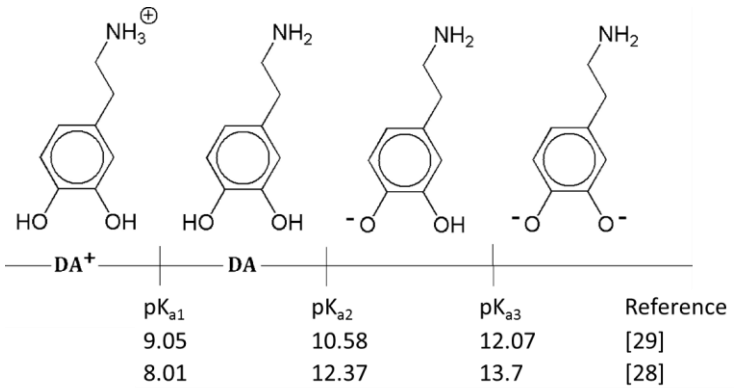

Figure 3. Predominance zone diagram for dopamine with the pK_a from two different references. At physiological pH (7.4) dopamine occurs as a protonated cation.

Kiss et al. have proposed that either one of the two hydroxyl groups in the catechol ring loses a proton and then the OH group in the amine follows before the final hydroxyl group in the catechol ring is deprotonated. [28] The study does not assign pK_{a1} and pK_{a2} exclusively to the catechol or amine deprotonation and suggests that the first step is a mixture of both. According to Corona-Avendano, the OH group that becomes deprotonated first has great biological importance, since a different chemical structure is produced. Based on their theoretical and experimental study with density functional theory, chemical shift calculations (NMR-GIAO) and C NMR spectra, Corona-Avendano et al. proposed a deprotonation pathway where the amine group loses a proton first, followed by the deprotonation of the hydroxyl groups of the catechol ring as seen in Figure 4. [26] Despite the proposed deprotonation pathway, the same group proposes that the first step in DA oxidation occurs via the deprotonation of both hydroxyl groups in the catechol while the amine group is unaffected in a subsequent article [32].

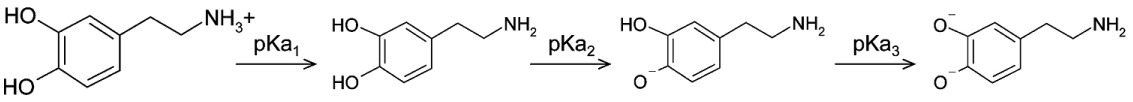

Figure 4. Deprotonation pathway of DA according to Corona-Avendano. [26]

2.2.2 Adsorption of dopamine

The heterogeneous electron transfer between an electrode and catechols such as dopamine is strongly dependent on catechol adsorption to the electrode surface [33-35]. DuVall and McCreery have shown that a chemisorbed monolayer on a glassy carbon (GC) electrode can completely inhibit heterogeneous electron transfer of catechols while it has little effect on outer-sphere systems that are not dependent on adsorption. They found that catechol adsorption was necessary for fast electron transfer and that the inhibition of electron transfer is caused by prevention of the adsorption. [35]

In a subsequent article, DuVall and McCreery investigated the nature of adsorption between catechols and a GC electrode. They concluded that a layer of adsorbed catechols or quinones catalyzes the electron transfer of catechols in solution. The catalytic effect could be a result of hydrogen bonding between a surface quinone oxygen and the catechol accelerating the overall redox process. In addition, they observed that fast electron transfer kinetics for catechols on electrochemically oxidized GC is caused by an increase in DA adsorption or an increase in the level of surface oxides or both. [34]

Bath et al. suggested that the amine was involved in the adsorption of dopamine to carbon fiber electrodes instead of the catechol. They attributed the disagreement on the role of catechol or amine in the adsorption process to the different conditions under which adsorption is studied and the use of microelectrodes and electrodes of conventional size in literature. [33]

2.2.3 Interference with Dopamine Detection

Catecholamine compounds show a similar two-electron redox reaction with approximately the same oxidation potential at physiological pH, which makes it difficult to distinguish between them. Moreover, most of these compounds undergo secondary reactions after the initial redox reaction further complicating their detection. A suitable choice of detection method can, however, simplify detection: in the case of the secondary reaction of dopamine from LDAC to DAC, the reaction can be outrun by using fast-scan methods because the electrochemical rate constant for the reaction is slow, on the order of $k = 0.1\ s^{-1}$. [3]

The main interferents for the electrochemical measurement of dopamine in the brain are ascorbic acid and uric acid. The oxidation potential of AA is the same as that of catecholamines, +0.2 V and that of UA is also very close, at +0.3 V. This results in overlap of the voltammetric responses. The concentration of ascorbic acid in the extracellular fluid is approximately 0.5 mM, which is $10^4 – 10^6$ times higher than that of dopamine. [3] DA basal concentration is estimated to be only 5-100 nM in the brain.

Dopamine transients have much higher concentrations, in the micromolar range, but their duration is very short because the uptake of dopamine is very fast. The transients last from milliseconds to a few seconds. [9, 11, 36] Robinson et al. have shown in their experiments that mass transport of dopamine in the brain is a competition between uptake and diffusion of dopamine. The uptake is caused by transporters that remove dopamine from the extracellular fluid. Simulations show that the diffusion distance of dopamine is only a few micrometers. [3]

To distinguish between ascorbic acid and dopamine, fast scan methods or surface modification of the electrode to reject ascorbic acid can be utilized. The use of fast scan methods at carbon electrodes shifts the oxidation potential of ascorbic acid to more positive values separating it from the oxidation peak of dopamine. This results from the slow electron transfer kinetics of AA oxidation. [3, 37]

In addition to direct electrochemical interference, ascorbic acid can interfere indirectly with the measured signal. As the major antioxidant in the body, it can reduce DAQ back to DA. This provides more dopamine for oxidation with the net result that the dopamine signal is proportional to both dopamine and ascorbic acid. [3] This catalytic reaction is not a problem with small electrodes (20-50 um carbon fiber electrodes), because the extensive diffusion associated with such small electrodes allows the oxidized product to diffuse away from the electrode before it is reduced back to dopamine. [37] Furthermore, the antioxidant effect of AA on DAQ prevents the formation of melanin-like polymers in biological systems as was discussed in section 2.2.1 [22, 23].

2.3 Techniques to measure neurotransmitters in the brain

The most widely used method to assess chemical communication between neurons in the brain is microdialysis. Other useful methods include spectroscopic and electrochemical techniques. [3]

2.3.1 Microdialysis

Microdialysis is a minimally-invasive technique that uses a small microdialysis probe that is inserted into the brain tissue of interest. A perfusion fluid is pumped at a low flow rate (generally 1 µL/min) through an inlet and outlet tubing to a semipermeable dialysis membrane. Small molecules from the extracellular fluid can diffuse across the dialysis membrane and the dialysate (the solution leaving the probe) is collected for analysis at certain time intervals. [3]

The advantages of microdialysis in neurotransmitter measurement comprise easy implementation to study a variety of neurotransmitters and a high chemical resolution, because the dialysate can be analyzed with several external techniques. The major disadvantage is the invasive nature of the technique. Despite efforts in making smaller probes, tissue damage is likely because its size (typically >200 µm in diameter) is large compared to nerve terminals (approximately 1 µm). Damaged tissue, inflammatory

response and wound healing can affect the uptake and diffusion of neurotransmitters near the probe. Another disadvantage is the low sampling rate due to the low flow rate required for extraction efficiency i.e. a sufficient amount of the measured molecule diffuses across the membrane. Rapid microdialysis to enhance the low sampling rate has recently emerged. [3]

2.3.2 Spectroscopic Methods

The two most used spectroscopic methods are positron emission tomography (PET) and functional magnetic resonance imaging (fMRI). Both of these methods are non-invasive and provide a three-dimensional map of neural activity in the brain. [3]

PET requires the introduction of a positron-emitting chemical agent in the body. The chemical agent is usually an activator or inhibitor of receptors for the neurotransmitter of interest. Displacement of the endogenous ligand by the chemical agent provides insight into the neurotransmitter processes. [3]

fMRI measures brain activity based on blood oxygen levels: when neurons become active, local flow of oxygen-rich blood increases in those regions reaching a peak after a few seconds and then falling back to the original level. The degree of oxygen in hemoglobin causes an alteration in the local magnetic field that the fMRI detects. This technique has been used to provide strong evidence, that brain regions containing dopamine are activated during reward-associated behavior. [3]

2.3.3 Electrochemical Methods

Several neurotransmitters are inherently electroactive or can be made electroactive by the use of enzymes as it was explained in section 2.1. These neurotransmitters can undergo redox processes and can thus be measured with electrochemical methods.

Electrochemistry is a powerful analytical technique for monitoring electroactive species in living organisms. Among all the techniques for the detection of electroactive neurotransmitters, electrochemical sensing techniques are the most straightforward, rapid and cost-effective. [2] They provide several advantages such as high temporal resolution, high accuracy and relatively easy operation and allow for very small electrodes that can be used in vivo. However, the poor selectivity of electrochemical methods remains a challenge. Selectivity and sensitivity can be enhanced by surface modification of the electrodes. Other limitations include high concentration of interfering electroactive species, electrode passivation and fouling. [2, 3]

The most common electrochemical methods used to directly detect electroactive neurotransmitters are constant-potential amperometry or DC amperometry, chronoamperometry, differential pulse voltammetry (DPV) and fast-scan cyclic voltammetry (FSCV). [2, 3] In all of the methods presented in this section the potential is held constant or varied in a predetermined manner as the current is measured as a function of potential or time. Cyclic voltammetry will be presented more in detail in section 6.1.

The focus of recent research and development of electrochemical sensors has been the improvement of their sensitivity, selectivity, biocompatibility and miniaturization. Miniaturization affects temporal and spatial resolution of the electrodes and prevents extensive tissue damage and trauma during implantation and in in-vivo applications. [2]

Constant-potential Amperometry

In constant-potential amperometry or DC amperometry, the potential is held constant at a sufficiently large value to oxidize or reduce the compound of interest at the electrode surface (Figure 5). The electron transfer of the electrochemical reaction produces a measurable current that is proportional to the amount of chemical species electrolyzed by Faraday's law (see section 4.1). [2, 3, 10]

The advantages of this method include very high time resolution, below millisecond time scale, and the independence on adsorption effects, because the compounds are electrolyzed immediately upon contact with the electrode surface. Hence, adsorption processes do not slow down the response to concentration changes in the same way as in voltammetric methods. On the other hand, amperometry is essentially non-selective, because all the electroactive compounds that undergo redox processes within the applied potential will generate a current. To measure and confirm the current produced by the compound of interest, all the compounds producing a current must be identified. Despite the non-selectivity, constant-potential amperometry has been used to measure vesicular neurotransmitter release from single cells and catecholamine concentrations in the brain and brain slices. [2, 3]

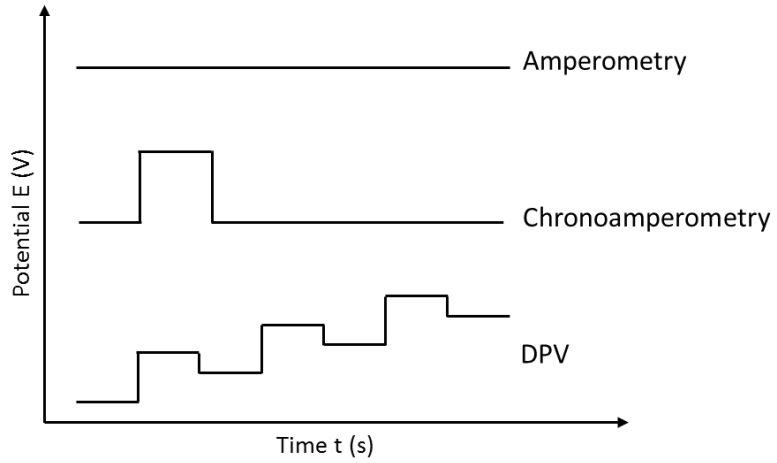

Figure 5. Potential waveforms of amperometry, chronoamperometry and differential pulse voltammetry (DPV). The potential in amperometry is constant and non-zero.

Chronoamperometry

In chronoamperometry, the potential of the working electrode is altered with a rectangular waveform (Figure 5). At the initial potential, no chemical reactions occur. The potential is then stepped to a value at which a redox process occurs and the resulting current is monitored as a function of time before stepping back to the initial potential. The current is proportional to the concentration of the electroactive species and decays as described by the Cottrell equation (5.15). The compounds that were oxidized on the rising step are reduced as the potential is lowered to the initial value. The ratio of the peak oxidation current versus the peak reduction current provides information about the stability of the chemical species and offers somewhat greater selectivity compared to constant-potential amperometry, although selectivity is limited compared to other methods. Chronoamperometry has been used to measure dopamine concentrations in the extracellular fluid of the brain in real-time [3] and to study neurotransmitter dynamics following injection of chemical agents or electric deep-brain stimulus (DBS). [2, 3]

Differential Pulse Voltammetry

Differential pulse voltammetry (DPV) combines linear sweep voltammetry and square wave techniques: the potential is increased or decreased linearly and a square wave pulse is superimposed at a constant frequency (Figure 5). The difference between the currents is measured right before the pulse starts and before it ends, and it is plotted against the potential of the linear sweep. The amplitude of the differential current is proportional to the concentration of the analyte. The current peak position shows the half-wave potential for reversible systems [2]. DPV is more selective and sensitive than the amperometric methods discussed above. For instance, it is possible to simultaneously measure different compounds as long as their oxidation potentials differ by more than 100 mV [3]. The major drawback of this method is its relatively poor time resolution as one scan takes over 30 s. DPV has been used for the in vivo detection of catecholamines. [2, 3]

Cyclic Voltammetry

Cyclic voltammetry is dealt with in more detail in Chapter 6.

3. Electrode Potential and Thermodynamics of Cells

In this chapter we will examine through thermodynamics how the electrode potential is established. The electrode potential is related to the difference in electrochemical potential between the electrode and the electrolyte. Thermodynamics provide a description of the behavior of electrochemical systems at equilibrium and predict the spontaneity and feasibility of chemical reactions according to the change in Gibbs free energy in the electrochemical system.

3.1 Electric Double Layer

The charge on the metal electrode is composed of an excess or deficiency of electrons that reside on a very thin layer on the metal surface, approximately <0.01 nm. The charge in the solution is made up of an excess of anions or cations near the electrode surface. The distribution of charge depends in each case on the potential difference between the electrode and the solution. The electrode-electrolyte interface can be thus thought of as an electrical double layer (EDL) that is characterized by the double layer capacitance C_d (see section 6.1.3). Several models of the double layer exist such as the Helmholtz, Gouy-Chapman and Stern's models. [10, 38, 39]

The structure of the EDL in solution is formed by several layers visible in Figure 6. The inner layer, right on the electrode surface, comprises specifically adsorbed solvent molecules and ions. The specifically adsorbed species are desolvated and bind chemically to the electrode surface, forming the inner Helmholtz plane (IHP). The IHP extends to the electrical centers of the specifically adsorbed ions. The outer Helmholtz plane (OHP) is made up of solvated ions that are attracted to the charged electrode only by long-range electrostatic forces. The solvated ions are said to be non-specifically adsorbed. The OHP extends from the IHP to the electrical centers of these nearest solvated ions. Beyond the OHP is the diffuse layer where the non-specifically adsorbed ions are distributed because of thermal motion. The thickness of the diffuse layer depends on the total ionic concentration and is less than ~10 nm for concentrations greater than 0.01 M. The inner layer and diffuse layer have a net electrical charge equal in magnitude to that of the electrode surface but of opposite polarity. As a result the complete structure is electrically neutral. [10, 38]

The structure of the EDL can affect the rate of electrode processes. For example an electroactive species that is non-specifically adsorbed in the OHP experiences a potential that is less than the total potential between the electrode and the solution by an amount equal to the charge of the diffuse layer. In electrode kinetic models such as the Butler-Volmer model presented in chapter 4, the concentrations are taken in the OHP instead of the bulk solution because the tunneling distance is 1-2 nm. Sometimes the effect of EDL can be neglected, however at low concentrations of electroactive species these effects can become important and must be taken into account. [10, 38]

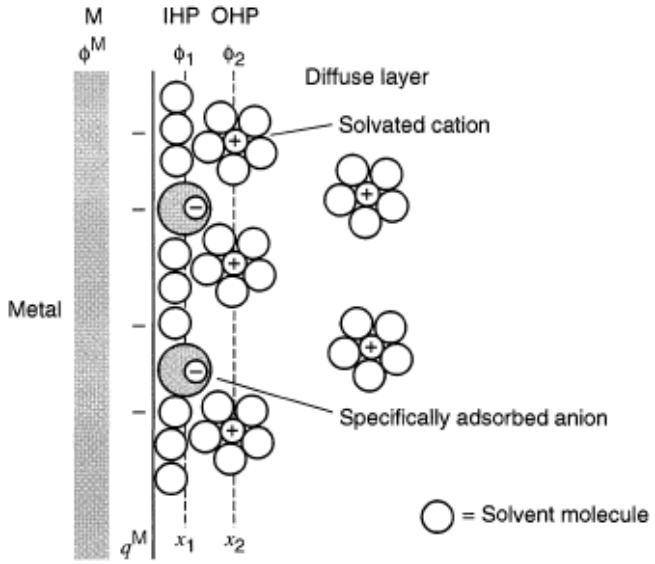

Figure 6. The electrical double layer according to the Helmholtz model. [10]

3.2 Establishment of Electrode Potential

The establishment of the electrode potential between a metallic electrode and the electrolyte, a solution composed of dissolved ions, can be explained by considering the energy levels of the two different phases.

The electrons in the electrode are delocalized because of metallic bonding between the atoms, and form a conduction band. The conduction band is a continuum of energy levels filled up to an energy maximum known as the Fermi level. [40] In contrast, the ions in the solution have discrete energy levels called electron shells. The electrons fill up these electron shells beginning from the inner shells (the ones closest to the nucleus) until the valence shell (the outermost shell). The ions will react in order to fill vacancies in the valence shell to gain a stable electronic configuration. The electrons will transfer between the two phases depending on the difference in energy between the electrode and the ions in the solution. [40] If the electrode is driven to a more negative potential by connecting it to an external power supply, the electrons will gain energy and thus can reach a level high enough to transfer into a vacancy in the valence shell of an ion. When the electrons flow from electrode to solution, the current is called cathodic. The ion in the solution gains an electron and is said to be reduced. This reaction can be written as

$$M^{z+}(aq) + z\,e^- \rightarrow M(s), \qquad (3.1)$$

where z is the charge number and s and aq refer to the solid (metal) and aqueous (solution) phases, respectively.

If the electron transfer occurs in the opposite direction, from solution to metal, it will cause an anodic current and the metal atom loses an electron and is said to be oxidized:

$$M(s) \rightarrow M^{z+}(aq) + z\, e^{-}. \quad (3.2)$$

In general, we can write the reduction and oxidation i.e. redox reactions as

$$Ox + ne^{-} \leftrightarrow Red. \quad (3.3)$$

The energy difference between the metal electrode and the solution is the driving force of the electron transfer between the phases and it will determine the energetically favorable direction of charge transfer [40]. Since there is a transfer of charge between the metal electrode and the solution, it will give rise to a potential difference between the phases. This is the electrode potential. [38, 40]

3.3 Electrochemical Potential and Equilibrium State

In an electrochemical system, a chemical species j has an electrochemical potential $\bar{\mu_j}$ (kJ mol^{-1}) defined by

$$\bar{\mu_j} = \mu_j + Z_j \mathrm{F}\phi, \quad (3.4)$$

where μ_j is the chemical potential and Z is the charge on species j, F is the Faraday constant (C mol^{-1}) and ϕ is the potential of the electrode or the solution in which the molecule j is found. The electrochemical potential is the sum of the chemical potential μ_j and the electrical energy $Z_j F\phi$ that will affect the charged species because of the potential difference between the phases. As a consequence, equation (3.4) will reduce to the chemical potential μ_j for uncharged species.

The chemical potential, in turn, can be written as

$$\mu_j = \mu_j^0 + \mathrm{RT} \ln a_j, \quad (3.5)$$

where μ_j^0 is the standard chemical potential and a_j is the activity of a chemical species j, R is the universal gas constant (J K^{-1} mol^{-1}) and T is the temperature (K). The standard chemical potential is the energy of species j at standard state (constant temperature and pressure). In addition, the chemical potential will depend on the activity of the chemical species that accounts for the non-ideality of the solution. The non-ideality can be modelled for example by the Debye-Huckel theory and reflects ion-ion and ion-solvent interactions in the electrolyte [40]. Additionally, electrolytes tend to deviate from ideal solutions because of long-distance electrostatic interactions between charged ions. [38] For solutions, the activity of a species j is dependent on its concentration c_j, its activity coefficient γ_j and the standard concentration c_0 (1 mol dm^{-3}) as determined by

$$a_j = \gamma_j \left(\frac{c_j}{c_0}\right). \quad (3.6)$$

The electrochemical potential $\overline{\mu_j}$ can also be expressed as the change in Gibbs energy per mole n of chemical species j:

$$\overline{\mu_j} = \left(\frac{\partial \overline{G}}{\partial n_j}\right). \quad (3.7)$$

The electrochemical potential is equivalent to the Fermi level, the highest energy level of the electrons in a certain phase, discussed in the previous section. [10] For the metal electrode, the Fermi level corresponds to the highest occupied electronic state in its conduction band whereas for a solution, it is a function of the electrochemical potential of the dissolved oxidized and reduced chemical species.

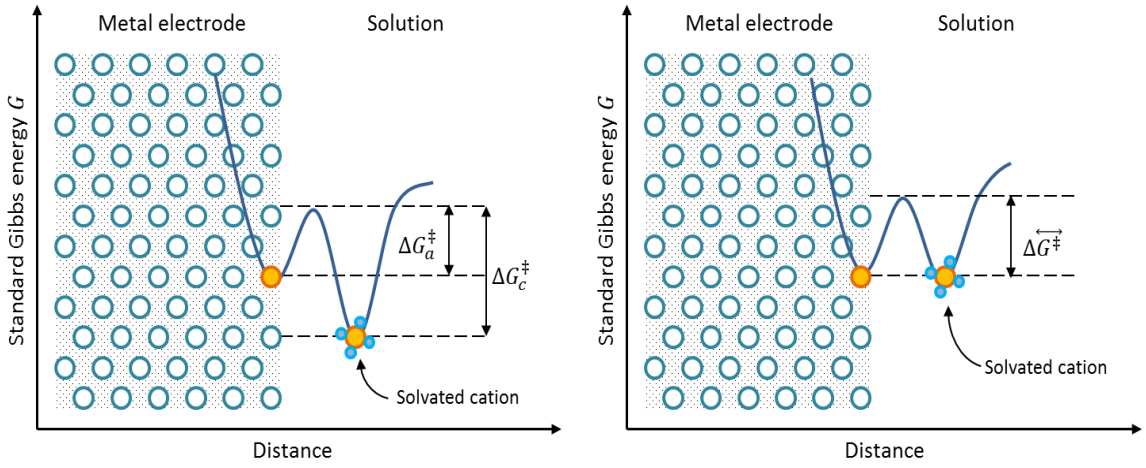

Figure 7. Energy profile for the oxidation of a metal atom on the left and when the system is at equilibrium on the right. The change in Gibbs energy for oxidation $\Delta G_a^{\ddagger}$ is smaller than that for reduction $\Delta G_c^{\ddagger}$, so oxidation is the energetically favorable reaction. At equilibrium $\Delta G_a^{\ddagger}$ and $\Delta G_c^{\ddagger}$ are equal and both redox reactions occur at the same rate.

The energetically favorable direction of electron transfer is from the phase with the higher Fermi level (higher electrochemical potential) to the phase with the lower Fermi level across the electrode-solution interface. In terms of Gibbs energy, it means that the redox reaction (equations 3.1 and 3.2) with the negative change in Gibbs energy given by

$$\Delta \bar{G} = \bar{G}_{products} - \bar{G}_{reactants} \quad (3.8)$$

is the spontaneous reaction. [38] As the electrons are transferred between the phases, the electrochemical potentials of the phases will gradually shift closer to each other and the spontaneous reaction will slow down until a point is reached when the potentials are equal in both phases. At this point the change in Gibbs energy $\Delta\bar{G}$ is zero and both redox reactions occur at the same rate. The Fermi level of the electrode and the solution are equal i.e. the electrochemical potential of electrons in both phases are equal. This is the point of electrochemical equilibrium. [10]

Because the electrochemical potential of electrons in both phases are equal, the rate at which the solution gives up electrons is equal to the rate at which electrons are released by the metal electrode. Consequently no net current flows, because the anodic and cathodic reactions of equations (3.1) and (3.2) are of equal magnitude and opposite direction. This is defined as dynamic equilibrium. Since at this point the potential difference between the phases vanishes, we can see from equations (3.5) and (3.6), that the activity and hence concentrations of both reactants and products must be equal at equilibrium. [10, 40]

3.3.1 Standard Electrode Potential

The absolute value of electrode potential cannot be measured for a single electrode in solution because there is only a single electrode-solution interface. For this reason a reference electrode is required, so that the potential between the two electrodes can be measured. This is analogous to closing an electric circuit. The electrode potential of the standard hydrogen electrode (SHE) has been chosen by convention to be zero at all temperatures and it forms the basis of comparison with all the other electrode potentials. For example the electrode potential of the Ag/AgCl electrode compared to SHE is +0.197 V [10]. This potential is called the standard electrode potential of the Ag/AgCl electrode.

The measurement of standard potentials at equilibrium requires knowledge of the activity coefficients of the chemical species involved in the reactions. Because the activity coefficients are usually unknown and the ionic strength and composition of the solution will lead to deviations from solution ideality, it is more convenient to measure the formal potential E_f^0. The formal potential is an empirical value that includes the standard potential E_0 and activity coefficients γ in it. In the case of a reactant A and product B, the formal potential is

$$E_f^0 = E_0 + \frac{RT}{F}\ln\left(\frac{\gamma_A}{\gamma_B}\right). \qquad (3.9)$$

The values of standard potential are determined by measuring formal potential values at different ionic strengths and extrapolating to zero ionic strength, where the activity coefficients approach unity. [10, 40]

3.4 Electromotive Force and Overpotential

In an electrochemical cell, when two electrodes are connected together, two independent half-reactions occur, one at each electrode. Each half-reaction will depend on the interfacial potential difference at the corresponding electrode-electrolyte interface. If the impedance between the electrodes is made large enough so that no current flows in the circuit, a potential difference between the two electrodes will form. This is the electromotive force E^0. [10, 38]

The maximum amount of work from the electrochemical cell is obtained at the equilibrium state, because there is no net current flow in the cell and thus no IR-drop. The maximum amount of electrical work is equal to the product of charge and potential difference through which the charged is moved, E^0, and it is directly related to the amount of chemical work by

$$\Delta G^0 = -nFE^o, \qquad (3.10)$$

where n is the number of moles of electrons involved in the redox reaction and F is the Faraday constant.

If the reactions occur spontaneously, the cell is called a galvanic cell and if the potential has to be shifted in order for chemical reactions to occur, it is an electrolytic cell. When an electrode is shifted to a positive value compared to its equilibrium potential by an external power supply, an anodic current will flow and the metal atoms will be oxidized. However, if this reaction is not fast enough to oxidize metal atoms to maintain equilibrium between the positive potential building up on the electrode and the amount of positive ions in the solution, the electrode will become positively charged. The departure of the electrode potential from the thermodynamic equilibrium potential is termed polarization and in this case the electrode is said to be polarized anodically. Correspondingly, if the electrode is shifted to a more negative potential and the cathodic reactions cannot keep up, the electrode will be polarized cathodically. The overpotential η measures the extent of polarization and is defined as

$$\eta = E - E^0, \ ^{(*)} \qquad (3.11)$$

where E^0 is the equilibrium potential. The overpotential can also be calculated using the formal potential E_f^0 when the activity coefficients differ from unity. [10, 38]

Polarization is caused by the sluggishness of the electrode processes. The overpotential is the sum of the different types of retarding processes that cause polarization. The most common types of overpotentials and their cause are listed in Table 2.

(*) Typically $E^0 = E_f^0$

Table 2: Different types of overpotential and their causes. [38]

Type of overpotential	Cause
Activation overpotential	Electron transfer between the electrode and the chemical species undergoing redox reactions
Diffusion overpotential	Diffusion of the reacting chemical species to the surface of the electrode
Reaction overpotential	Chemical reactions that precede electron transfer
Crystallization overpotential	Lattice formation
Resistance overpotential	Solution resistance and other resistances caused by cell design

4. Electrode Kinetics

Electrode kinetics provide information about the reaction rates at the electrode-electrolyte interface with regard to potential and concentration. Thermodynamics, introduced in the previous chapter, describe the electrochemical system only at equilibrium. For the kinetic theories to be valid and accurate, the kinetic equations must collapse to thermodynamic relations at equilibrium. [10]

The reactions that occur at the electrode-electrolyte interface are called heterogeneous reactions, because the reactants undergo chemical changes at an interface between two phases. Conversely, homogeneous reactions occur in the same phase.

4.1 Faraday's laws

The electrochemical reactions taking place at the electrode surface are governed by Faraday's laws:

1) The electrochemical reactions occur only at the surface of an electrode.
2) The mass of substance altered at an electrode is directly proportional to the quantity of electrical charge Q transferred at that electrode.
3) For a given amount of electricity, the mass of a substance altered at an electrode is directly proportional to the equivalent weight of the substance (molar mass M divided by charge number z). [38]

4.2 Current and Rate of Reaction

The electron transfer between the chemical species in solution and the electrode leads to an electrical current i and it is proportional to the rate of reaction υ, electrode area A and the amount of electric charge consumed in the reaction, nF, via the following equation:

$$i = nFA\upsilon. \qquad (4.1)$$

The rate of reaction υ (mol cm^{-2} s^{-1}) measures the rate at which electrochemical reactions occur at the interface between the electrode and the solution, i.e. the rate of heterogeneous electrochemical reactions. The net rate for a reaction such as the redox reaction $Ox + ne^- \leftrightarrow Red$ is given by:

$$\upsilon = k_c\, c_{ox} - k_a\, c_{red}\,, \qquad (4.2)$$

where k is the first order electrochemical rate constant with unit of velocity (cm s^{-1}) and the subscripts c and a denote the cathodic and anodic reactions, respectively. The electrochemical rate constant is a measure of the speed of the electrochemical reaction in question. The concentrations of the reactants, c_{ox} and c_{red}, are taken within the

distance at which electron transfer can occur as opposed to bulk concentration. The concentration is not uniform close to the electrode, because the passage of current through the electrode-solution interface will lead to the reaction and consequent depletion of reactants at the electrode surface. Chapter 5 deals with the effect of mass transfer on electrode kinetics. [10, 40]

Combining equations (4.1) and (4.2) we have

$$i = i_c - i_a = nFA(k_c\, c_{ox} - \, k_a\, c_{red}) \qquad (4.3)$$

In the above equation it is emphasized that the total current i is composed of the cathodic and anodic currents i_c and i_a, respectively. In a cathodic reaction the reactant is reduced, while in an anodic reaction the reactant is oxidized.

At dynamic equilibrium the anodic and cathodic reactions are of equal magnitude but opposite direction. The net rate of reaction is zero and thus $i = 0$ in the above equation, resulting in

$$\frac{k_c}{k_a} = K = \frac{c_{ox}}{c_{red}}. \qquad (4.4)$$

This result is in agreement with the thermodynamic approach used in section 3.3 in so far as concentration of reactants and products is constant at equilibrium, because the conversion rate in both directions is of equal magnitude. [10, 40]

4.3 The Arrhenius Equation and Transition State Theory

The Arrhenius equation relates the rate constant to the Gibbs free energy of activation. The cathodic and anodic rate constants for redox reactions can be expressed, respectively, in the form:

$$k_c = A_c \exp\frac{-\Delta G_c^{\ddagger}}{RT} \qquad (4.5)$$

and

$$k_a = A_a \exp\frac{-\Delta G_a^{\ddagger}}{RT}, \qquad (4.6)$$

where $G^{\ddagger}$ is the Gibbs energy of activation for the chemical reaction and the subscripts *c* and *a* refer to cathodic and anodic respectively. *R* and *T* have their usual meaning. The exponential term represents the probability that the activation energy is overcome by using thermal energy, and the pre-exponential factors A_c and A_a describe the number of

collisions with the electrode surface or the attempts at surmounting the activation energy (also the failed attempts).

The idea of activation energy can be depicted as shown in Figure 8 by a reaction path in terms of potential energy along a reaction coordinate [10]. The reaction coordinate is a geometric parameter that changes during the conversion of reactants to products and its value is a measure of the progress of a reaction. The bond length and bond angle of a molecule are examples of geometric parameters, although for more complex reactions non-geometric parameters such as bond order must be used. [40] Reactants and products are stable molecules and they correspond to energy minima separated by an energy maximum, the activation energy. [10] According to transition state theory, the reaction proceeds through a fairly well-defined transition state or activated complex that corresponds to this energy maximum. The activated complexes are in equilibrium with the reactants and can convert into products. Kinetic theory can be used to calculate the rate of this conversion. [10, 38]

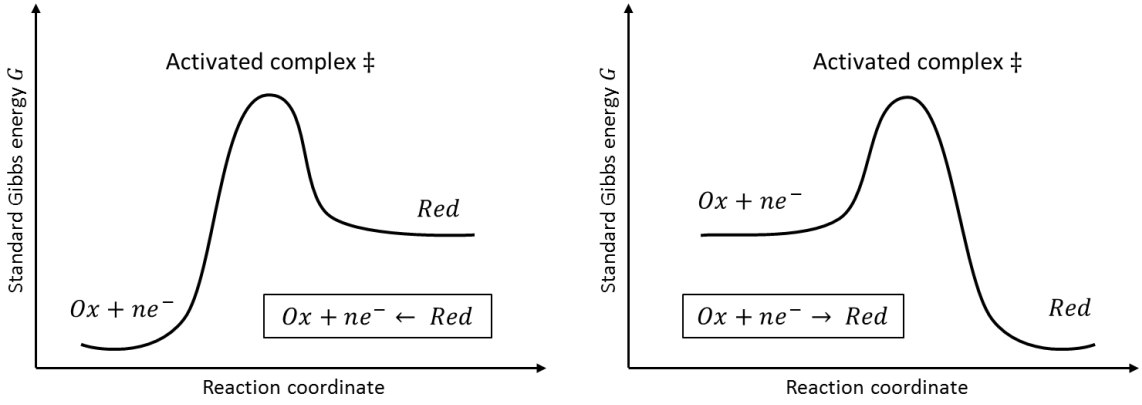

Figure 8. Energy profiles for simple redox processes. Altering the potential of the electrode will change the Gibbs energy of the reactants and products. If the electrode is made more positive compared to the solution, oxidation occurs (left) whereas if the electrode is made more negative, reduction occurs (right).

4.4 Butler-Volmer Kinetics

The heterogeneous electrochemical rate constants k_a and k_c introduced in the previous section are strongly sensitive to potential, since the chemical species involved in the electrochemical reaction are charged. If the electrode potential is altered, the interface potential will change. The change will take place for the most part in the electrical double layer while its effect on the bulk solution remains unchanged. All the charged species in the electrode and the double layer will be affected. [38]

In a simple redox reaction such as $Ox + ne^- \leftrightarrow Red$, if the electrode becomes more negatively charged, the main effect is that the electrons on the reactant side gain energy. Thus $Ox + ne^-$ will be raised in energy compared to Red. Since the activation energy for reduction is lowered and that for oxidation is raised, the net conversion will be from

$Ox + ne^-$ to Red and the energetically favorable reaction will be reduction as shown on the right side of Figure 8. Conversely, if the electrode potential is made more positive, the electrons on the reactant side will lose energy and $Ox + ne^-$ will be lowered in energy compared to Red. The net conversion will be from Red to $Ox + ne^-$and oxidation will occur as depicted on the left side of Figure 8. [40]

The cathodic and anodic activation energies at equilibrium potential E^0 are $\Delta G_{0c}^{\ddagger}$ and $\Delta G_{0a}^{\ddagger}$, respectively. If the potential is changed from the equilibrium potential to a new value *E*, the relative energy of electrons on the electrode changes by $-nF(E - E^0) = -nF\Delta E$ per mole of electrons. For a negative change ΔE, the activation energy for reduction is lowered implying that $\Delta G_c^{\ddagger}$ becomes less than $\Delta G_{0c}^{\ddagger}$ by a fraction of the total energy change as can be seen in Figure 9. [10, 38, 40]

The fraction by which the Gibbs free energy of activation for cathodic and anodic processes is changed is dependent on the transfer coefficients α and β according to

$$\Delta G_c^{\ddagger} = \Delta G_{0c}^{\ddagger} + \alpha nF\Delta E \qquad (4.7)$$

and

$$\Delta G_a^{\ddagger} = \Delta G_{0a}^{\ddagger} - (1-\alpha)nF\Delta E = \Delta G_{0a}^{\ddagger} - \beta nF\Delta E\,, \qquad (4.8)$$

where the transfer coefficients are defined so that $\alpha + \beta = 1$. The transfer coefficients are a measure of the symmetry of the energy barrier and in most electrochemical systems α lies between 0.3 and 0.7. It can usually be approximated by 0.5 ($\alpha \sim \beta \sim 0.5$). The transfer coefficient tells us how much of the change in potential energy is used to overcome the activation energy. [10, 40]

From the above equations we can determine that if the potential change $E - E^0$ is negative, the activation energy for reduction is lowered by $\alpha nF\Delta E$ while at the same time the activation energy for oxidation is raised by $(1-\alpha)nF\Delta E$ as reference to Figure 9 shows. [10, 25]

At equilibrium, where $E = E_f^0$ and the redox reactions are of equal magnitude, the rates of anodic and cathodic reaction must have the same value so that $k_c = k_a = k^0$. This value is known as the standard electrochemical rate constant with units of velocity (cm s^{-1}). When the Gibbs free energies given by equations (4.7) and (4.8) are inserted into the Arrhenius equations of (4.5) and (4.6), we obtain

$$k_c = k^0 \exp\frac{-\alpha F(E - E_f^0)}{RT} \qquad (4.9)$$

and

$$k_a = k^0 \exp\frac{(1-\alpha)\,F(E - E_f^0)}{RT} = k^0 \exp\frac{\beta F(E - E_f^0)}{RT}, \qquad (4.10)$$

where E_f^0 is the formal potential given by eq. (3.9). [10, 38, 40]

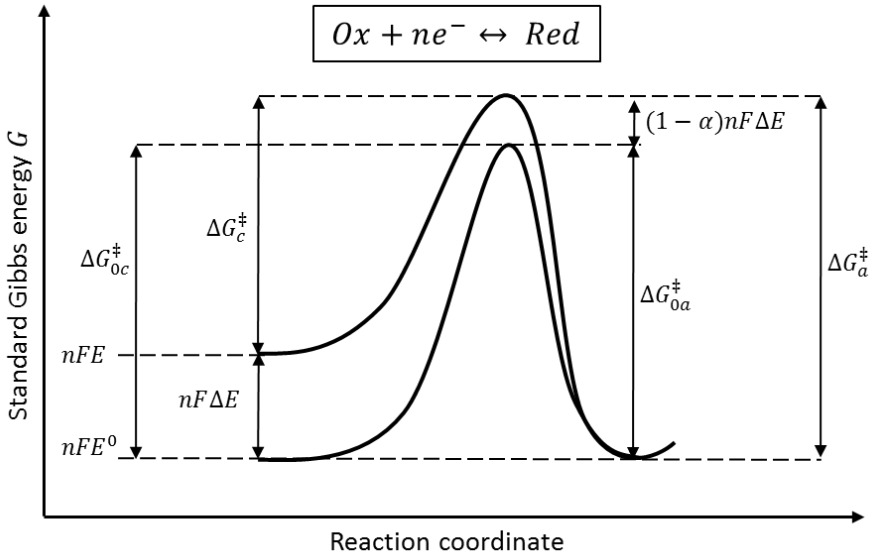

Figure 9. Effects of a potential change on the standard Gibbs free energies of activation for oxidation and reduction. When the potential is changed from the equilibrium potential E^0 to a more negative value E (the change in Gibbs free energy is positive by eq. (3.10)), the activation energy for cathodic processes is decreased and that for anodic processes increased.

The standard rate constant is used to express rate constants at potentials deviating from the equilibrium potential. It is a measure of the kinetic facility of a redox couple: a system with a large value of k^0 will reach equilibrium rapidly, while a system with a small k^0 will be sluggish. The largest values are obtained for redox reactions involving only electron transfer and resolvation. On the other hand, processes that require significant molecular rearrangements upon electron transfer will have a small standard rate constant and the thus the reactions will be sluggish (see section 4.6 on Marcus theory) The largest measured standard rate constants are in the range of 1 to 10 cm/s, while the smallest reported values have been less than 10^{-9} cm/s. The anodic and cathodic rate constants can become quite large, even if k^0 is small, by providing a large overpotential to overcome the activation energy.

It can be seen from equations (4.9) and (4.10) that the electrochemical rate constants depend exponentially on the electrode potential. The rate constant for reduction, k_c, increases as the electrode is made more negative whilst the oxidation rate constant, k_a, increases as the electrode is made more positive. For $\alpha \sim \beta \sim 0.5$, if the term $E - E_f^0$ is changed by 1 V, then the rate constants are changed by a factor of circa 10^9. This demonstrates that the sensitivity of rate constants on electrode potential dominates the behavior of electrode kinetics. This is also the reason behind the narrow potential window of many systems as the electron transfer rises exponentially with potential. [40]

Finally, insertion of the equations for the electrochemical rate constant (4.9) and (4.10) into equation (4.3) yields the complete current-potential characteristics

$$i = i_c - i_a = nFAk^0 \left[c_{ox} \exp\frac{-\alpha F(E - E_f^0)}{RT} - c_{red} \frac{(1-\alpha)F\left(E - E_f^0\right)}{RT} \right] \quad (4.11)$$

This equation is known as the Butler-Volmer formulation of electrode kinetics and it is central to the field of electrochemistry. The first component inside the bracket describes the contribution of the cathodic current i_c while the second term that of the anodic current i_a. [10, 40]

4.5 Special Cases of the Butler-Volmer Kinetics

4.5.1 The Nernst Equation

From the thermodynamic inspection in section 3.3, we saw that at equilibrium the activity and concentration of redox species must be equal. If the Butler-Volmer kinetic theory is to hold, then it must reduce to thermodynamic relations at equilibrium. At equilibrium the net current is zero and the terms in equation (4.11) can be rearranged to give

$$\exp\frac{F(E - E_f^0)}{RT} = \frac{c_{ox}}{c_{red}} \quad (4.12)$$

which is the exponential form of the Nernst equation, which is used to characterize electrode reactions at equilibrium:

$$E = E_f^0 + \frac{RT}{F}\ln\left(\frac{c_{ox}}{c_{red}}\right). \quad (4.13)$$

The Nernst equation relates the electrode potential to the concentrations of the redox species at the electrode surface and it is valid for reversible reactions. The Butler-Volmer kinetic theory gives correctly the Nernst equation at equilibrium and reduces, consequently, to thermodynamic relations. [10, 38]

4.5.2 The Current-Overpotential Equation

Although the net current is zero at equilibrium, the cathodic and anodic components i_c and i_a will be non-zero and equal in magnitude. This current is called the exchange current $i_0 = i_c = i_a$.

The exchange current can be expressed in terms of the standard electrochemical rate constant k^0 by

$$i_0 = nFAk^0 c_{ox}^{(1-\alpha)} c_{red}^{\alpha} \quad (4.14)$$

The exchange current can be stated per unit area to provide the exchange current density

$$j_0 = \frac{i_o}{A}. \quad (4.15)$$

The current is proportional to the amount of reactants consumed in the process as explained by Faraday's laws, whereas the current density gives information about the speed of the reaction. [39]

By expressing the current i in terms of i_0 rather than k^0 will allow us to use the overpotential η instead of the formal potential E_f^0. By dividing the Butler-Volmer kinetic formulation in (4.11) by (4.14) gives the current-overpotential equation:

$$i = i_0 \left[\frac{c_{ox}}{c_{ox}^*} \exp \frac{-\alpha F \eta}{RT} - \frac{c_{red}}{c_{red}^*} \exp \frac{(1-\alpha)\, F\eta}{RT} \right]. \quad (4.16)$$

c_{ox}^* and c_{red}^* are the bulk concentrations of the redox species. The total current is the sum of the anodic and cathodic components as depicted in Figure 10. When the potential deviates considerably from the equilibrium potential, one of the exponential terms becomes negligible. For large negative overpotentials, the anodic component approaches zero and hence the total current curve merges with the cathodic current and vice versa for large positive overpotentials. As the potential increases in either direction, the current rises sharply, because of the exponential dependency. However, at sufficiently large values of η, the current flattens out as mass transfer becomes rate-limiting. This behavior could be predicted from the concentration factors in the above equation that account for the reactant supply. The effects of mass-transfer on electrode kinetics will be discussed further in chapter 5. [10]

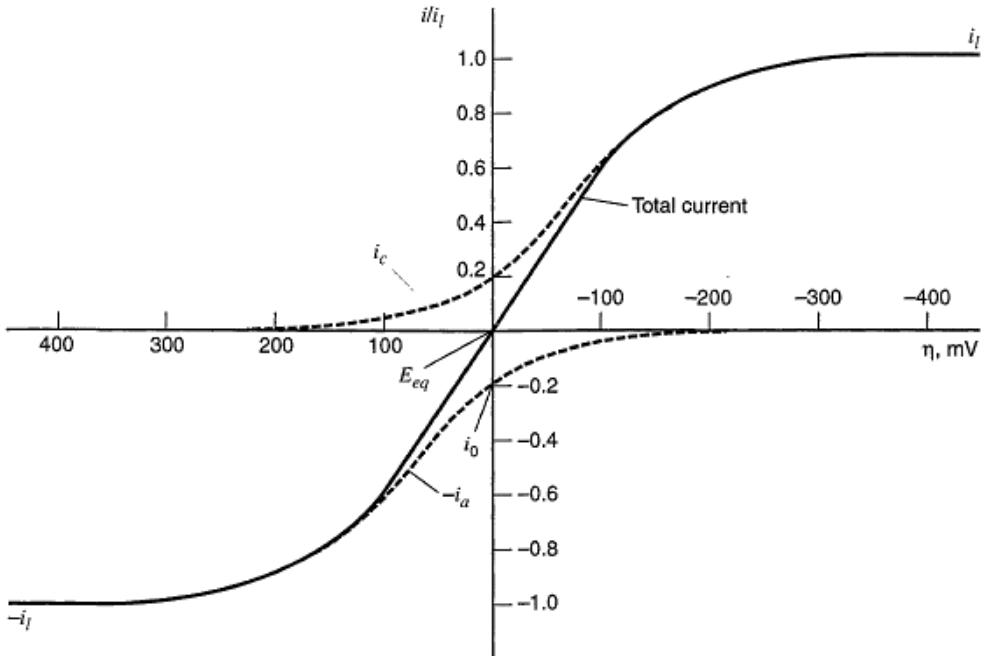

Figure 10. Current-overpotential curves for a simple redox system with α = 0.5 and T = 298 K. The dashed lines indicate the cathodic and anodic components and the normal line to total current. i_l is the rate-limiting current.

4.5.3 The Butler-Volmer Equation

If the surface concentrations of the redox species do not vary appreciably from the bulk concentrations, for example in the case of small currents, the mass-transfer effects can be omitted and the current-overpotential equation (4.16) becomes

$$i = i_0 \left[\exp\frac{-\alpha F\eta}{RT} - \exp\frac{(1-\alpha)\,F\eta}{RT} \right], \qquad (4.17)$$

which is known as the Butler-Volmer equation.

The effect of exchange current densities on the Butler-Volmer equation are shown in Figure 11. In each plot $\alpha = 0.5$. Since mass-transfer effects are not included, the overpotential serves solely to overcome the activation energy and drive the heterogeneous process at the rate reflected by the current. In the case of a large exchange current (curve a), there is no significant activation overpotential and the system can supply large currents. Any observed overpotential is related to concentration overpotential i.e. the activation energy required to drive mass transfer to provide enough reactants to maintain the current. From curve c, we see that the lower the exchange current, the more sluggish the kinetics. This implies that a larger activation overpotential must be applied to obtain any particular net current. This is the case for systems with a very low standard electrochemical rate constant k^0. At a sufficiently large potential, mass transfer will limit the current (Figure 11). This means that the concentration overpotential will also contribute to the total overpotential even if it is

small compared to the activation energy required for charge transfer. The exchange current can be thought of as a measure of any system's ability to deliver a net current without a significant energy loss due to activation. [10]

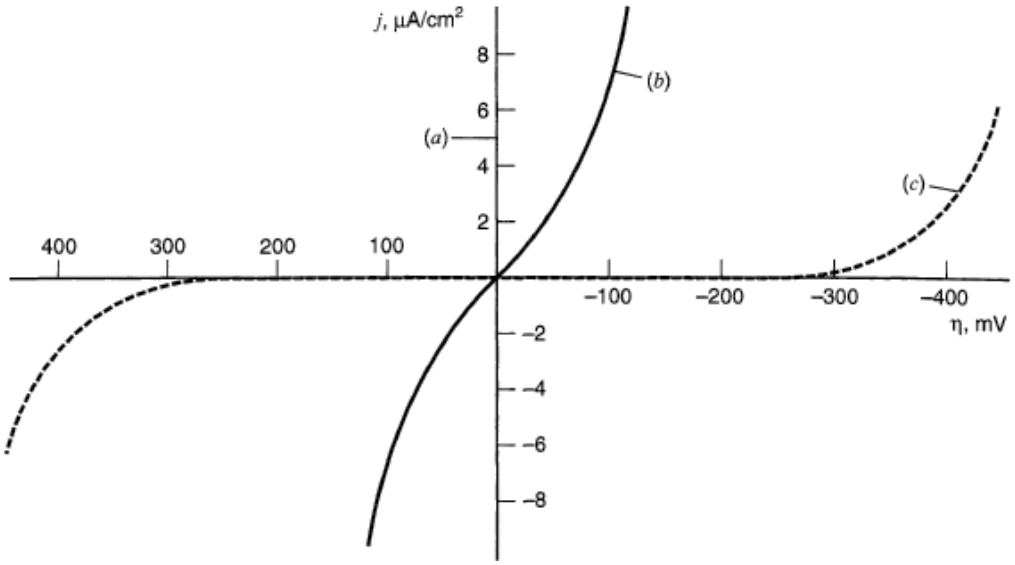

Figure 11. Effect of exchange current on the activation overpotential required to obtain a net current density for a simple redox system with α = 0.5 and T = 298 K. Curve (a) $j_0 = 10^{-3}$ A/cm^2, (b) $j_0 = 10^{-6}$ A/cm^2 and (c) $j_0 = 10^{-9}$ A/cm^2. The curve (a) is equal to the current density axis.

4.5.4 Tafel Equation

When the imposed potential is much larger or much smaller than the formal potential, the overpotential η becomes very large and one of the bracketed terms in the Butler-Volmer equation (4.17) becomes negligible. For example at large negative overpotentials, where reduction is dominant, $\exp(-\alpha F\eta) \gg \exp((1-\alpha)\,F\eta)$ and the Butler-Volmer equation becomes

$$\eta = \frac{RT}{\alpha F}\ln i_0 - \frac{RT}{\alpha F}\ln i. \qquad (4.18)$$

This is of the same form as the Tafel equation, which predicts the exponential relation between the current i and the overpotential η:

$$\eta = a + b\log i. \qquad (4.19)$$

The Tafel constants a and b can be written using the 10-base logarithm as

$$a = \frac{2{,}3RT}{\alpha F}\log i_0 \qquad (4.20)$$

and

$$b = \frac{-2{,}3RT}{\alpha F} \log i_0 \qquad (4.21)$$

Adequate Tafel relationships can be observed when the kinetics are slow and high overpotentials are needed to pass a current underscoring the fact that Tafel behavior indicates irreversible kinetics. In fact, the Tafel form is valid when the reverse reaction (for example anodic reaction when reduction is considered) contributes less than 1% to the total current. [10, 40]

Tafel plots provide information on the kinetic parameters of a system. On the linear segment of the plot, the current *i* can be evaluated if the overpotential is known. As the overpotential approaches zero, the plot is no longer linear, because the reverse reaction can no longer be neglected. Extrapolating the linear segment, we can obtain the Tafel constant a and the exchange current i_0 from the intercept of $log|i|$. The magnitude of the transfer coefficients α and β can also be estimated from Tafel plots. [10, 40] For example, in a two-electron transfer process with $\alpha \sim \beta \sim 0.5$, a Tafel slope of ca. 0.5 indicates that the first electron transfer is rate-determining whereas a slope of ca. 1.5 indicates that the second electron transfer process is the determining step [40].

Since there will be reactant depletion at the electrode surface due to electrochemical processes, the restriction imposed on the concentrations will no longer be valid.

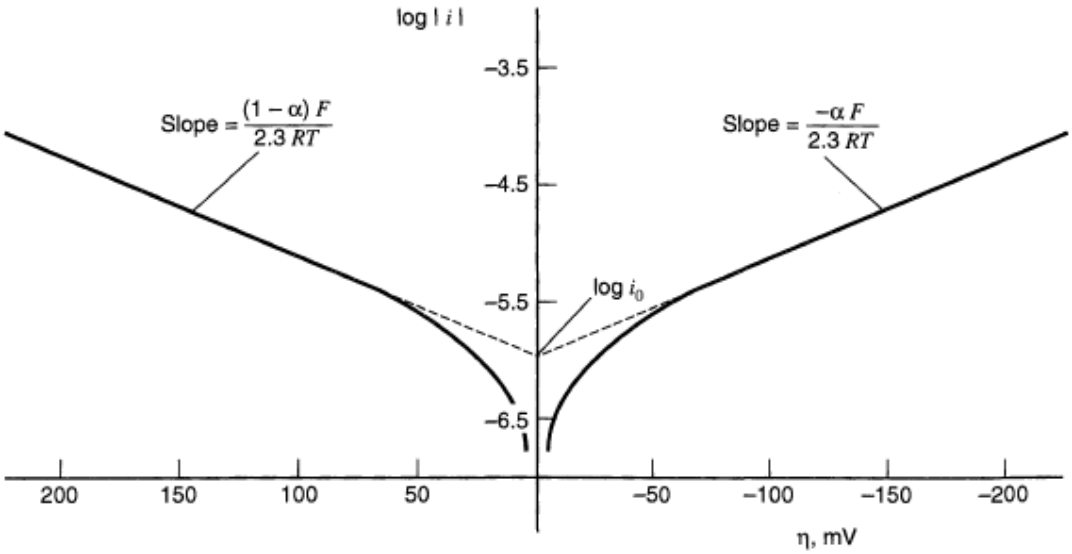

Figure 12 . Tafel plot for a simple redox system with with α = 0.5 and T = 298 K and $j_0 = 10^{-3}$ A/cm^2. Oxidation reaction on the left side and reduction on the right side of the current axis.

4.6 Marcus Theory

The driving force for the electron transfer that results in electrode potential is the difference in the Fermi level of the metal electrode and the electronic state of the species in the solution. The Marcus theory is a widely used microscopic theory in electrochemistry that predicts how molecular structure and environment such as the solvent and electrode material affect the electron transfer process. [10]

The electron transfer process between the electrode and a chemical species in solution takes place via quantum mechanical tunneling, The chemical species undergoing a redox reaction must be located within approximately 1-2 nm from the electrode surface, because the rate of tunneling falls off sharply as the distance increases, as it requires overlap of the quantum mechanical wavefunctions describing the electron location. [40]

4.6.1 Inner and Outer-Sphere Electron Transfer

A coordination sphere consists of a central atom or ion to which ligands, usually solvent molecules, are attached. The first coordination sphere refers to the molecules that are attached directly to the central atom. Several coordination spheres can surround the central atom. For example in an aqueous solution water molecules can form a primary, secondary, etc. solvation shell around a dissolved ion. [38]

Outer-sphere electron transfer is characterized by weak interaction of the reactive species with the inner coordination spheres remaining intact in the activated complex during electron transfer. The reactant and product are generally at a distance of at least one solvent layer from the electrode and do not interact strongly with the electrode surface. [Bard, Compton] Outer-sphere redox systems are generally considered to lack any electrocatalytic or adsorption step and often have low reorganization energies. Examples of such systems are ferrocene and $Ru(NH_3)_6^{3+/2+}$. [14]

In contrast, inner-sphere electron transfer involves a common ligand between the central atoms or ions in the activated complex and the structure of the coordination shells is altered. Reactants, intermediates or products are specifically adsorbed on the electrode surface and thus have kinetics that are strongly dependent on the chemical nature of the electrode surface. [10, 40] Examples include $Fe(CN)_6^{-3/-4}$ and dopamine [14].

4.6.2 Relationship between Marcus Theory and Butler-Volmer Kinetics

The potential energy curves of reactants (R) and products (P) as a function of reaction coordinate (as explained in section 4.3) are shown in Figure 13. According to Marcus theory, the electron moves from an initial state to a receiving state of the same energy due to the principle of conservation of energy. Additionally, during the actual electron tunneling, the reactant and product have a common nuclear composition, because the timescale of electron transfer is much shorter than that of nuclear vibrations. It follows that the electron tunneling takes place where the potential curves of the reactants and products meet. This also corresponds to the reaction coordinates of the transition state, where the reactants and products have the same configuration (see Figure 13). [10]

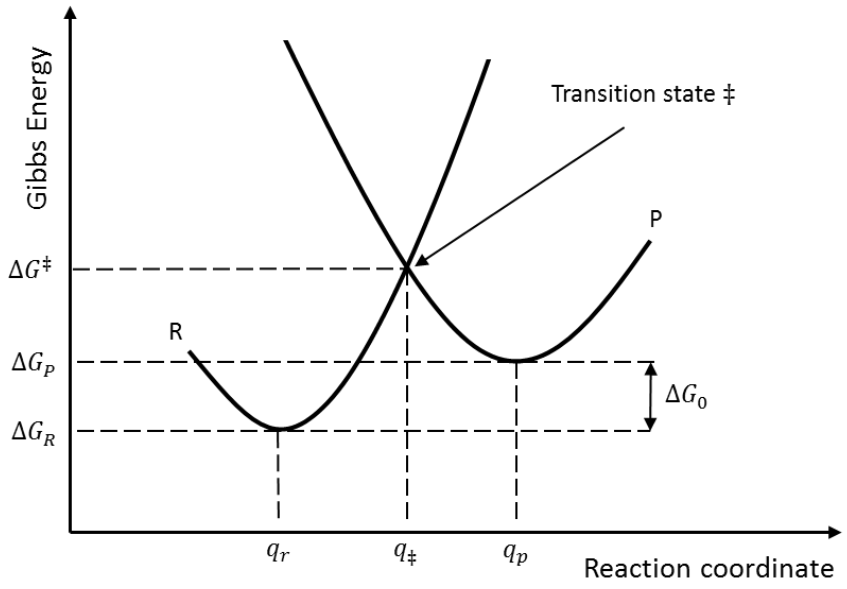

Figure 13. Potential energy curves for reactants (R) and products (P). The transition state is the cross-over point of the curves.

At the transition state, the bond lengths and angles within the reactant species become stretched, compressed or distorted by changes in thermal energy and the structure of solvation shells may also be altered. [10]

In reference to Figure 13, the free energy of activation $\Delta G^{‡}$ for the electron transfer may be expressed as

$$\Delta G^{‡} = \frac{\lambda}{4}\left(1 + \frac{\Delta G_0}{\lambda}\right)^2 = \frac{\lambda}{4}\left(1 + \frac{F(E - E_0)}{\lambda}\right)^2 \qquad (4.22)$$

where the standard free energy $\Delta G_0 = \Delta G_P - \Delta G_R$. The potential energy curve for R in Figure 13 is the sum of energies for species R and for an electron on the electrode at the Fermi level corresponding to potential E. Thus for electrode reactions we can write $\Delta G_0 = F(E - E_0)$. The reorganization energy λ is the energy required to transform the reactant into the product state and is expressed as

$$\lambda = \frac{1}{2}k(q_R - q_P)^2 \qquad (4.23)$$

The constant k is the force constant for a change in bond length and q_R and q_P are the values of the the reaction coordinate for the equilibrium atomic configuration of the reactants and products, respectively. The reorganization energy can be divided into an inner component, λ_i, representing the change in the nuclear configuration of the reactant and an outer component, λ_o, representing the reorganization of the solvation shells so that

$$\lambda = \lambda_i + \lambda_o. \quad (4.24)$$

From equations (4.22) and (4.23) we can obtain qualitative information about reaction kinetics. Since a change in reaction coordinate implies a change in the structure of the molecule (alterations in bond lengths or bond angles), a large difference in reaction coordinates between the ground state of reactants and products results in a large reorganization energy. Thus for reactants and products with a differing molecular geometry, the free energy of activation is appreciable and the reaction kinetics are sluggish. This corresponds to a small standard rate constant k^0 for the electron transfer process. On the other hand, for reactants and products with a similar molecular geometry, the free energy of activation is small and k^0 is large. [10]

From equation (4.22), we can obtain a value for the transfer coefficient α as

$$\alpha = \frac{1}{2}\left[1 + \frac{F(E - E_0)}{\lambda}\right] \quad (4.25)$$

This equation provides a link between Marcus theory and Butler-Volmer kinetics. In Butler-Volmer kinetics the value of α is usually taken as constant ($\alpha \sim 0.5$) but Marcus theory predicts that its value depends on potential. Near the equilibrium potential ($E \approx E_0$), α is approximately 0.5, which is generally assumed in Butler-Volmer kinetics. The potential-dependent term in (4.25) is generally not very large so a clear potential dependency has been difficult to observe experimentally. [10]

If $\Delta G_0 \gg 0$ and the reaction is thermodynamically unfavorable, then $\Delta G_0 \sim \lambda$ and we see from the above equation that α approaches 1. Conversely, when $\Delta G_0 \ll 0$ and the electrode potential strongly drives the reaction, $\Delta G_0 \sim -\lambda$ and α approaches 0. [40]

5. Mass Transfer

Mass transfer at electrodes takes place due to electron transfer reactions, where the species involved in the reactions are either depleted or produced at the electrode surface. As a consequence, concentration differences are created in the vicinity of the electrode, which gives rise to mass transfer. In this chapter we have assumed steady-state situations. Transient phenomena have not been taken into account except for the Cottrell equation in section 5.5.

5.1 Modes of Mass Transfer

Mass transfer is the movement of material in the solution and results from differences in chemical or electrical potential at two different locations in the solution or the physical movement of the solution. The modes of mass transport are

1. Diffusion, which is the movement of a chemical species caused by a chemical gradient i.e. a difference in concentration.
2. Migration, which is the movement of a charged species under the effect of an electric field.
3. Convection, resulting from a fluid flow that occurs naturally as a consequence of density gradients or forced by the cell design (for example a rotating disk electrode).

The mass transfer to an electrode is described by the Nernst-Planck equation. An exact solution of the Nernst-Planck equation that takes into account all of the three modes of mass transfer is difficult. Therefore, electrochemical systems are usually designed so that the mass transfer of an electroactive species at the electrode can be restricted to diffusion alone. [10]

In the bulk of the solution, away from the electrode where the electrochemical reactions take place, the concentrations of the species are for the most part unchanged and mass transport occurs mainly by migration. The addition of a supporting electrolyte at a concentration much larger than that of the electroactive species eliminates the contribution of migration to mass transport. The supporting electrolyte is composed of an excess of non-electroactive ions that do not participate in the electrochemical reactions and carry the current in the bulk solution. The supporting electrolyte also ensures that the double layer remains thin compared to the diffusion layer. [10]

The use of a supporting electrolyte has also additional benefits. The high concentration of ions decreases the solution resistance and lowers the ohmic drop caused by the uncompensated resistance (see section 6.1.4), hence, improving the accuracy with which the working electrode's potential is measured. A lower solution resistance also reduces power dissipation and can lead to simplification in the cell apparatus. The reaction conditions (pH, ionic strength, ligand concentration) can be controlled by altering the

supporting electrolyte and it can therefore serve to reduce or eliminate sample matrix effects. Some disadvantages are also associated with high concentrations of supporting electrolytes. The impurities in the electrolyte can be the source of interference by giving rise to small faradaic processes or by reacting with intended reaction products. Electrode kinetics can also change if the impurities adsorb on the electrode surface. Therefore a suitable supporting electrolyte must be chosen for a particular solvent and electrode process. [10]

The effect of convection can be minimized by preventing stirring and vibrations in the electrochemical cell. [10]

5.2 Physical View of Diffusion

The mathematical model of diffusion was given by Einstein and Smoluchowksi and is based on the random walk process of diffusing particles. The moving molecules advance by colliding with solvent molecules under brownian motion and their location can only be estimated by giving the probability that it is found there. From Einstein and Smoluchowksi's findings, a simple equation can be derived to relate the root mean square distance diffused by a molecule to the diffusion coefficient and time:

$$x = \sqrt{2Dt}. \qquad (5.1)$$

The diffusion coefficient D has units $cm^2\ s^{-1}$. This equation is useful because the average distant x diffused by the molecule from the electrode in a time t provides an estimate of the thickness of the diffusion layer. A diffusional velocity can also be derived from the above equation by dividing both sides by the time t:

$$v_d = \frac{x}{t} = \sqrt{\frac{2D}{t}}. \qquad (5.2)$$

It can be seen that the speed of a diffusing molecule decreases with time because random walk processes favor small displacement instead of large ones. A particle can only move in a given direction at high velocity over a short distance before it collides with other solvent molecules and changes direction. [10, 40]

A typical value of D for an aqueous solution is $5\times10^{-6}\ cm^2/s$. Using equation (5.1) we can estimate the scale of the diffusion layer to be 32 μm for t = 1 s [40].

5.3 Fick's Laws of Diffusion

Fick's laws describe the flux of a substance and its concentration as functions of time and position. The physical basis of Fick's laws was explained by Einstein and Smoluchowski and outlined in the previous section.

The flux *j* of a substance expresses the net mass-transfer rate of that substance at a certain location *x* at which the concentration is known. Fick's first law relates the diffusive flux to the concentration gradient:

$$j(x) = -D\frac{\partial c(x)}{\partial x}. \qquad (5.3)$$

The flux *j* corresponds to the number of moles passing per unit area per unit time (mol m^{-2} s^{-1}), *D* is the diffusion coefficient with the minus sign implying that the flux is taken down the concentration gradient from high to low concentration and $\partial c/\partial x$ is the concentration gradient. [40]

Fick's second law predicts how the concentration varies with time *t*. It can be derived from Fick's first law and mass conservation. Its general formulation is given by

$$\frac{\partial c}{\partial t} = D\,\nabla^2 c, \qquad (5.4)$$

where ∇^2 is the Laplace operator that will take different forms depending on the coordinate system used. The choice of coordinate systems depends on the electrode geometry. For a planar electrode, diffusion occurs in one dimension so the linear diffusion equation is

$$\frac{\partial c(x,t)}{\partial t} = D\frac{\partial^2 c(x,t)}{\partial x^2}. \qquad (5.5)$$

For cylindrical microelectrodes, the properties of which are similar to the electrodes used in this work, equation (5.4) becomes

$$\frac{\partial c(r,z,t)}{\partial t} = D\left(\frac{\partial^2 c(r,z,t)}{\partial r^2} + \frac{1}{r}\frac{\partial c(r,z,t)}{\partial r} + \frac{\partial^2 c(r,z,t)}{\partial z^2}\right). \qquad (5.6)$$

The variables *r* and *z* are the radial distance measured from the center of the disk and the distance normal to the disk surface, respectively. The solutions of Fick's second law yield concentration profiles at the electrode surface. The geometry of the electrode will affect the concentration profile and must be taken into account when solving equation (5.4). The difference between a linear and cylindrical electrode arises because

cylindrical diffusion takes place through an increasing area as the radius increases from the center of the electrode. [10]

In solving diffusion equations to obtain an expression for the concentration of a species, an initial condition and two boundary conditions are required. The initial condition describes the concentration of the species at time $t = 0$. Usually, the species is either uniformly distributed in the solution at bulk concentration (reactant) or it is absent from the solution (product) at the beginning of the experiment. In most cases, the electrochemical cell is large compared to the length of diffusion and we can assume that far away from the electrode, where $x \rightarrow \infty$, the concentration reaches a constant value at a time $t > 0$. Usually, the constant value is the same as the initial value and these conditions constitute the necessary boundary conditions for solving the diffusion equation. Additional boundary condition can for example relate the concentration of a species to the electrode potential, for example through the Nernst equation (4.13). [10]

In most voltammetric studies, the changes in solution composition caused by electrolysis are sufficiently small that variations in diffusion coefficient can be neglected [10, 40]. A reasonable solution to Fick's second law could not be obtained if the diffusion coefficient was varying and thus it is assumed to be constant. However, when the electroactive component is present at a high concentration, electrolysis can lead to large changes in the solution properties and migrational effects can also become notable. [10]

5.4 Mass Transfer and Electrode Kinetics

When an electroactive species undergoes an electron transfer reaction of the type $Ox + ne^- \leftrightarrow Red$ at the electrode, a current proportional to the amount of reactant is produced according to Faraday's law (see section 4.1). In a situation where this electroactive species is transported solely by diffusion to the surface of the electrode, and no other reactions occur, then the current is related to the amount of species diffused to the electrode. Namely, the total number of electrons transferred at the electrode must be proportional to the quantity of reactant reaching the electrode. The diffusive flux is hence related to the rate of reaction υ described in section 4.2. By solving equation (4.1) for the rate of reaction υ and equating it to the flux j given in (5.3), we obtain

$$-j(x,t) = \frac{i}{nFA} = D\frac{\partial c(x,t)}{\partial x}, \qquad (5.7)$$

where n is the number of electrons passed in the electrode reaction, F is the Faraday constant and A is the electrode area. Both υ and j have the same units (mol m^{-2} s^{-1}). The importance of this equation lies in the fact that it connects the evolving concentration

profile at the electrode surface to the current flowing in the electrochemical experiment. [10]

Let us consider the reduction of the species Ox according to the reaction $Ox + ne^- \leftrightarrow Red$. The initial concentration of Ox is equal to the bulk concentration c_{ox}^* everywhere in the solution. Then, once the reduction of Ox begins, its concentration at the electrode surface $c_{ox}(x = 0)$ becomes smaller than the bulk value. This simplified model is based on the idea that a Nernst diffusion layer of thickness δ_0 forms at the electrode surface as shown in Figure 14. The Nernst diffusion layer is the depletion zone near the electrode where the concentration differs from the bulk value. [10] Assuming that the concentration gradient is linear within the diffusion layer, we can write from Fick's first law

$$j = D\frac{[c_{ox}^* - c_{ox}(\mathrm{x} = 0)]}{\delta_0}. \qquad (5.8)$$

Since the diffusion layer thickness δ_0 is usually unknown, it is convenient to incorporate it with the diffusion coefficient *D* into a new constant m_T, the mass transfer coefficient:

$$m_T = \frac{\mathrm{D}}{\delta_0}. \qquad (5.9)$$

The mass transfer coefficient has the same units (cm/s) as the first-order heterogeneous electrochemical rate constant k_c (and k_a in the case of oxidation), so that a direct comparison of the two values is feasible and can provide information on the relative speeds of electron transfer and mass transfer. [10] When equations (5.8) and (5.9) are inserted into 5.8, we obtain for the cathodic reaction

$$\frac{i}{nFA} = m_T\,[c_{ox}^* - c_{ox}(\mathrm{x} = 0)]. \qquad (5.10)$$

The reduction of Ox produces Red at the electrode surface, so that $c_{red}(x = 0)$ becomes larger than the bulk concentration of Red, c_{red}^*. Therefore

$$\frac{i}{nFA} = m_T\,[c_{red}(\mathrm{x} = 0) - c_{red}^*]. \qquad (5.11)$$

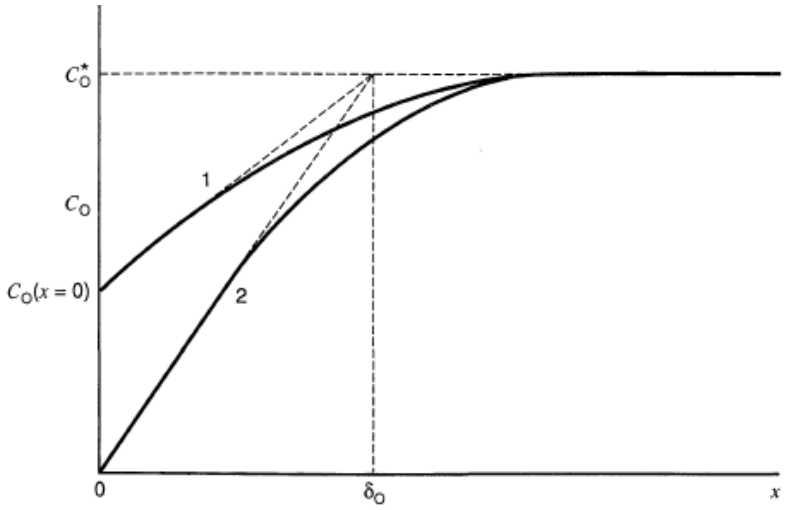

Figure 14. The solid lines indicate the concentration profile near an electrode. x = 0 corresponds to the electrode surface and δ_0 is the thickness of the diffusion layer. The Nernst diffusion layer is approximated by the dashed lines. The concentration profiles 1 and 2 correspond to different electrode potentials. (1) $c_{ox}(\mathrm{x} = 0) = c_{ox}^*/2$; (2) $c_{ox}(\mathrm{x} = 0) = 0$. [10]

5.4.1 Limiting Current

When the current in the electrochemical cell is low, mass transport doesn't limit the rate of reaction since the amount of reactants required to produce the current is small. In such a case, the current is limited by the electrode kinetics introduced in chapter 4. Yet, when the current becomes higher, an increasing amount of reactants must be provided to the electrode. When the reactant concentration falls to zero at the electrode surface, the mass-transfer becomes rate-limiting and a concentration overpotential is established. The concentration overpotential restricts the current at the electrode to a value known as the limiting current i_l.

As the reactant is depleted from the surface of the electrode i.e. $c_{ox}(x = 0) \ll c_{ox}^*$, the rate of mass transport reaches its maximum value and thus we can express the limiting current for a cathodic reaction as

$$i_{l,c} = nFAm_T c_{ox}^* \qquad (5.12)$$

For the anodic limiting current we have

$$i_{l,a} = -nFAm_T c_{red}^*. \qquad (5.13)$$

The minus sign is due to the convention that anodic currents are taken as negative and cathodic ones as positive. From the above equations we see that the limiting current is proportional to the concentration of the reactant and the diffusion coefficient and inversely proportional to the thickness of the diffusion layer. [10, 38]

5.4.2 Reversible, Quasi-reversible and Irreversible Reactions

In general, the electrochemical experiments can be studied by using the current-potential characteristics in conjunction with mass transfer. Butler-Volmer kinetics (equation (4.11)) can be combined with Fick's laws, which give the concentration of the electroactive species at the electrode surface. Experiments are usually designed so that simpler mathematical treatments can be utilized.

If the electrode kinetics are so fast that the net rate of reaction is totally controlled by the rate at which the electroactive species is transported by diffusion to the electrode surface, we can say that electrochemical reaction is reversible or nernstian. Compton defines a reversible reaction as one for which the standard electrochemical rate constant $k^0 \gg m_T$. Reversible chemical reactions obey thermodynamic relationships. Consequently the concentrations of Ox and Red at the electrode surface can be assumed to be at equilibrium with E and obey the Nernst equation (4.13), which is also the origin of the name nernstian reaction:

$$E = E_f^0 + \frac{RT}{nF} \ln\left(\frac{c_{ox}(\mathrm{x} = 0)}{c_{red}(\mathrm{x} = 0)}\right). \qquad (5.14)$$

The mathematical treatment of reversible reactions is often greatly simplified, because the electrochemical rate constant k^0 is not involved and for example the determination of the surface concentration is straightforward with the Nernst equation. [10, 40]

An electrochemically irreversible reaction corresponds to the case $k^0 \ll m_T$. Only negligible currents flow for potentials close to the equilibrium potential because the electrode kinetics are very sluggish and cannot keep up with a change in the potential. Thus large overpotentials must be applied to observe a net current. Mass transfer does not limit the reaction. If a cathodic current is applied, the anodic current is negligibly small and vice versa. Thus, the treatment of irreversible reactions can be narrowed down to the Tafel region (see section 4.5.4). [10]

An intermediate case between reversible and irreversible reactions occurs when $k^0 \sim m_T$. This corresponds to electrochemically quasi-reversible reactions. In quasi-reversible cases both forward and reverse charge transfer are activated and the whole i-e characteristics must usually be considered, which complicates the mathematical treatment of such systems. [10, 40]

Most likely, the above situations are further complicated by irreversible chemical reactions such as homogeneous reactions of products following an electron transfer reaction. Even in the absence of coupled homogeneous reactions, heterogeneous electron transfer reactions can be complicated by multistep heterogeneous electron transfer or multiple electron transfer. [10]

5.5 Cottrell Equation

An important solution of the linear diffusion equation (5.5) is the Cottrell equation, which is valid for a planar electrode when a potential step function changes the potential instantaneously from a value where no electrolysis occurs to a value in the mass-transfer-controlled region. The Cottrell equation describes a transient phenomenon and the current i is a function of time (rather than distance from the electrode):

$$i = \frac{nFA\sqrt{D}c^*}{\sqrt{\pi t}} \qquad (5.15)$$

where n is the number of electrons passed in the electrode reaction, F is the Faraday constant, A is the electrode area, D is the diffusion constant, c^* is the bulk concentration and t is the time. The Cottrell equation shows that the current is inversely proportional to the square root of time. Thus, the current will eventually decay to zero. This means that mass transfer controls the current. However, in real potential step experiments the predicted dependence on $t^{-1/2}$ is observed only for up to a few seconds except at very short times in the order of milliseconds or less when the charging current contributes greatly to the total measured current. After a few seconds, the measured current reaches a steady value because the diffusion layer does not expand and the concentrations of electroactive species approach the bulk values. This result is consistent with the Nernst diffusion layer model and arises because of natural convection. [40] Convection results in currents larger than those predict by the Cottrell equation. However, with the use of microelectrodes, it is possible to reach a steady state where convective effects are negligible and diffusion dominates [10].

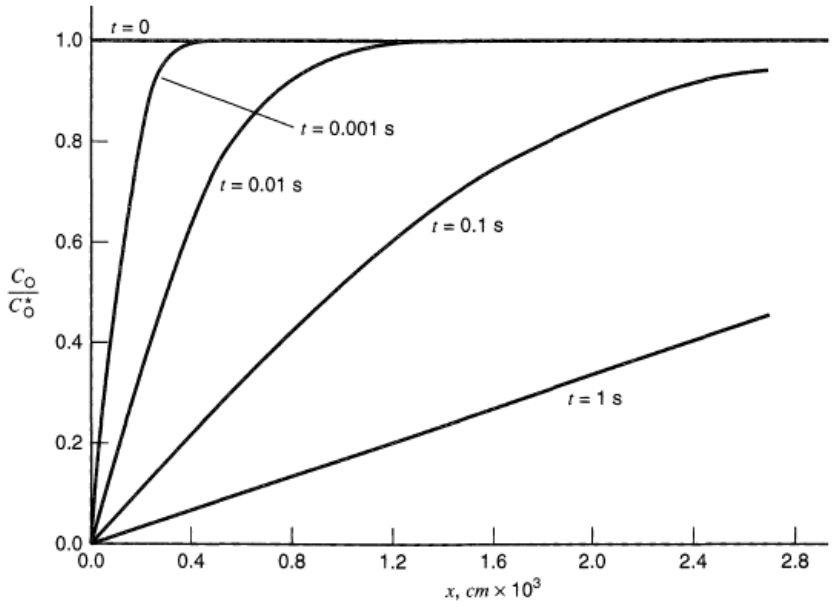

Figure 15. Concentration profiles for different values of t in a potential step experiment. D = 1×10^{-5} cm^2/s. [10]

In reference to Figure 15 we notice that the diffusion layer thickness is not constant and depends on the time scale of the experiment. The thickness of the diffusion layer can be well approximated by equation (5.1) or simply as a multiple of $\sqrt{Dt}$.

6. Measurement of Dopamine by Cyclic Voltammetry

Electrochemistry is a powerful analytical technique for monitoring electroactive species in living organisms. Several neurotransmitters, including dopamine, are inherently electroactive or can be made electroactive as it was explained in section 2.1. Thus, electrochemical methods are well-suited for monitoring the redox processes of neurotransmitters both in vitro and in vivo.

Among the electrochemical techniques presented in section 2.3.3, cyclic voltammetry (CV) is a very popular technique for the electrochemical study of redox systems and it is perhaps the most frequently used technique for the investigation of rapid neurotransmission events. [2, 11] Its strength lies in the qualitative evaluation of the electrochemical systems whereas other methods such as amperometry are often better suited for precise quantitative assessment. [10] CV provides high temporal resolution without compromising very good selectivity and this technique has proved effective for the multi-analyte detection of catecholamines. [2, 11] Fast scanning can also minimize electrode fouling [2].

Comparing to other techniques, cyclic voltammetry has several advantage for in vivo measurement of dopamine: it can measure DA concentration on a subsecond timescale, detect DA concentration changes in the nanomolar range and it can be combined with electrodes in the micrometer scale (for example carbon fiber electrodes) to give good spatial resolution with minimal tissue damage. [11]

6.1 Cyclic Voltammetry

In a cyclic voltammetry experiment, the potential of the working electrode is swept linearly with time from an initial potential E_i until a switching potential E_λ is reached at $t = \lambda$. At this point the direction of the linear sweep is switched until the initial potential is attained (see Figure 16). The potential limits are chosen so that the oxidation and reduction of the desired electroactive species lie within this potential window.

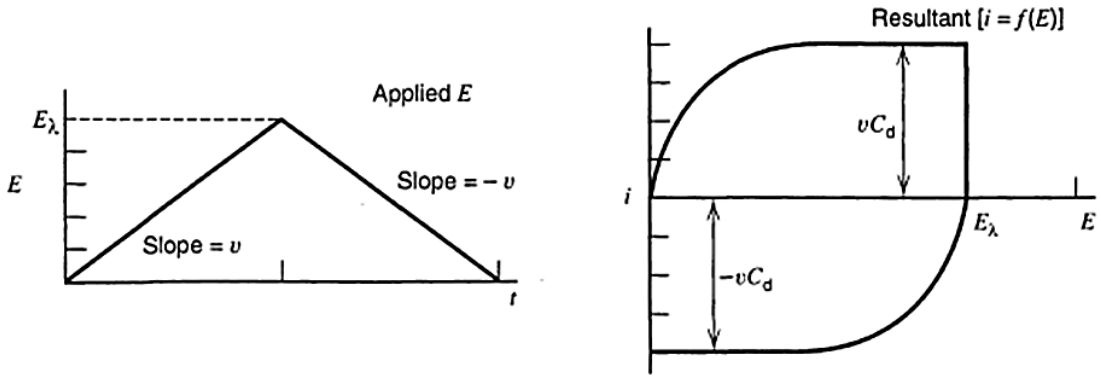

Figure 16. Applied potential in CV experiments and the resulting current-potential plot for an RC-circuit.

The forward scan (potential in the positive direction) produces an anodic current for any analyte that can be oxidized within the scanned potential range. When the applied potential approaches the oxidation potential, the analyte starts to oxidize and a current begins to flow (A in Figure 17). The oxidation causes the concentration of the analyte to decrease at the electrode surface even though mass transfer brings new analyte from the bulk solution to the vicinity of the electrode (B in Figure 17). As the potential increases, more and more analyte is oxidized and it becomes completely depleted from the electrode surface. At this point mass transfer reaches its maximum value and a peak current is observed (C in Figure 17). As the potential still increases, the zone of depletion i.e. the diffusion layer widens and mass transfer slows down, which in turn causes the current to decrease (D in Figure 17). After the switching potential is reached, on the reverse scan, the oxidized species is reduced to its original state if the electrochemical reaction is reversible. The cathodic current produced by the reduction has a similar shape much like that of the anodic current. The current is generally recorded as a function of potential, albeit current plots against time are also used since the potential is varied with time according to the scan rate. The result is a cyclic voltammogram from which information about the electrochemical reactions of the system under study can be obtained. [10, 40]

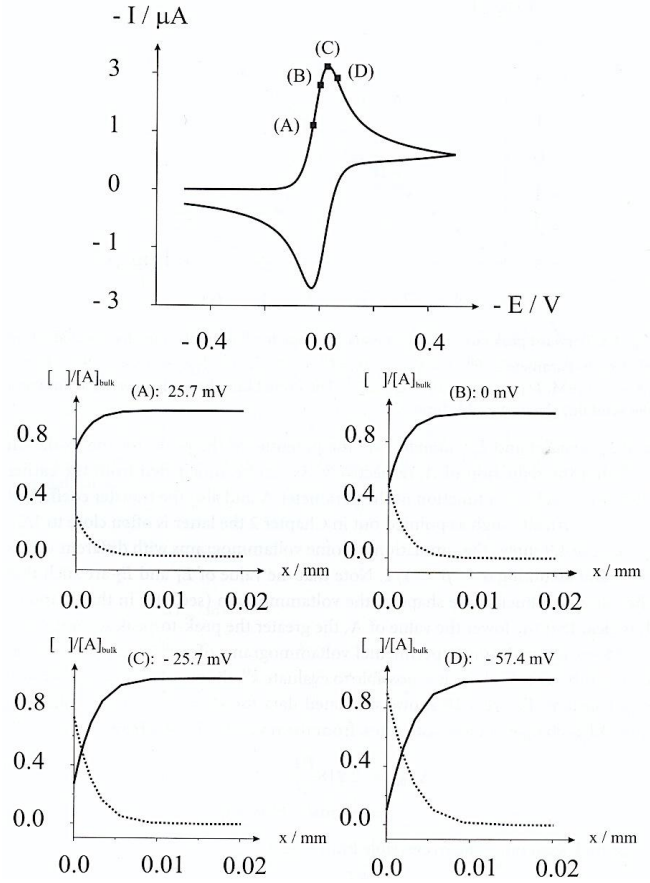

Figure 17. CV for the reversible reduction of A to B. The concentration profiles show the distributions of A (solid line) and B (dashed line) at the four locations indicated on the CV. CV parameters: E^0 = 0 V; α = 0.5; k^0 = 1 cm/s; υ = 10 V/s; A = 1 cm^2; [A_0] = 1 mM; D = 10^{-5} cm^2/s. [40]

The sweep rate or scan rate υ ranges from 10 mV/s to 10^6 mV/s for microelectrodes. The potential of the working electrode can be written as

$$0 < t \leq \lambda \qquad E = E_i + \upsilon t \tag{6.1}$$

$$t \geq \lambda \qquad E = E_i + 2\upsilon\lambda - \upsilon t \tag{6.2}$$

Two parameters of interest obtained from this voltammogram are the ratio of the peak currents, i_{pa}/i_{pc}, and the separation of peak potentials, $E_{pa} - E_{pc}$ as shown in Figure 18 [10, 40]. These parameters are discussed more in depth in the following sections.

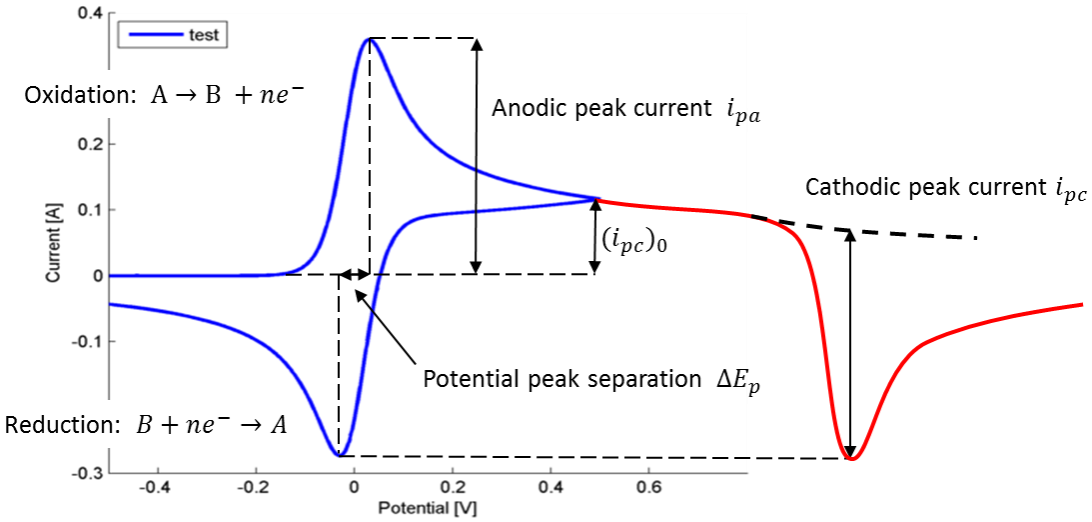

Figure 18. Parameters obtained from a CV experiments. The reverse scan has been plotted in red as if the current was plotted against time. This presentation clearly shows the baseline from which the cathodic peak current must be calculated.

The potential window, also called water window, occurs in aqueous electrolytes. It is the potential range between hydrogen evolution, where proton reduction occurs, and oxygen evolution, where water oxidation occurs.

6.1.1 The Electrochemical Cell

The overall electrochemical reaction taking place in a electrochemical cell is made up of two independent half-reactions occurring at the working and counter electrodes. Each half-reaction will depend on the interfacial potential difference at the corresponding electrode-electrolyte interface as was discussed in chapter 3. The working and counter electrodes are separated with an electrolyte through which an ionic current transports charge. The electrodes are connected to an external potentiostat which is used to measure and apply the desired potential in the experiment. The electrode-electrolyte

interfaces of the two electrodes, the electrolyte separating them and the potentiostat form a closed electric circuit also known as the electrochemical cell. [10]

In cyclic voltammetry we are interested in the electrochemical reactions taking place at the working electrode. A potentiostat measures the current through the working electrode as a function of the applied potential. The potentiostat drives the current of the counter electrode so that it passes the same current as that flowing through the working electrode. In other words, at the counter electrode, a reaction opposite to that at the working electrode is produced in order to balance the overall redox reaction. In a two-electrode setup, the counter electrode also serves to measure the potential of the working electrode. Usually, a three-electrode setup, in which a reference electrode is used to measure the working electrode's potential, is more common as will be discussed further in section 6.1.4. [40]

6.1.2 Faradaic and Non-faradaic Processes

The two types of processes that occur at the electrode are faradaic and non-faradaic processes. Faradaic processes involve the transfer of electrons across the electrode-solution interface and arise from the reduction and oxidation reactions of the chemical species. Non-faradaic processes do not involve transfer of electrons and stem from changes in the structure of the electrode-solution interface. These changes can be caused by adsorption and desorption of molecules and ions on the electrode surface and/or the charging of the electrical double layer (EDL). Over limited potential ranges no charge transfer occurs because it is thermodynamically or kinetically unfavorable. Thus, in this range charge will build up, carried by a charging current, and this leads to the electrode-solution interface behaving as a capacitor. [10] Non-faradaic currents can also be caused by electrochemical reactions of solution impurities (for example metal ions, oxygen and organic species) on the electrode surface, but it is usually quite small in clean systems [10].

At very low concentrations of electroactive species, the charging current can exceed the faradaic current. Furthermore, the capacitances will lower the potential between the electrode and solution experienced by the electroactive species. Hence the non-faradaic processes must often be taken into account when measuring the faradaic processes of interest. [10] Non-faradaic currents are often also called background currents.

6.1.3 Double-layer Capacitance and Charging Current

As it was explained in the previous section, the electric double layer can be characterized by a double layer capacitance C_d. The charge on the metal electrode is composed of an excess or deficiency of electrons, while the charge in the solution is made of an excess of cations or anions in the vicinity of the electrode. The double layer capacitance is a function of potential and applies only at a certain potential. If the potential changes during the experiment, approximate results can be obtained using an average C_d over the potential range.[10]

The magnitude of the charging current depends on the resistance of the electrochemical cell. The cell resistance can be approximated by an electrical circuit with a resistorR_S,

representing the solution resistance and a capacitor C_d, representing the double layer capacitance. Hence we have an RC-circuit.[10]

The double layer capacitance can be expressed as

$$C_d = \frac{q}{E_C}, \quad (6.3)$$

where q is the charge and E_C the voltage across the capacitor (double layer).

The potential across a resistor (solution resistance) is obtained from Ohm's law

$$E_R = iR_S \quad (6.4)$$

The sum of the voltage across the resistor, E_R, and the capacitor, E_d, must be equal to the applied voltage of the circuit, thus from the previous equations:

$$E = E_R + E_C = iR_S + \frac{q}{C_d} \quad (6.5)$$

In cyclic voltammetry, the potential is increased linearly with time at a scan rate v. Assuming the initial potential to be 0, the applied potential E is

$$E = vt = iR_S + \frac{q}{C_d}. \quad (6.6)$$

If we assume that $q = 0$ at $t = 0$ and noting that $i = dq/dt$, we obtain the current

$$i = vC_d\,(1 - \exp\left(-\frac{t}{R_S C_d}\right). \quad (6.7)$$

The current rises from zero as the scan rate increases to reach a steady-state value of vC_d in the anodic region and then decreases to reach $-vC_d$ in the cathodic region (Fig. 11) The time required for the current to rise to vC_d depends on the electrode time constant $R_u C_d$, where R_u is the uncompensated resistance (see the following section).[10]

In a potential step experiment the charging current decays exponentially with the cell time constant $R_u C_d$. For a period of approximately 5 time constants, the charging current contributes greatly to the total measured current and may obscure the faradaic current [10]. However, in cyclic voltammetry experiments, the potential is continuously changing and a charging current always flows as equation (6.7) demonstrates. This implies that the peak current i_p of a redox reaction must always be measured from the baseline of charging current. The peak current i_p is proportional to $v^{1/2}$ whereas the

charging current i_c is proportional to v and thus i_c becomes relatively more important at faster scan rates. This results in the peak currents being covered by the non-faradaic background current and appearing relatively lower. [10] To monitor the smaller faradaic currents, it is often necessary to eliminate the capacitive contribution by background subtraction [2, 3].

6.1.4 IR-drop

We saw in the previous section, that the solution resistance R_S causes an ohmic drop iR_S in the potential applied to the electrochemical cell. The applied potential is required to support the electrochemical reaction corresponding to the current. Part of this potential is used to encompass the solution resistance. The ohmic drop is not a form of overpotential, because it is not involved in the electrode reactions and is rather regarded as a characteristic of the bulk solution. In fact, the resistivity depends on the type of solution. For example non-aqueous solvents are typically highly resistive.

The contribution of the ohmic drop to the measured potential can be minimized by cell design and good instrumentation. From Ohm's law (equation (6.4)) we can deduce that the current i and the resistance R_S should be reduced. This can be achieved by using small electrodes that only permit the passage of small currents in the order of nano-amperes. The use of a supporting electrolyte also decreases the solution resistance, because of a high concentration of ions that carry the current in the bulk solution as was discussed in section 5.1. In both cases iR_S is lowered and it remains acceptably small. [10, 40]

Two-electrode cells are usually used with microelectrodes, because they pass very low currents, and thus the ohmic drop is negligibly small. In addition, low currents do not alter the solution-electrode interface as much as high currents and the counter electrode's potential is unchanged. [40] If the ohmic drop is large, three-electrode cells are preferable. In this setup, the current flows between the working electrode and a counter electrode chosen so that its redox products do not interfere at the working electrode. Since no current flows into the reference electrode, its potential remains stable and the potential between the reference and working electrode is not disrupted. [10]

Even in the three-electrode setup, the ohmic drop cannot be totally neglected. A small fraction of iR_S, namely iR_u, where R_u is the uncompensated resistance, appears in the measured potential if the reference electrode is not placed exactly at the working electrode surface as depicted in Figure 19. The reference electrode cannot be placed closer than two times its diameter to the working electrode without causing appreciable shielding error. Shielding error arises, because part of the ionic current at the working electrode is blocked, which causes non-uniform current densities at the electrode surface. R_u also includes any resistances in the working electrode, such as in the wires used to make it. [10]

Since the error caused by the uncompensated resistance cannot be totally eliminated, the measured potential is $E + iR_u$ rather than the true potential of the working electrode. In cyclic voltammetry, when the current peaks are measured, if i_pR_u is considerable compared to the accuracy of the measurement, the sweep will not be linear and the potential given by $E = vt$ does not hold. Moreover, the uncompensated resistance flattens the wave that results from faradaic currents and shifts the oxidation and reduction peak potential E_p in a voltammogram. Because the peak current is proportional to $v^{1/2}$, the larger the scan rate, the more the E_p will be shifted. Large R_u causes the peak potential to be a function of scan rate. It moves in a positive direction with increasing v for oxidation and in a negative direction for reduction. With microelectrodes, the effect of R_u does not perturb the measured potential nor distort the voltammogram as much as for larger. Nonetheless, even with microelectrodes, the effects of uncompensated resistance cannot be totally neglected. [10]

Modern instrumentation usually includes circuitry for electronic compensation of the uncompensated resistance.

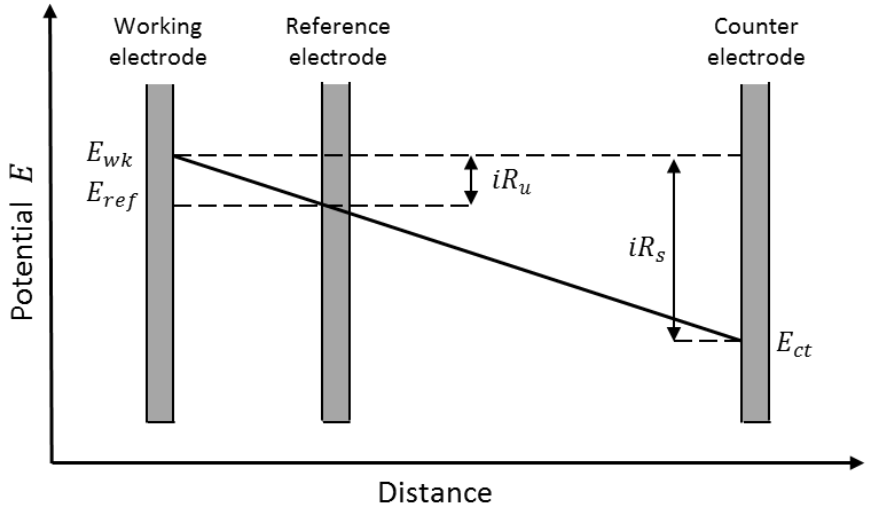

Figure 19. Potential drops between the working, reference and counter electrodes caused by the solution resistance.

6.1.5 Microelectrodes

Microelectrodes or sometimes ultramicroelectrodes (UMEs) are generally defined as electrodes with dimensions smaller than the scale of the diffusion layer developed during experiments, although a precise definition has not been established. For instance Bard defines UMEs as electrodes having a critical dimension (such as the radius of a disk electrode) smaller than 25 μm [10]. Microelectrodess have several advantages over conventional electrodes (typically on the scale of millimeters or centimeters) attributed to their small size. Microelectrodes have improved signal-to-noise ratios, because

Faraday currents are substantially increased by higher rates of mass-transfer. Their response times are much faster because of small charging currents and time-constants. Additionally, the IR-drop is of less concern because the total currents are much smaller with microelectrodes than those of large-scale electrodes. [2, 10, 40]

6.1.6 Peak Current Ratio and Peak Potential Separation

In a reversible reaction, if the product is chemically stable and does not undergo homogeneous reactions, the peak current ratio i_{pa}/i_{pc} is equal to 1 regardless of scan rate, switching potential and diffusion coefficients. Any deviation of i_{pa}/i_{pc} from unity points to homogeneous kinetic or other complications in the electrode process, because ideally all the reactants that were oxidized during the forward scan would be reduced back to the reactants in the reverse scan. Hence the oxidation and reduction currents would be equal in both scan directions. [10, 40]

Since the peak currents are superimposed on the charging current, they must be measured from the baseline (see Figure 18) If the baseline cannot be determined from the voltammogram or interpolated, Nicholson has proposed an alternative way of calculating the peak current ratio:

$$\frac{i_{pa}}{i_{pc}} = \frac{(i_{pa})_0}{i_{pc}} + \frac{0{,}485(i_{pc})_0}{i_{pc}} + 0{,}086 \qquad (6.8)$$

where $(i_{pa})_0$ is the current corresponding to E_λ and $(i_{pc})_0$ is the cathodic peak current measured from the zero current baseline. The measurement of peak current is generally not accurate, because the charging current is difficult to define precisely. Especially for the reverse peak, the baseline to use as a reference for measurement is often imprecise. Therefore, cyclic voltammetry is not an ideal method for quantitative analysis of the electrochemical system, because properties such as the concentration of electroactive species or the rate constant of a coupled homogeneous reaction are obtained from peak heights. The strength of cyclic voltammetry lies in qualitative evaluation of the system whereas other methods are often better suited for the precise assessment of parameters. [10]

The separation of the peak potentials E_{pa} and E_{pc} gives information on the reversibility of the electrode reaction. Although the separation of peak potentials, ΔE_p, varies slightly as a function of E_λ, for reversible reaction it is $2{,}3RT/nF$ or $59/n$ mV at 25°C according to the Nernst equation (n is the number of electrons consumed in the reaction). For repeated cycling the cathodic peak current decreases and the anodic one increases until steady-state values are attained. [10, 40]

7. Carbon Electrodes in Electrochemistry

Carbon materials are widely used in analytical electrochemistry, because of their electrocatalytic activity towards a variety of redox reactions, wide potential window, relatively inert chemistry and low cost. Often the electrochemical properties of carbon are better than those of noble metals for the oxidation and reduction of organic and biological molecules. In recent years many new carbon materials such as boron-doped diamond (BDD), carbon nanotubes (CNT), graphene and microfabricated carbon structures have emerged offering distinct properties compared to the commonly used graphitic electrodes and allowing new applications in sensing and electrocatalysis. [14]

In a recent review on the latest trends in the electrochemical sensing of dopamine, Jackowska and Krysinski focused on some of the new materials that have been used for electrode modification in the past few years. [2] These materials included graphene, BDD, ionic liquids and nanoparticles. Many electrodes modified with nanoparticles contain glassy carbon or carbon paste as a substrate and some are modified with either single-walled or multi-walled carbon nanotubes. For in vivo measurements carbon fiber is still the most popular material although boron-doped diamond is emerging as a potential material for in-vivo detection of dopamine. [2]

7.1 Electochemical Properties of Carbon Materials

7.1.1 Electronic Properties of Carbon Materials

The density of electronic states (DOS) is a factor that contributes greatly to the electronic properties of electrode materials. Electron transfer between the electrode and a chemical species in solution or adsorbed on the electrode surface is fastest when the energy of the electron is equal in both phases. A high DOS increases the probability that an electron of the appropriate energy is available for electron transfer and will affect the heterogeneous electron transfer rate of that electrode material. A low DOS results in gap regions near the Fermi level lowering the probability of electron transfer between the electrode and the thermally activated species in solution. [14]

The high conductivity of metals is a result of a high DOS, because a large number of atomic orbitals overlap to form a band with a high density of electronic states. By contrast, the DOS of carbon materials varies greatly. The DOS of graphene sheets is low at the Fermi level, which explains partially the lower conductivity of graphite materials compared with metals. The low DOS of graphite also affects its electrochemical reactivity. On the other end, undoped diamond has a low electrical conductivity because it has no electronic states within its band gap, which covers most of the electrochemical potential scale. Termination, disorder and defects in the lattice, for example by introduction of dopants, creates a range of energy states in the gap region that increase conductivity and electron transfer reactivity as in the case of BDD electrodes. [14]

7.1.2 Surface Structure of Carbon Electrode Materials

Since electrochemistry is based on interfacial phenomena, the nature of the electrode surface is of uttermost importance. The surface chemistry of carbon materials is much more complex than that of metals, because carbon forms a wider range of surface bonds and functional groups. Surface termination is therefore an important factor in regard to electrode properties. [14]

The basal plane is relatively unreactive although it may contain defects such as step edges and grain boundaries. The edge plane, on the contrary, contains unsatisfied valences that are reactive and easily form bonds with oxygen and water to form various oxygen-containing functional groups. The electron transfer rate is much faster at the edge plane than at the basal plane [41]. Polishing is one of the most common procedures for preparing carbon electrodes, but it results in a quite complex surface because of reactions with air and water. Even though surface oxides are often unavoidable unless special pre-treatments are used, functional groups can also be used to one's advantage. For example BDD and GC electrodes terminated with hydrogen are more stable and react slowly with oxygen. Negative surface charges from carboxyl functional groups can have significant effects on adsorption and electron transfer rates. [14]

7.1.3 Adsorption

Adsorption depends strongly on the type of carbon, its surface chemistry and the structure of the adsorbate. The interactions between the carbon surface and the adsorbate that govern adsorption include dipole-dipole interactions, induced dipoles, hydrophobic and electrostatic effects and covalent bonding. These interactions will be affected by the carbon allotrope, its preparation, the exposure of basal and edge planes, and surface oxides. [14]

Adsorption can be an advantage or a disadvantage depending on the application of the carbon electrode. Carbon electrodes are often subject to adsorption of impurities during electrode preparation, which can affect electron transfer rates and catalytic activity of the electrodes. Several activation procedures for carbon electrodes such as polishing, heat treatments, solvent treatment, laser activation and ultrasonication among others improve electrochemical performance in part by removing adsorbed impurities from the electrode surface. [14]

7.2 Graphite

The most common carbon electrodes are based on graphite. There exists a variety of graphitic materials with different structural and electronic properties, for example graphene, highly-oriented pyrolytic graphite (HOPG), carbon fiber, glassy carbon (GC) and amorphous carbon including diamond-like carbon (DLC). [14]

The simplest graphitic material is a two-dimensional graphene sheet composed of carbon atoms arranged in a hexagonal configuration. Graphitic materials are composed of one or several graphene sheets stacked in parallel and kept together by van der Waals forces [17]. The carbon atoms in graphite are all sp^2 hybridized. [14, 42]

Graphitic materials are often characterized by the size of the crystallites. L_a describes the crystallite size in the in-plane axis or the basal plane whereas L_c is the plane perpendicular to the graphene plane, the edge plane. The edge plane is irregular and contains various sites, like armchair or zig-zag sites and various oxygen-containing functional groups. The basal and edge plane differ greatly in electrochemical reactivity and underlie the electrochemical behavior of the electrode. [14]

Despite the very different properties of graphitic materials, the crystallite size, long-range order and anisotropy are critical factors in determining their electrochemical activity. [14]

7.2.1 Graphene

Due to its unique structure described above, graphene has many intriguing properties including a very large surface area (2630 m^2/g), a tunable band gap, high mechanical strength, high elasticity and thermal conductivity. It is a very promising material for electrochemistry due to its very large electrical conductivity, large surface area and low cost. Comparing to CNTs, its apparent advantages are that it does not contain metallic impurities, it is inexpensive and its production is accessible. The metallic impurities of CNTs, introduced by the fabrication process, can dominate the electrochemical response of CNT electrodes. [42]

Graphene monolayers can be prepared with a high yield (90%) but they tend to stack to form multi-layered structures [42, 43]. Most methods of synthesis produce multi-layered graphene also known as stacked graphene platelets (GNPs) [42].

The good electrochemical properties of graphene are a result of the fast heterogeneous electron transfer of the edge plane whereas the basal plane is inert electrochemically [42]. According to Ambrosi and Pumera, the heterogeneous rate constant of graphitic materials and carbon nanotubes is similar, because CNTs contain nanographite impurities that impart its good electrochemical properties. Comparing to pure CNTS, graphitic materials have a higher heterogeneous transfer rate. [42, 44]

Graphene electrodes have also been used for the detection of dopamine. Kim et al. reported that they observed peak separation of DA and AA with cyclic voltammetry in mixture of 100 μM DA and 1 mM AA at a graphene modified electrode [45]. Shang et al. demonstrated selective electrocatalytic activity of an electrode with a multi-layer graphene nanoflake film towards the oxidation of DA, AA and UA in a mixture of 50 mM PBS with 0,1 mM DA, 1 mM AA and 0,1 mM UA using CV. Distinct oxidation peaks could be obtained for all three of these biomolecules. [46]

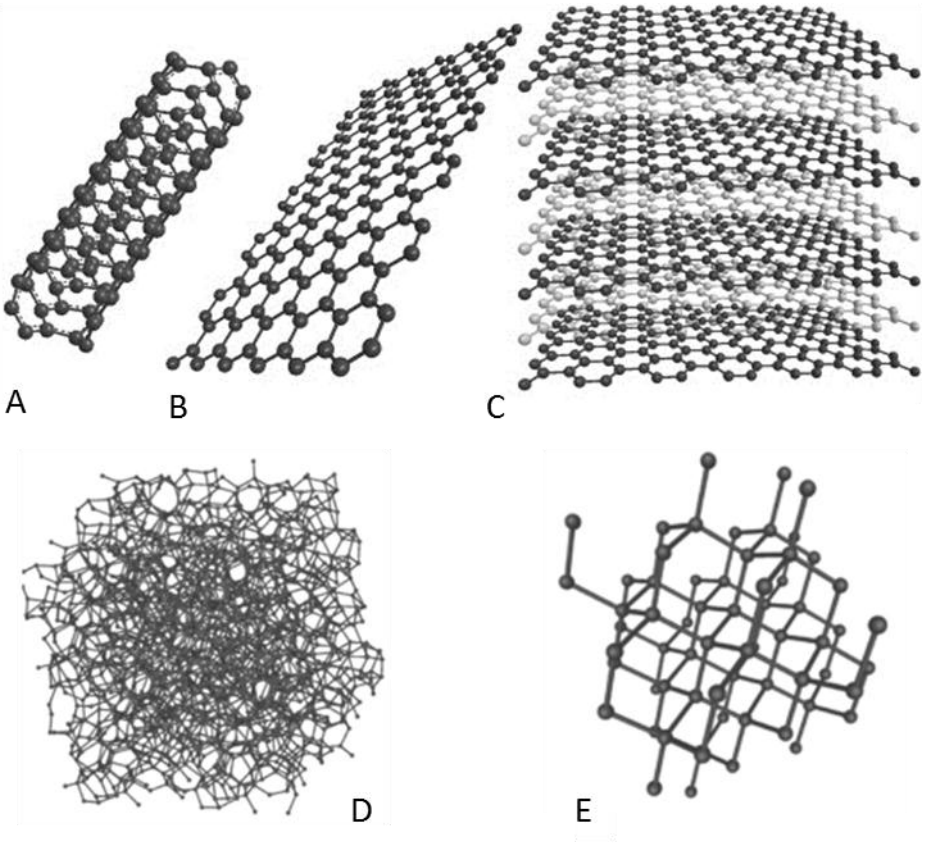

Figure 20. Different carbon allotropes: CNT (A), graphene (B), graphite (C), amorphous carbon (D) and diamond (E).

7.2.2 Carbon Fiber

Carbon fiber electrodes have been used extensively in electrochemistry since the 1980s. Many of their applications have been biological, because of their small size (generally the diameters are in the range of 5-50 μm) and their activity toward a variety of biochemically important molecules such as neurotransmitters and nucleotides. [11, 14, 47]

Three general types of carbon fiber can be distinguished depending on their order and crystallite size. Radial carbon fibers have graphene planes radiating from the center of the fiber, onion fibers are composed of concentric cylinders of graphene planes in the same manner as CNTs and random fibers have a random orientation of graphene sheets. However, no particular type of carbon fiber is used in electrochemical applications. The edge/basal ratio on the exposed surface of carbon fibers determines adsorption and electrocatalytic activity as in the case of glassy carbon. To enhance selectivity and reactivity, carbon fibers can be subject to several types of surface modification such as Pt or CNT deposition, Nafion or polypyrrole coatings or electrooxidation. [2, 14]

Carbon fiber electrodes have been used in analytical applications for example in in vivo monitoring of neurotransmitters in living animals and to examine transmitter release and

uptake by single cells and nucleotides [3, 14]. Carbon fiber microelectrode have been shown to be relatively unsusceptible to fouling by products of DA oxidation [2].

7.2.3 Glassy Carbon

The crystallites in glassy carbon (GC) are small, in the range of 3-7 nm, because the C-C bonds do not break in the fabrication process and the graphitic planes do not form parallel graphene sheets i.e. do not graphitize. The microstructure is disordered and not known in detail, because the characterization is difficult due to the randomness of the structure. [14]

Traditionally, GC has been widely used as a working electrode material, because of its relatively wide potential window in comparison with noble metal electrodes such as Pt and Au. The electronic and electrochemical properties depend on several factors including surface preparation, microstructure and presence of oxygen-containing functional groups. [48] The edge/basal ratio on the exposed surface of carbon fibers determines adsorption and electrocatalytic activity of GC [14].

The surface of GC electrodes can become deactivated when it is exposed to laboratory atmosphere or working solutions and the problem becomes more acute when biological solutions are used. Several investigations on the surface activation of GC electrodes have been carried out. [48]

7.2.4 Diamond-like Carbon

Diamond-like carbon (DLC) is a variant of amorphous carbon. Amorphous carbons are disordered materials with a combination of sp^2 and sp^3 hybridized carbon atoms and often small amounts of hydrogen. There is no long-range order in the arrangement of carbon bonds but a short-range still occurs. [14, 15] Different forms of amorphous carbon can be grouped into graphite-like carbon with prevailing sp^2 hybridization or diamond-like carbon with a high fraction of sp^3 hybridization [19]. Accordingly, DLC is sometimes called amorphous carbon (a-C) or amorphous hydrogenated carbon (a-C:H) if it is more graphite-like in its structure and properties, and tetrahedral amorphous carbon (ta-C) if it is more diamond-like [15, 17, 18].

The ratio of sp^2 and sp^3 bonding and amount of hydrogen vary considerably with preparation conditions [14, 15, 17]. Thin films of hydrogen-free DLC with a very high amount of sp^3 bonds can be prepared by filtered cathodic vacuum arc, pulsed laser deposition or mass-selected ion beam deposition. Alternatively, hydrogenated amorphous carbon with a sp^2 configuration is usually made by plasma enhanced chemical vapor deposition (PECVD) or reactive sputtering. An advantage in the synthesis of DLC comparing to diamond is that it can be deposited at low temperatures (25-100 °C), allowing the use of a wider variety of substrates. [15, 18, 49] Yet, the deposition on metal substrate needs to be developed [50]. To avoid delamination caused by internal stress, ta-C films need to thin (hundreds of nanometers) [49].

DLC has some unique properties such as very low surface roughness, high mechanical hardness and high elastic modulus. It is chemically inert, has good corrosion resistance

and shows a wide potential range. DLC films have been shown to enhance biocompatibility and reduce biofouling [16]. The semiconductor electrical properties of DLC result from its large band gap (approximately 1 to 4 eV). [15, 19] The high electrical resistivity of DLC films can be decreased by doping with boron [51], nickel[52, 53], nitrogen [54] or platinum [55]. Doped DLC electrodes have been reported to have low background currents and a wide potential range, comparable or superior to that of BDD. [15, 19, 51, 54]

DLC is a relatively new research area in electrochemistry and its applications are still few. DLC has been used amongst other things in glucose amperometric biosensors[52, 53], glucose oxidase biosensors [52], as nitrogenated DLC films in metal tracing analysis [56] and in commercial ELISA kits for diagnosis of viruses such as HIV [57]. A few studies on DA detection with amorphous carbon have been published [49, 51]. Naragino et al. examined the behavior of B-doped DLC, N-doped DLC and BDD electrodes in 20 µM DA in 0.1 M $HClO_4$ at a scan rate of 10 mV/s. The doped DLC electrodes showed a similar value (427-440 mV) for the peak separation ΔE_p that was lower than that of BDD (656 mV). The authors attributed the faster kinetics on the DLC electrodes to oxygen containing surface functional groups that bonded to sp^2 hybridized carbon atoms. These functional groups are not found on the BDD surface. [51]

7.3 Diamond

The tetrahedrally bonded carbon atoms are completely sp^3 hybridized and result in the hardness and low electrical conductivity of diamond. Introduction of impurities, for example boron or hydrogen, in the diamond lattice increases its conductivity sufficiently to allow its use as an electrode. The most common diamond electrode is the microcrystalline boron-doped diamond (BDD) electrode. [14]

The BDD electrode is p-doped and has usually a high level of doping in the range of 10^{18}-10^{20} atoms/cm^3. BDD is microcrystalline with randomly oriented crystallites a few micrometers in size. [14]

Nanocrystalline diamond has randomly oriented crystallites with dimensions of a few tens of nanometers. Nitrogen and boron are used to dope nanocrystalline diamond negatively or positively, respectively. The surface has significant π-bonding and sp^2 hybridization compared to microcrystalline diamond, which results in higher electrical conductivity. [14]

In comparison to graphitic materials, BDD and nanocrystalline diamond are much more inert and have a wider potential window and lower capacitive current in electrochemical applications. This allows the study of electrochemical reactions occurring at high overpotentials. [14] In addition, diamond electrodes have been found to show high resistance to deactivation by fouling, which is attributed to hydrogen termination of the surface making it hydrophobic and inert [48]. It has been suggested that extensive

anodic polarization before in-vivo use of BDD electrodes improved their selectivity for DA, most probably because of the formation of carboxyl or hydroxyl groups on the surface. [2]

A disadvantage of diamond is the high temperature (600-800 °C) required for deposition, which limits the choice of substrates. [49]

7.4 Carbon Nanotubes (CNTs)

The walls of the carbon nanotube (CNT) consist of rolled graphene sheets with hexagonally arranged carbon atoms like in basal plane graphite. The tube ends are terminated with a fullerene structure incorporating pentagons or functional groups similarly to edge plane graphite. Carbon nanotubes are divided into two categories: single-walled carbon nanotubes (SWNTs) which consist of a single graphene sheet rolled into a tube and multi-walled carbon nanotubes (MWNTs) which contain several concentric tubes with a common axis. CNT electrodes are usually bundles of nanotubes of different sizes. [14]

CNTs hold promise for many new applications because of their unique properties such as high aspect ratio, conductivity, thermal stability, flexibility, mechanical strength and reactivity. Individual nanotubes have metallic or semiconducting electronic properties depending on the number of carbon hexagons around the circumference of the tube. Most electrochemical applications using nanotubes involve large numbers of tubes with different diameters and DOS distribution, so the effective DOS will be broadened by the combination of many different DOS profiles. [14]

Defects and oxides on CNTs have important effects on their electrochemical behavior. Defects can occur in the basal plane, and the unterminated tube ends are prone to form oxygen-containing functional groups. It is uncertain in some cases whether the behavior of CNTs is determined by special properties of the tubes themselves, a variable level of oxides and defects or metal catalysts that were not completely removed after synthesis. However, there is little doubt that defects play an important role in the electrochemical behavior of CNT electrodes, because edge-plane like sites are exposed. The reactivity of a single nanotube or a bundle of tubes depends strongly on the defect density and edge/basal ratio. [14] Banks et al. have shown that the edge-plane like sites are responsible for the electrocatalytic properties of CNTs. In addition, they suggest that it is the combination of edge-plane like sites and the special morphology and small size of CNTs that lead to their special applications. [41] CNTs may also be doped with nitrogen to produce defects. [14]

CNTs are very attractive for use in different biosensors such as amperometric enzyme electrodes, immunosensors and DNA sensing devices. [15] To enhance their performance and expand their applications, various chemical and physical modifications have been used to modify the CNT walls. Various hybrid composites based on CNTs

with organic and inorganic materials such as metal nanoparticles, metal oxides and semiconductor nanoparticles have been reported for electrochemical applications. [58] There have been reports of high electrocatalytic activity of CNTs toward the oxidation of catecholamines [59, 60] and SWNT films on GC modified with ferrocene have exhibited selective oxidation of DA in the presence of AA and UA [59].

8. Experimental

In the experimental part of this work, measurements in sulphuric acid, phosphate-buffered saline and dopamine solutions were carried out with DLC/Pt composite electrodes using cyclic voltammetry to assess their electrochemical response. SEM images were taken of the surface of some electrodes to detect possible surface defects resulting from the fabrication process and delamination that could have occurred during the cyclic voltammetry experiments.

Table 3 shows the six different types of DLC/Pt electrodes that were prepared. All the DLC electrodes (except control group) used a platinum wire as the substrate material, which was coated with a 30 nm thick titanium layer to enhance adhesion of the DLC coatings. Electrodes of group 1 were coated with a 30 nm thick DLC coating whereas electrodes in groups 2 with a 7.5 nm thick DLC coating. Additionally roughly half of the electrodes in each group underwent vacuum annealing in order to form oxides on the carbon surface. As discussed in section 7.1, surface oxides affect the electrochemical performance of electrodes and play an important role in the adsorption of chemical species. Additionally, a 30 nm Ti and DLC coating on silicon wafer and an uncoated Pt wire were used as control group electrodes. The control group was used to examine the function of platinum and DLC separately on the electrode response of groups 1 and 2.

Table 3: Specifications and grouping of the different electrodes used in the experimental part of this work.

Group 1 Pt + 30 nm Ti + 30 nm DLC		Group 2 Pt + 30 nm Ti + 7.5 nm DLC		Control electrodes
No annealing	Annealing	No annealing	Annealing	
1-1	1-1V	4-3	4-2V	Si+DLC (Si + 30 nm Ti + 30 nm DLC)
1-2	1-2V	4-5	4-5V	
1-4	1-3V	4-6	4-6V	
1-5	1-4V	4-7	4-7V	Pt (uncoated Pt wire)
1-6	1-5V	4-8		
	1-6V			

The single electrodes are denominated so that the first number stands for a group and the second number for a specific electrode. The letter V is assigned to electrodes that were vacuum annealed. The numbering of single electrodes is not continuous, because some electrodes were broken during the fabrication process. Also group 2 electrodes are marked with the number 4 instead of 2, because some additional groups of electrodes have been used in the course of this work, but their results are not reported here.

The electrochemical properties of the vacuum annealed electrodes were nearly identical with those of the electrodes that didn't undergo annealing. Most likely the vacuum annealing didn't affect the adsorption of DA and thus the results inside groups 1 and 2 were so much alike regardless of vacuum annealing.

8.1 Coating and Electrode Fabrication

The electrodes were prepared by coating a thin titanium and diamond-like carbon layer on platinum-iridium wires (Goodfellow Cambridge Ltd., Huntingdon, England). The composition of the Pt-Ir wire was 90% Pt / 10% Ir with a diameter of 30 μm. The control sample was prepared by coating a 30 nm thick Ti and DLC layer on 1 x 2 cm piece of silicon wafer (Okmetic Oyj, Vantaa, Finland).

8.1.1 Pre-treatments

Before applying the titanium and DLC layers, the Pt-Ir wire was cleaned ultrasonically in an acetone bath for 10 min and immersed in 40% hydrofluoric acid (HF) to remove the native platinum oxide layer. The wire was then electrochemically etched in a solution composed of 100 mL of 38% hydrochloric acid (HCl) and 400 mL of DI-water saturated with sodium chloride (NaCl) for 5 min. The Pt-Ir wire was then connected as an anode to the positive terminal of a DC power supply. A pure platinum wire was connected to the negative terminal and served as the cathode. The applied potential was 6 V. The electrochemical etching evens out the surface roughness and longitudinal grooves on the Pt-Ir wire surface and removes impurities. [61]

After the pre-treatments, the wire was inserted in a glass capillary with 1-mm diameter (World Precision Instruments, Inc., Sarasota, USA) and pulled with a micropipette puller. The length of the wire was adjusted so that approximately 2 cm protrude from the tapered tip for the application of the coating.

The control sample made on silicon was pre-treated by immersion in HF before the coatings were applied. A contact was made on the uncoated side of the silicon piece by scratching grooves on the silicon surface oxide and fixing a conducting wire with silver paste. A plastic sample holder was used to constrain the measuring area to the coated side of the wafer piece.

8.1.2 DLC Coating

The titanium and DLC coatings were prepared by cathodic arc discharge method under the supervision of Professor Jari Koskinen from the Department of Materials Science and Engineering, Aalto University. The coatings were done at VTT.

The glass capillaries were protected with aluminum foil so that only the Pt wire protruded out from it for the duration of the coating. The foil also served as a good attachment point to hang the samples from the sample holder inside the vacuum chamber. After the vacuum was pumped (approximately $2x10^{-3}$ Pa) inside the chamber, the samples were sputtered with argon for 15 min to remove surface impurities. A pulsed mode with 2 Hz frequency was used. The 30 nm titanium coatings were sputtered for 35 s, the 30 nm DLC coatings for 6 min 30 s and the 7.5 nm DLC coatings for 1 min 45 s.

The thin films were characterized by X-ray reflectivity (XRR), Raman spectroscopy and transmission electron microscopy (TEM) to verify that they were in fact DLC. [61]

8.1.3 Vacuum Annealing

The coated Pt-Ir wires were covered with 3 aluminum foils and put inside the vacuum chamber. The vacuum was pumped for 2 days until it reached a pressure of 3.2×10^{8} Pa. Then, the temperature was raised to 600 °C (60 min) with a dwell time of 15 min and allowed to cool down for 1 day. During the heating the pressure was 1.2×10^{6} Pa.

8.1.4 Electrode fabrication

After the titanium and DLC coatings were applied, the capillary was filled with epoxy (EpoFix, Struers A/S, Ballerup, Denmark) and the wire was carefully pulled so that the protruding tip was roughly 2-mm long. A conducting wire was then inserted from the untapered end of the capillary. The insulation from the conducting wire was stripped for a length of about 2 cm in order to achieve a good electrical contact with the DLC-coated wire. The epoxy fixes the measuring wire and the conducting wire inside the capillary and strengthens the electrode shaft. Additionally, the epoxy seals the tip of the electrode and the capillary at the tapered end to prevent the solution from leaking inside the capillary during measurements. The solution increases the effective surface area of the electrode-solution interface and causes fluctuations in the background signal that can lead to increased noise [62].

After letting the epoxy dry for 24 h, the wires were soldered to enhance the electrical contact. A poor contact can be responsible for high impedance and noise or in the worst case electrode failure [62]. The junction was covered with heat-shrinkable tubing.

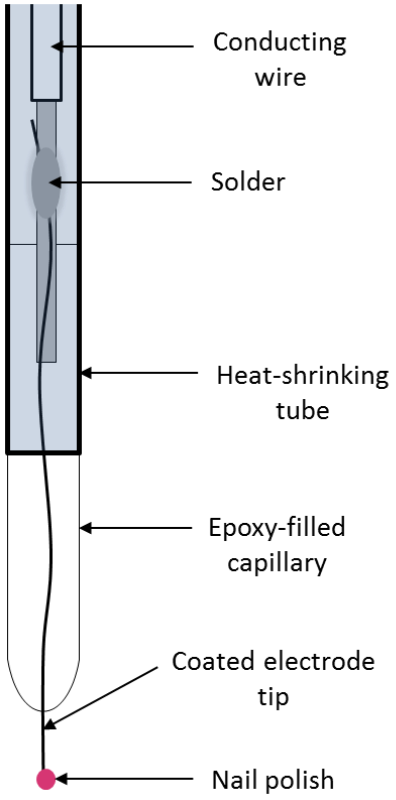

Figure 21. Structure of the electrode tip used in the CV measurements.

8.2 Cyclic Voltammetry

Cyclic voltammetry measurements were made with a potentiostat (QuadStat, eDAQ Pty Ltd, Denistone East, Australia) attached to a recording unit (e-corder 821, eDAQ) and computer. The Echem software (ADInstruments Pty ltd, Castle Hill, Australia) was used to enter the parameters of the experiment and control the potentiostat.

A three-electrode configuration, depicted in Figure 22, was used in a single compartment glass cell of approximately 15 mL. A titanium rod with 2.5 µm thick coating of platinum (ET078, eDAQ) served as the counter electrode and a commercial Ag/AgCl electrode (Sarissa Biomedical Ltd., Coventry, UK) was used as the reference. All measurements were made in a Faraday cage (VistaShield, Gamry Instruments, Warminster, USA) to avoid electrical interference.

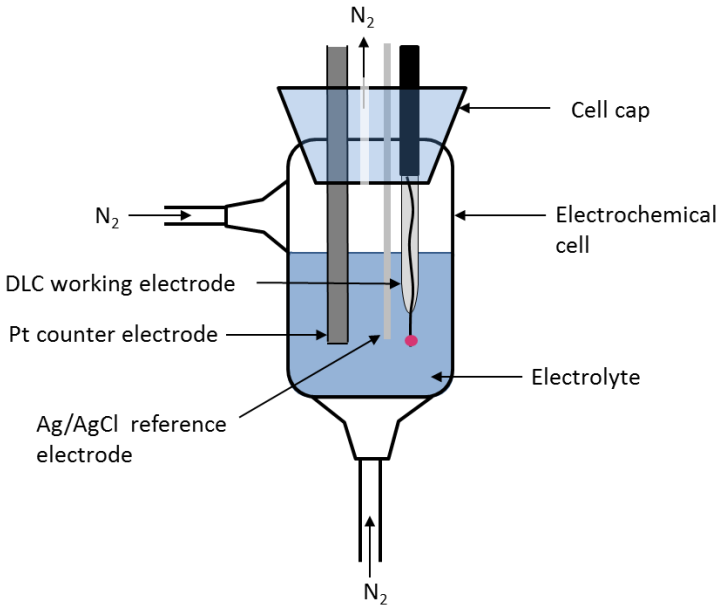

Figure 22. A three-electrode configuration and the electrochemical cell used in the CV measurements of this work.

The potential window was determined in 0.15 M sulphuric acid (Merck KGaA, Darmstadt, Germany) with pH 0.55 at a scan rate of 400 mV/s. During the first scans the appropriate parameters were chosen and the potential range was tested. Then the potential was cycled approximately 20 to 25 times until a steady-state CV was obtained. The capacitive currents were measured at -0.15 V vs Ag/AgCl in H_2SO_4 from steady-state CVs.

The dopamine solutions were always prepared on the day of the measurement, because it is easily oxidized in air. A 10 mM dopamine solution was prepared by dissolving 0.18964 g of dopamine hydrochloride (Sigma-Aldrich, St. Louis, USA) in 100 mL of phosphate-buffered saline (PBS Dulbecco, Biochrom AG, Berlin, Germany) that was diluted to obtain a series of dopamine solutions from a concentration of 1 mM to 1 nM.

The DA detection limit measurements were made starting with the lowest concentration of DA and the working electrode was dipped into PBS in-between measurements to rinse it. The initial potential was chosen as 0 V, since no redox reactions occurred at that potential. The scan rate was 400 mV/s. Three cycles were scanned at each DA concentration. The capacitive currents were measured at -0.3 V in PBS and DA solutions.

The effect of scan rate was studied for electrode 1-6, because its DA detection limit was the lowest in group 1. The CVs were scanned at 10, 50, 100, 200 and 400 mV/s. The solution was changed to a fresh one each time the scan rate was altered. The electrode was rinsed in PBS between each measurement. Only two scans were carried out at each concentration and scan rate. The anodic and cathodic currents to calculate the ratio i_{pa}/i_{pc} were obtained as depicted in Figure 18. Extrapolation to obtain the baseline for the cathodic current was done by hand on the plot in MATLAB.

All the solutions were deoxygenated with N_2 for 5 min prior to measurement and the air in the electrochemical cell was purged with N_2 during the measurements. All the measurements were conducted at room temperature. The tip of the electrodes was sealed with nail polish in order to avoid electron transfer from the uncoated part of the Pt wire.

The peak current values were calculated from the background-subtracted plots. The background-subtracted plots were obtained with the Echem software by setting the measurement in pure PBS as the background and subtracting the plots obtained in PBS + DA solutions from it. Data analysis was performed with MATLAB (MathWorks, Natick, USA). The average values of the electrode groups are presented with the standard deviation values.

8.3 SEM

The surfaces of the electrodes were examined by scanning electron microscopy (SEM, JSM-6330F, JEOL Ltd, Tokyo, Japan) to assess the effect of cyclic voltammetry on the DLC coating. Electrodes that were broken during fabrication and that did not pass any current in the electrochemical measurement were used as control. The SEM was operated in the secondary electron imaging mode.

The SEM samples were sputtered with chromium using a sputter coater (Emitech K575X, Quorum Technologies Ltd., Ashford, USA) to make them conductive for the analysis. Non-conductive samples tend to be charged by the electrons and a clear image cannot be formed.

10. Results

10.1 Cyclic Voltammetry

10.1.1 Platinum electrode in Sulphuric Acid

The voltammogram of the platinum electrode in sulphuric acid is presented in Figure 23. The potential window for the platinum electrode was 1.4 V and it extended from -0.5 V to +0.9 V vs Ag/AgCl. The peaks at -0.5 V and +0.9 V are caused by hydrogen evolution and oxygen evolution, respectively, and define the potential window. The capacitive current of Pt was 149.88 nA. The potential window and capacitive current values of all the electrodes used in the CV experiments are reported in Table 4.

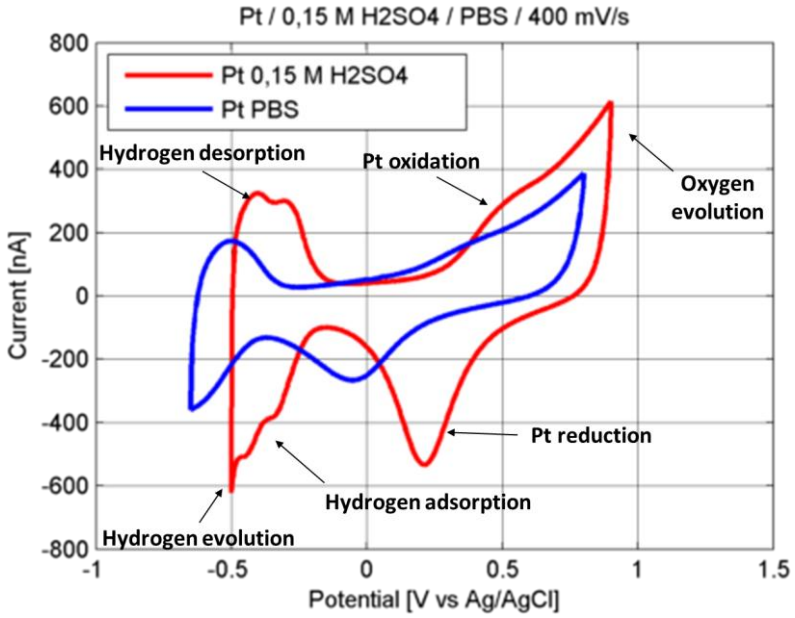

Figure 23. Cyclic voltammograms of the platinum electrode in 0.15 M H_2SO_4 (red) and in PBS (blue). Scan rate v was 400 mV/s and initial potential 0 V.

A shoulder with onset at +0.3 V and maximum value occurring at +0.5 V is assigned to platinum oxide formation and a reduction peak at +0.21 V to the corresponding platinum oxide reduction.

The reduction peaks at -0.34 V and -0.46 V are attributed to hydrogen adsorption, while the oxidation peaks at -0.43 V and -0.32 V to hydrogen desorption. These results are in agreement with literature [63, 64]. Hudak et al. reports that platinum has a conventional potential window of 1.5 V with limits at approximately -0.6 V and +0.9 V vs Ag/AgCl. The electrochemical phenomena and potential peak positions also correspond well to the results obtained by Hudak and Cogan. [64, 65]

Table 4: Potential window limits, range and capacitive current measured for Pt and the electrodes of groups 1 and 2 in H_2SO_4. The scan rate was 400 mV/s. Capacitive currents were measured at -0.15 V. The average values in bold are presented as average of the whole group ± standard deviation.

Electrode	Potential window in H_2SO_4 (mV)			Capacitive current in H_2SO_4 (nA)
	lower limit	upper limit	range	
Pt	**-500**	**900**	**1400**	**149.88**
1-1	-500	1000	1500	40,43
1-2	-550	1100	1650	27,66
1-4	-550	1100	1650	30,26
1-5	-550	1100	1650	23,04
1-6	-550	900	1450	36,34
Average	**-540 ± 20**	**1040 ± 80**	**1580 ± 87.2**	**32.0 ± 6.18**
4-3	-550	1100	1650	23,30
4-5	-500	600	1100	46,93
4-6	-500	600	1100	70,49
4-7	-550	900	1450	31,89
4-8	-500	650	1150	42,62
Average	**-520 ± 24.5**	**770 ± 199**	**1290 ± 222.3**	**43.05 ± 16.02**

10.1.2 Platinum electrode in PBS and DA Solutions

In PBS solution with varying dopamine concentration, the electrochemical characteristics of the platinum electrode, shown in Figure 24, were similar to those observed in H_2SO_4. The potential window was slightly wider though, from -0.65 V to +0.8 V vs Ag/AgCl.

The peak corresponding to Pt oxidation was found at +0.39 V in the form of a shoulder with onset at +0.2 V on the rising anodic current. This shoulder was clearly visible for DA concentrations up to 10 µM. At concentrations above 10 µM, the dopamine oxidation current dominates the response and the Pt oxidation current is completely covered. The Pt reduction peak is observed at -0.05 V at all concentrations

The peaks corresponding to hydrogen adsorption were not visible and only one peak was observed at -0.5 V for hydrogen desorption in comparison with the two peaks seen in H_2SO_4.

The minor shifts in potential peak positions observed for the same electrochemical phenomena in PBS and H_2SO_4 are most likely caused by the difference in pH (Figure 23). However, the changes were somewhat smaller than Hudak observed in his experiments. [65]

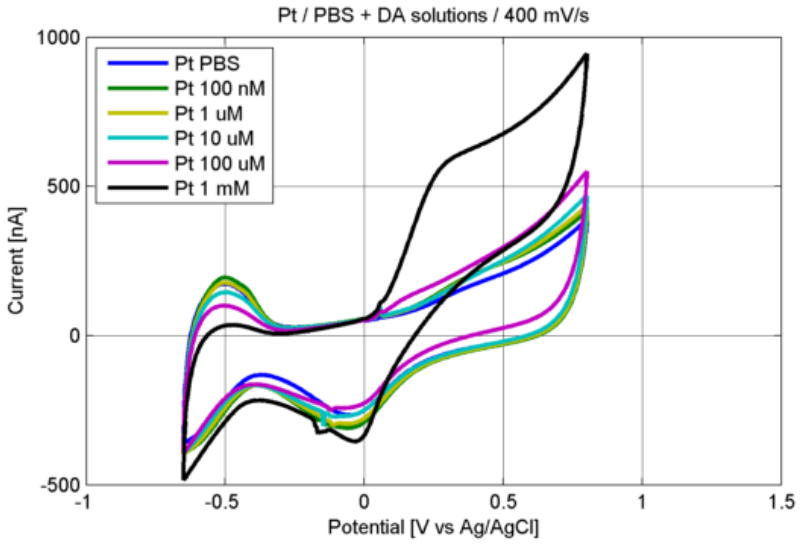

Figure 24. CVs of the Pt electrode in PBS at different concentrations of DA. v = 400 mV/s.

The DA detection limit is 100 µM with the platinum electrode. The dopamine oxidation peaks are at +0.18 V and 0.33 V at 100 µM and 1 mM concentrations, respectively. The DA reduction peak is observed only for 1 mM concentration at -0.02 V giving a peak separation ΔE_p of 0.35 V. This corresponds to slow heterogeneous electron transfer, since for reversible reactions ΔE_p = 59/n mV at room temperature, corresponding in the case of a two-electron transfer to approximately 0.03 V. The peak oxidation current of DA, $I_{p\ ox,}$ was 455.8 nA.

The peak current ratio i_{pa}/i_{pc} was 0.71. For a reversible reaction, deviation from unity means for example that there is a coupled homogeneous reaction and therefore all the DA that is oxidized in the anodic scan is not reduced in the cathodic scan. In this case, however, more oxidation product is reduced than was originally oxidized. This results most likely from the overlapping dopamine and Pt reduction peaks. The cathodic peak current has a large component resulting from the Pt reduction current summed on the DA reduction current. Thus i_{pa}/i_{pc} has a value less than unity. Additionally, the 1 mM oxidation peak was not very well-defined and the extrapolation to define a baseline for the cathodic peak current was difficult. This could have resulted in a considerable error in the peak current ratio.

ΔE_p, $I_{p\ ox}$ and i_{pa}/i_{pc} values of all the electrodes at a DA concentration of 1 mM in PBS are displayed in Table 5 for direct comparison of the data between the electrodes.

Table 5: Separation of DA oxidation and reduction peak potential ΔE_p, oxidation peak current $I_{p\ ox}$ and anodic and cathodic peak ratio i_{pa}/i_{pc} measured in PBS and 1 mM DA solution at a scan rate of 400 mV/s. The values in bold are the averages of the whole group ± standard deviation.

Electrode	ΔE_p (V)	$I_{p\ ox}$ (nA)	i_{pa}/i_{pc}
Pt	**0.35**	**455.8**	**0.71**
1-1	-	-	-
1-2	0.87	637.47	1.15
1-4	0.98	696.14	0.97
1-5	1.05	626.98	1.13
1-6	0.78	1026.68	1.02
Average	**0.92 ± 0.10**	**746.82 ± 163.71**	**1.07 ± 0.08**
4-3	0.68	365.91	0.95
4-5	0.54	750.88	0.84
4-6	0.51	623.84	0.86
4-7	0.48	800.35	0.96
4-8	0.47	520.19	-
Average	**0.54 ± 0.08**	**612.23 ± 157.41**	**0.90 ± 0.06**

10.1.3 Group 1 Electrodes in Sulphuric Acid

The cyclic voltammograms of the electrodes in group 1 are presented in Figure 25. The potential window of the electrodes ranged from -0.55 V up to +1.1 V and in average it spanned 1.58 V. The exact water windows for each electrode and platinum can be found in Table 4.

The redox reactions of platinum and hydrogen adsorption and desorption, which were observed in the Pt voltammograms, were clearly visible for electrodes 1-1, 1-2 and 1-6. Electrodes 1-4 and 1-5 exhibited the platinum reduction peak at +0.13 V but the other characteristics of the platinum CV were not observed.

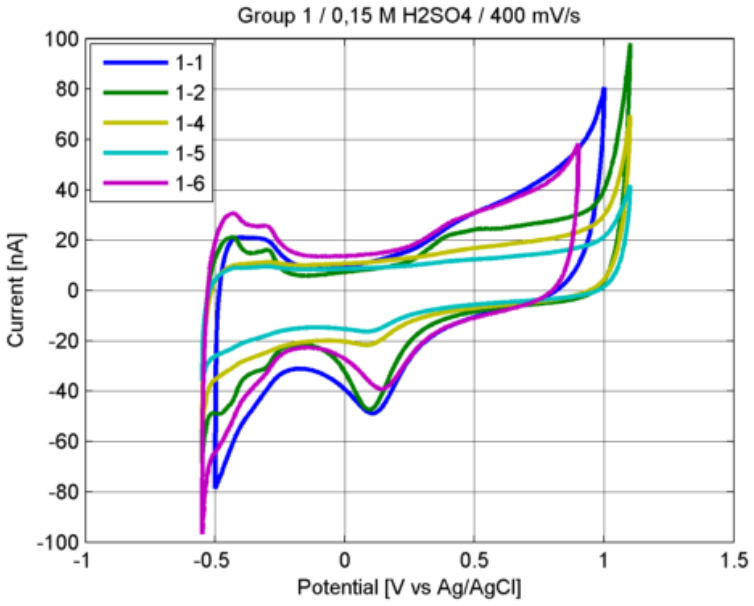

Figure 25. CVs of group 1 in 0.15 M H_2SO_4. Scan rate v was 400 mV/s.

The similarity with the platinum electrode response was accentuated as more scans were performed as can be seen in Figure 26, but this trend only occurred for the same electrodes (1-1, 1-2 an 1-6), for which the characteristics of the platinum CV were evident in the first scans. It is possible that the DLC layer was not homogeneous on these electrodes or that it was delaminated as more cycles were scanned.

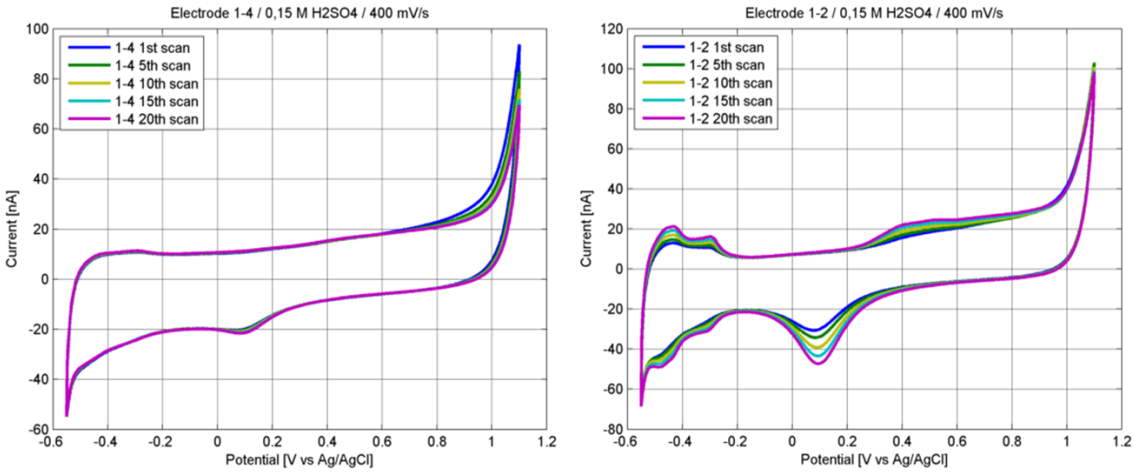

Figure 26. Effect of continuous scanning on electrodes 1-2 (right side) and 1-4 (left side) after 1, 5, 10, 15 and 20 scans. v = 400 mV/s.

In Figure 27 the CVs of group 1 are plotted against that of platinum. The capacitive currents of the DLC electrodes were on average 32.0 nA, while that of Pt was nearly five times larger, 149.88 nA (Table 4). The potential window was also wider for the group 1 electrodes and especially the oxygen evolution was shifted to higher potentials. These results clearly show that the 30 nm thick DLC coating made the electrodes considerably more inert than platinum in H_2SO_4.

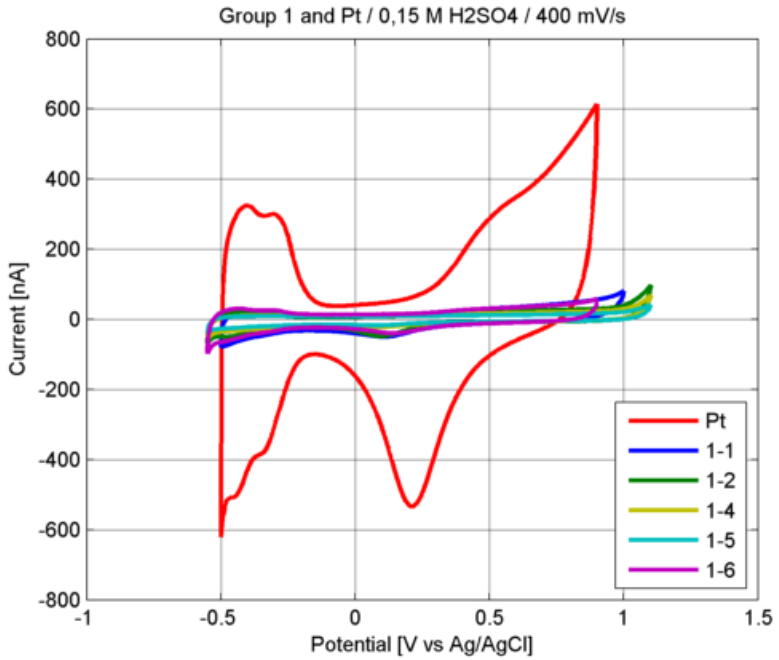

Figure 27. CVs of group 1 against that of Pt in 0.15 M H_2SO_4. v = 400 mV/s.

10.1.4 Group 1 in PBS and Dopamine Solutions

The cyclic voltammograms of the group 1 were very similar to each other in PBS (Figure 28). The potential windows were a little bit wider than in H_2SO_4. Contrary to what was observed in H_2SO_4, the peaks resulting from hydrogen adsorption and desorption were barely observable in PBS. Also, the Pt oxidation peak was not detected, while the corresponding reduction peak was still discernible at -0.12 V.

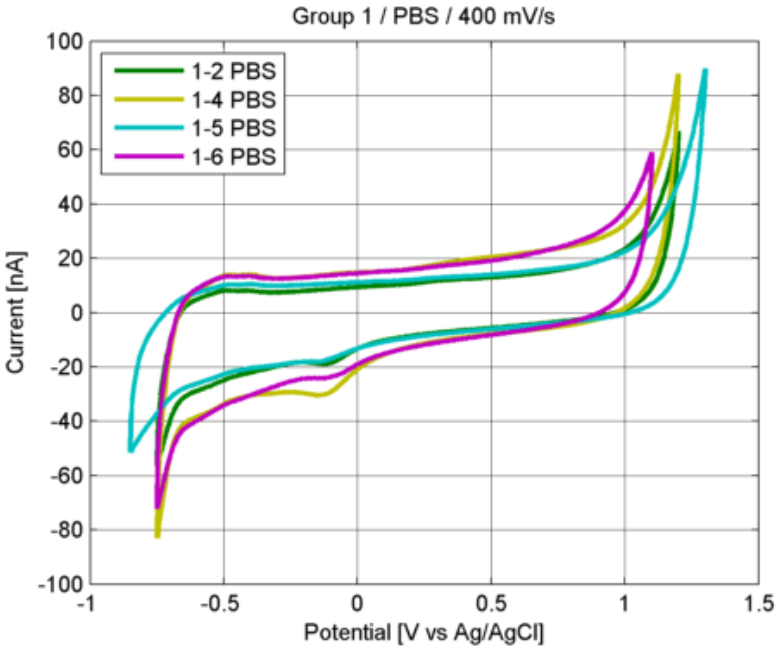

Figure 28. CVs of group 1 in PBS. v = 400 mV/s.

In Figure 29 the voltammograms of group 1 are compared to that of Pt in PBS. The electrodes of group 1 showed a lower capacitive current and wider potential window, as expected from the results in sulphuric acid.

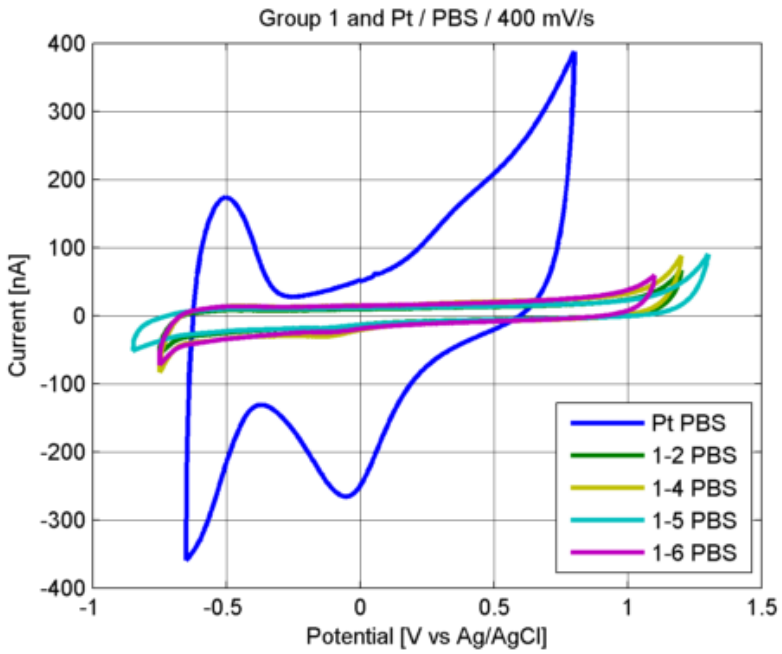

Figure 29. CVs of group 1 plotted against that of Pt in PBS. v = 400 mV/s.

In dopamine solution, all the electrodes showed an increase in the anodic current at a concentration of 10 µM as shown in Figure 30 for electrode 1-6. The voltammogram in 1 mM DA solution was omitted from Figure 30, because the current was so high that the properties of the voltammograms at lower concentrations were not distinguishable anymore. Clear dopamine oxidation and reduction peaks became visible only at 100 µM and above.

The DA oxidation and reduction potential difference ΔE_p, peak oxidation current $I_{p\,ox}$ and peak current ratio i_{pa}/i_{pc} values of each electrode are listed in Table 5. From the data, we see that ΔE_p is in average 0.92 V for group 1, which is nearly three times the value at the Pt electrode. This indicates that the heterogeneous electron transfer kinetics are far slower at the 30 nm thick DLC coating and that the redox reaction of DA is irreversible.

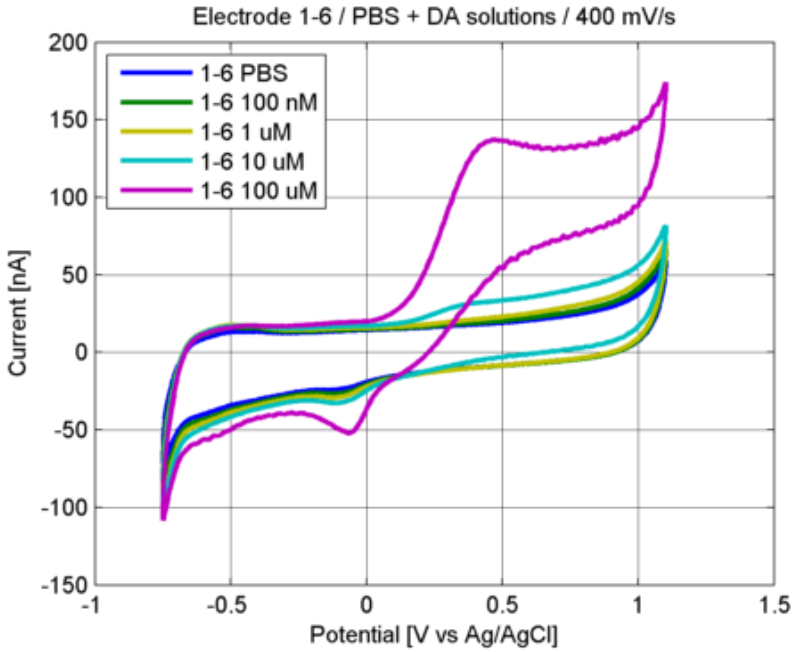

Figure 30. CV of electrode 1-6 in PBS and several concentrations of DA. v = 400 mV/s.

Also, we notice from Table 5 that the average $I_{p\,ox}$ value of group 1 is higher than that of Pt. This is a consequence of the low background current of DLC electrodes. Albeit the peak current of Pt is higher than that of any electrode in group 1, so is the capacitive current. When it is subtracted, $I_{p\,ox}$ is actually higher for the electrodes of group 1. This is a clear advantage of the low capacitive current of inert electrode materials such as DLC. Despite the inertness of the DLC electrodes and the slow electron transfer, DA detection is one order of magnitude better than that of Pt (10 µM compared to 100 µM).

The peak current ratio i_{pa}/i_{pc} was on average 1.07, which is quite close to unity. Even though the DA redox reaction was irreversible, it can be deduced that reaction was quite stable and no appreciable coupled homogeneous chemical reactions occurred.

Electrode 1-6 had some distinctive properties in group 1. Its ΔE_p was the lowest in the group (0.78 V) and its $I_{p\,ox}$ was the highest (1026.68 nA). The voltammogram of electrode 1-6 also had some evident characteristics that resembled the electrochemical response of the Pt electrode such as the narrowest potential window and one of the highest capacitive currents in the group. Peculiarly, it exhibited a slight rise in anodic current already at a dopamine concentration of 1 µM (Figure 30), which was the lowest observed among groups 1 and 2. Electrode 1-6 was chosen for further measurements presented in section 10.1.7.

10.1.5 Group 2 in Sulphuric Acid

The cyclic voltammograms of group 2 in H_2SO_4 are shown in Figure 31. Electrodes 4-5, 4-6 and 4-8 had a narrow potential window from -0.5 V to approximately or 0.6 V. Additionally, their capacitive currents were the highest in the group 2. Electrodes 4-3

and 4-7, in contrast, exhibited wider potential windows, ranging from -0.55 V to 1 and 0.9 V respectively, and lower capacitive currents than the above mentioned electrodes.

Peaks at approximately -0.4 V corresponding to hydrogen desorption are visible on all the electrodes, whereas the adsorption peaks are only seen for electrodes 4-3 and 4-7 around the same potential. Electrodes 4-5, 4-6 and 4-8 did not exhibit any of the other characteristic peaks of the Pt electrode. Conversely, the CVs of 4-3 and 4-7 show Pt oxidation and reduction peaks at 0.4 V and around 0.1 V, respectively.

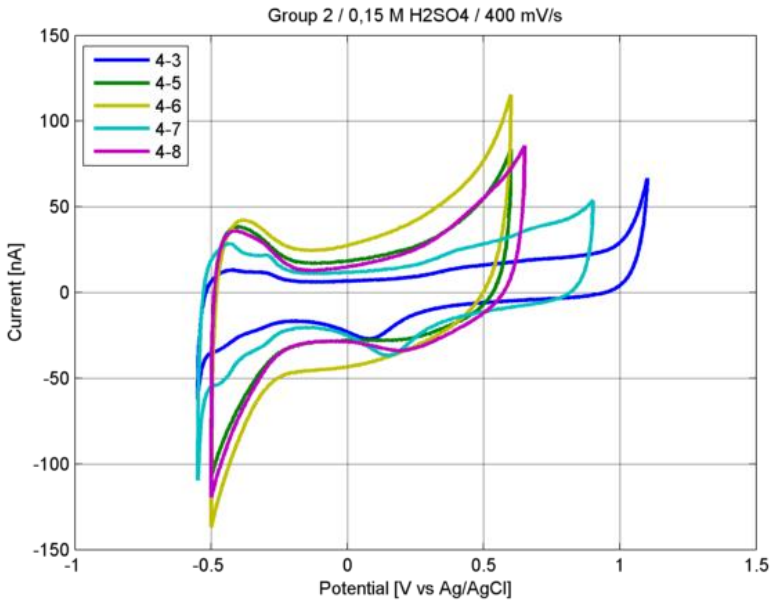

Figure 31. CVs of the electrodes of group 2 in 0.15 M H_2SO_4. v = 400 mV/s.

In comparison to the Pt electrode, the average potential window of group 2 was a little narrower, 1.29 V against 1.4 V. The standard deviation was quite significant though, because there was a lot of deviation between the different electrodes in group 2. Especially electrodes 4-5, 4-6 and 4-8 presented dissimilar results with electrodes 4-3 and 4-7. The capacitive currents were still considerably lower than that of Pt, which is obvious from Figure 32 and is an indication of the inertness of the electrodes of group 2.

The electrodes of group 1 had a wider potential window and lower capacitive current on average than group 2. This results most likely from the thinner, 7.5 nm thick DLC coating that is less homogeneous and more susceptible to show a response similar to that of the Pt electrode. In fact, the potential window and capacitive current values approached those of Pt.

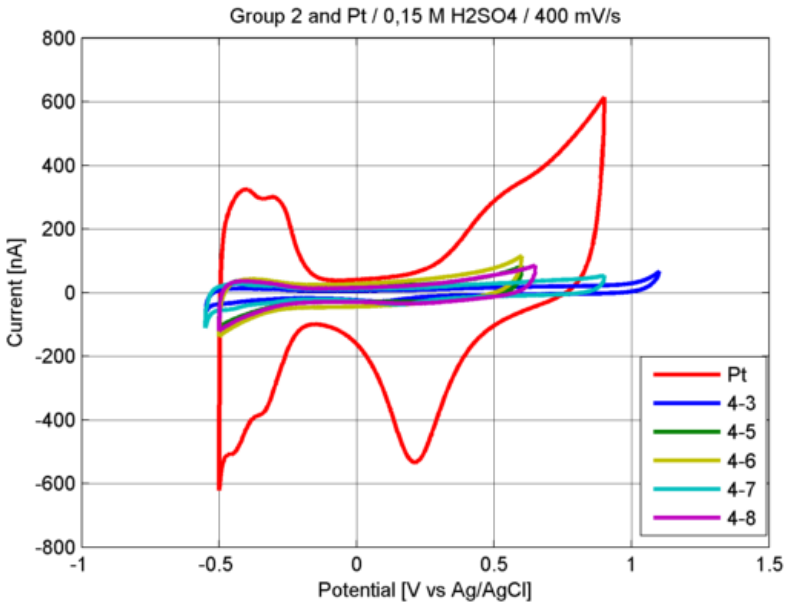

Figure 32. CVs of group 2 plotted against Pt in 0.15 M H_2SO_4. v = 400 mV/s.

10.1.6 Group 2 in PBS and Dopamine Solutions

Whereas the peaks of the Pt and group 1 electrodes corresponding to platinum redox reactions seemed to diminish in PBS (in relation to H_2SO_4), the opposite is seen for group 2 electrodes. The platinum oxidation peaks at approximately +0.34 V and reduction peaks at 0 V are evident in Figure 33. Electrode 4-3 was the only exception exhibiting no redox peaks at all. As in sulphuric acid, electrodes 4-3 and 4-7 had the widest potential windows and lowest capacitive currents.

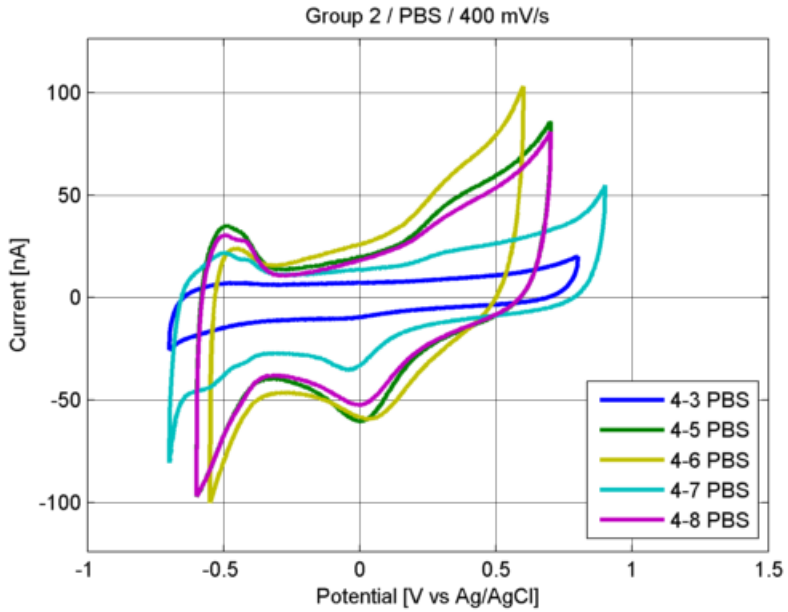

Figure 33. CVs of the electrodes of group 2 in PBS. v = 400 mV/s.

In Figure 34 the voltammograms of group 2 and Pt are plotted together. The potential windows were very similar and the DLC electrodes clearly had the same characteristics as Pt even if the potential peaks do not appear exactly at the same place. This similarity is more evident than in H_2SO_4 and could result from further delamination during the scanning of the voltammograms. Nevertheless, the background currents were considerably lower, indicating that the 7.5 nm thick DLC electrodes are more inert than the Pt electrode.

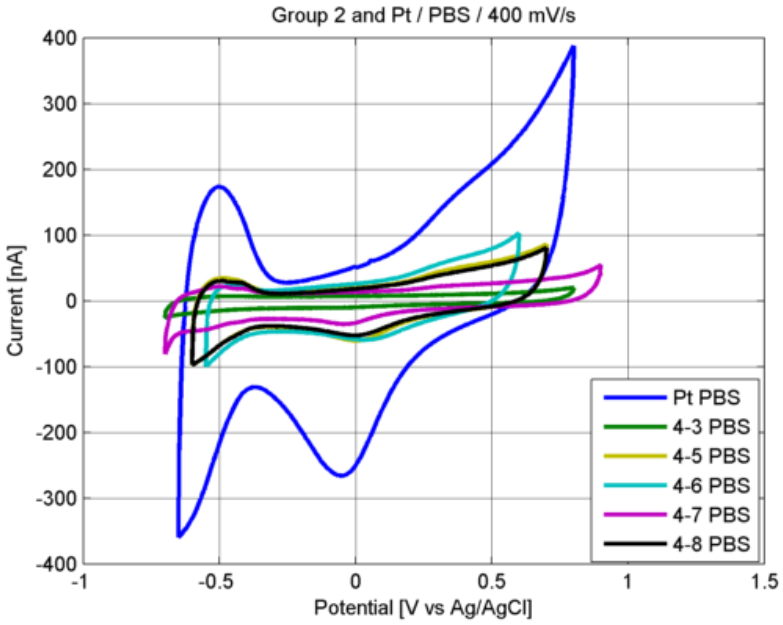

Figure 34. Cyclic voltammograms of Pt and group 2 electrodes in PBS. v = 400 mV/s.

All the electrodes in group 2 had a similar response in the dopamine solutions. Thus, only the CVs of electrode 4-5 are shown in Figure 35 at different DA concentrations in PBS. The voltammogram at 1 mM is not shown because the current was so high that the characteristics of other voltammograms at lower DA concentrations were not distinguishable anymore. All the electrodes except 4-6 showed an increase in the anodic current at a dopamine concentration of 10 µM. However, clear DA oxidation and reductions peaks were only visible at 100 µM and 1 mM concentrations. Dopamine detection was one order of magnitude better for the 7.5 nm thick DLC electrodes than Pt.

The peak potential separation ΔE_p of group 2 was on average 0.54 V at a DA concentration of 1 mM, which is higher than the value of the Pt electrode (0.35 V) and lower than that of group 1 (0.92 V). The heterogeneous electron transfer kinetics were slow and the DA redox reaction was irreversible. The oxidation peak current, $I_{p\,ox}$, was higher than that of Pt (455.8 versus 612.23 nA) and quite close to that of group 1, taking into consideration the large standard deviation of both groups.

The peak current ratio i_{pa}/i_{pc} was on average 0.90. This value is quite close to unity, but as in the case of the Pt electrode, the reduction of Pt probably contributes to the dopamine reduction current and therefore the value of i_{pa}/i_{pc} is less than unity.

The group 2 electrodes coated with a 7.5 nm thick DLC coating are more inert than Pt but much less so than group 1 electrodes with a 30 nm thick DLC coating. The electrochemical properties of group 2 approach those of Pt in regard to the potential window, the capacitive current, the potential peak separation of DA oxidation and reduction and the characteristics Pt redox peaks observed in the voltammograms of group 2.

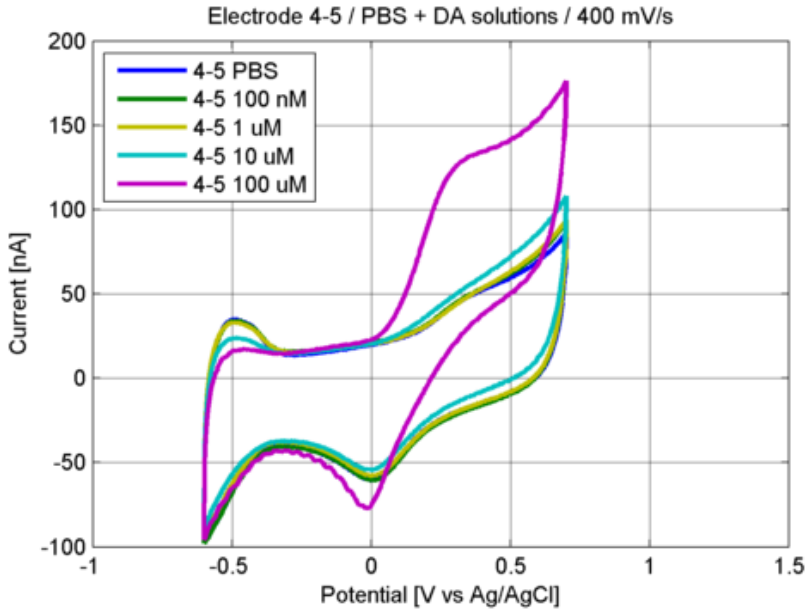

Figure 35. CVs of electrode 4-5 in the presence of varying concentrations of DA in PBS. υ = 400 mV/s.

10.1.7 Effect of Scan Rate on Electrode 1-6

The effect of scan rate was studied for electrode 1-6, because it showed interesting electrochemical properties (discussed in more detail in section 10.1.4). The cyclic voltammograms at different scan rates in a 100 μM DA solution are presented in Figure 36. The background current has been subtracted from the CVs so that the peaks are well-defined.

As the scan rate decreases, the DA reduction peak seems to gradually disappear implying that DAQ is not reduced back to DA. This was examined more thoroughly by calculating the peak current ratio i_{pa}/i_{pc} by extrapolation (explained in section 6.1.6). The results are shown in Table 6. At 10 mV/s, the reduction peak was not observed.

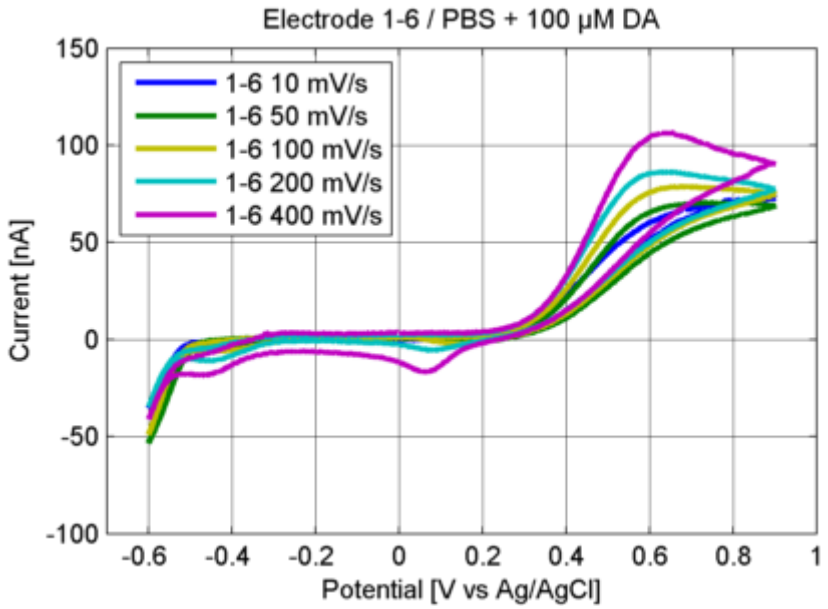

Figure 36. Effect of changing v on the CVs of electrode 1-6.

The peak current ratio i_{pa}/i_{pc} increases with decreasing scan rate (v), which demonstrates that the stability of the DA reaction changes. At high scan rates, DAQ is reduced to DA, because the chemical reaction to form LDAC has slow kinetics and does not have time to occur (the reaction pathway is depicted in Figure 2). On the other hand, at low scan rates the chemical reaction has time to occur forming LDAC. Therefore less and less DAQ is reduced to DA and the reduction current decreases resulting in an increase in the peak current ratio. As it was already discussed previously, the i_{pa}/i_{pc} value differs from unity even at fast scan rates, because of the contribution of Pt reduction current. At 100 µM DA this contribution is emphasized, because the Pt reduction current is higher relative to DA reduction current than at 1 mM DA.

Table 6: Oxidation and reduction peaks, peak separation and peak current values measured at different scan rates for electrode 1-6 in PBS with 100 µM DA.

Scan rate (mV/s)	Oxidation potential (V)	Reduction potential (V)	ΔE_p (V)	i_{pa}/i_{pc}
400	0.64	0.05	0.59	0.85
200	0.64	0.08	0.56	0.98
100	0.69	0.15	0.54	1.09
50	0.78	0.17	0.61	1.10
10	0.88			

We also note from Table 6, that ΔE_p changes as the scan rate is altered, which implies that the DA redox reaction is not reversible [40], confirming our previous results.

Furthermore, an increase in oxidation and reduction current as a function of increasing scan rate is noticeable. The peak oxidation and reduction currents, $I_{p\,ox}$ and $I_{p\,red}$, were plotted as a function of scan rate v and square root of the scan rate $v^{1/2}$. The data fitted better the linear model as a function of v, presented in Figure 37, with a squared R value

of 0.9644 for oxidation and 0.9774 for reduction of DA. A linear increase in $I_{p\ ox}$ and $I_{p\ red}$ with v indicates that the electrochemical reaction is controlled by adsorption. [40] This result is in agreement with the findings of DuVall and McCreery. [34, 35]

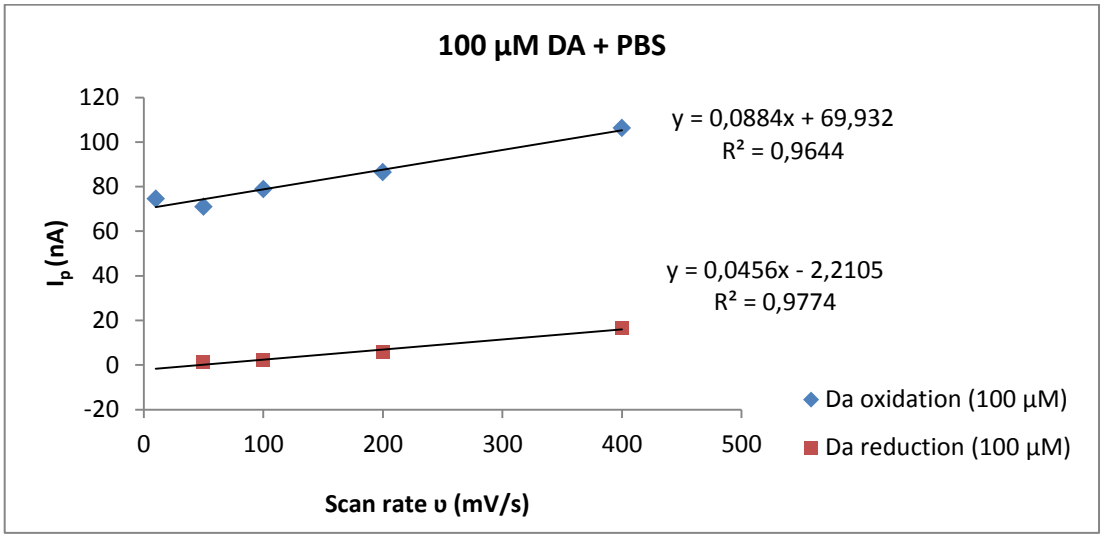

Figure 37. Peak oxidation and reduction current I_p as a function of scan rate v.

10.1.8 Silicon control electrode

The electrochemical characteristics of Pt were evident for the electrodes with a 7.5 nm thick layer and some of them were also seen for the more inert 30 nm thick DLC electrodes. In order to understand what was the individual contribution of Pt and DLC to the overall response of electrodes in groups 1 and 2, a DLC electrode was prepared on a silicon wafer substrate (denominated Si+DLC). The CVs at different DA concentrations are shown in Figure 38 and with the background subtracted in Figure 39.

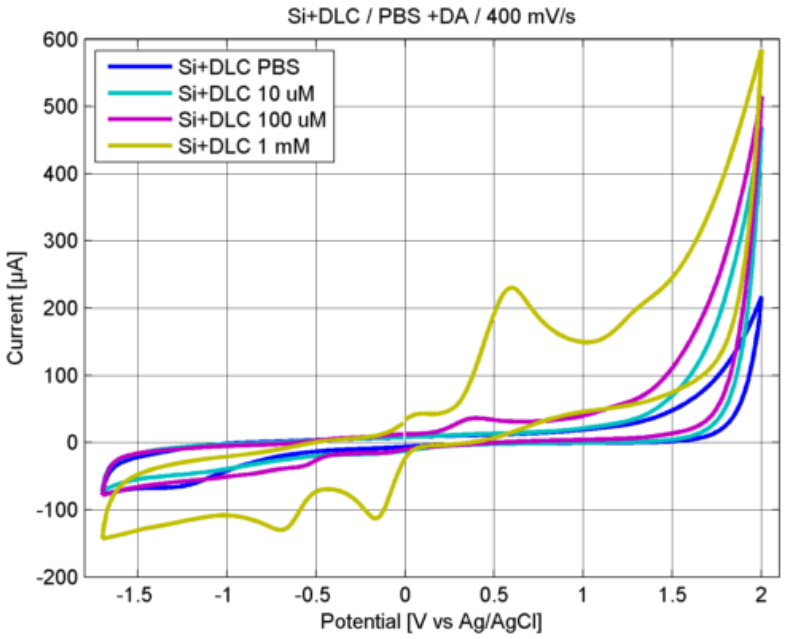

Figure 38. CVs of Si+DLC electrode in PBS at different DA concentrations.

The potential window was very wide, from -1.7 V to +2 V, which demonstrates how inert the DLC coating is in the absence of the platinum substrate. Dopamine was detected at a concentration of 100 µM with two oxidation and two reduction peaks appearing. From the background subtracted CVs (Figure 39), we clearly see that at 10 µM no peaks can be identified. The origin of the double peaks is not precisely known. One hypothesis is that the first oxidation peak is from the oxidation of dopamine in the solution, while the second peak results from the oxidation of surface adsorbed dopamine. The DA molecules in solution and those adsorbed to the surface have different energy levels and thus their oxidation occurs at different potential. For the same reason two reduction peaks are also observed.

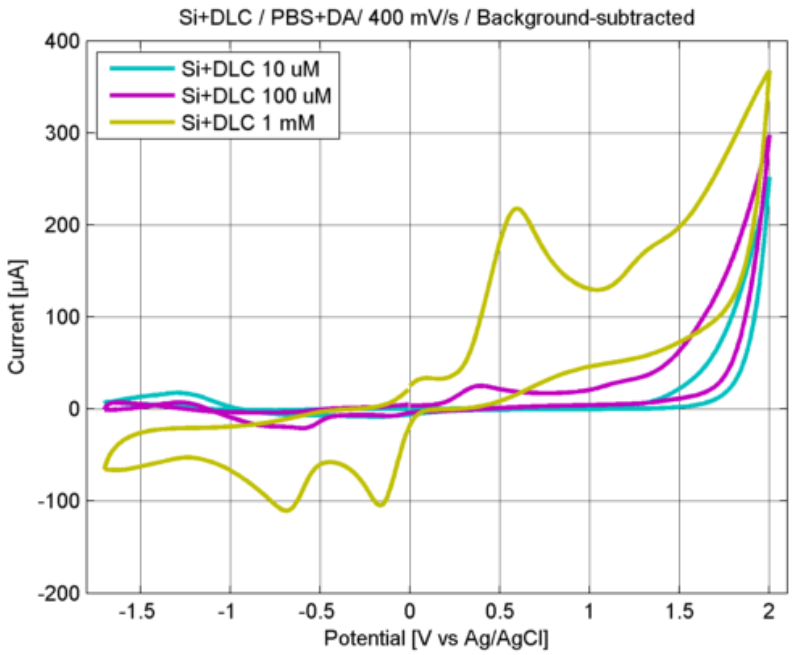

Figure 39. CVs of Si+DLC electrode in PBS at different DA concentrations with the background in PBS subtracted from the data.

For the Pt and Si+DLC electrodes the detection of dopamine occurred at a concentration of 100 µM whereas for the DLC-coated electrodes of groups 1 and 2 the detection was an order of magnitude better, nearly two for electrode 1-6. Since the lower detection limit cannot be attributed to either Pt or DLC, it must result from their combination.

The enhanced detection of DA with DLC-coated electrodes with Pt as a substrate could be a combination of two factors. Firstly, the inertness of DLC layer lowers the capacitive current sufficiently so that smaller faradaic currents can be detected and secondly, the Pt substrate offers small sites where the heterogeneous electron transfer kinetics are faster compared to DLC. In this regard, the platinum substrate offers catalytic sites where the DA redox reactions are fast and with the inertness provided by DLC coating the sensitivity is improved.

10.2 SEM images

The SEM images displayed several delaminated areas on the electrodes. Figure 40 and Figure 41 show different types of surface defects for electrode 1-4 from group 1. In Figure 40 a large delaminated area 30 x 10 µM in size is seen at the top. Similar delamination is also visible at the bottom right side of the figure. The arrows point at a number of small holes approximately 1 µM in diameter. In Figure 41 another large delaminated area is seen at the bottom as well as many cracks that spread at the surface of the electrode. All the electrodes that underwent cyclic voltammetric experiments and were observed under SEM exhibited some kind of delamination or surfaces defects.

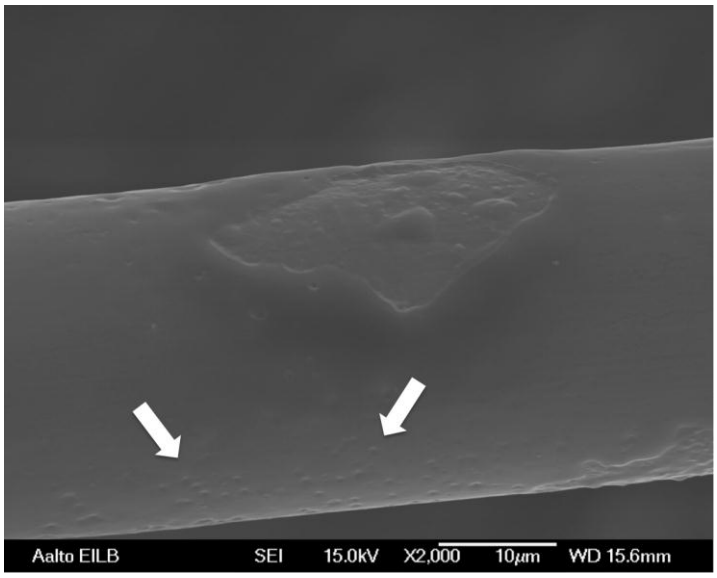

Figure 40. SEM image of the surface of electrode 1-4. The arrows show small holes in the DLC coating. Two large delaminated are also seen.

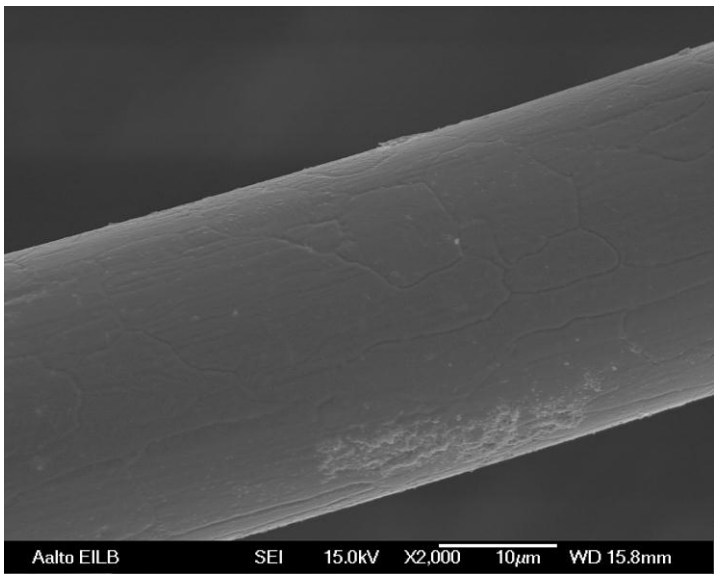

Figure 41. SEM image of the surface of electrode 1-4. Several cracks can be seen on the electrode surface.

11. Conclusion

Cyclic voltammetric experiments were carried out in sulphuric acid, PBS and varying concentrations of dopamine in PBS to evaluate the performance of DLC/Pt composite electrodes.

The results in sulphuric acid demonstrated that DLC coatings result in an increase in the potential window width and decrease in the capacitive current. This effect is accentuated at the thicker 30 nm DLC coatings, whereas the electrochemical response of the electrodes with a 7.5 nm coating approaches those of the platinum substrate. Nevertheless, the direct comparison of the cyclic voltammograms of the platinum and DLC/Pt composite electrodes made it evident that DLC improves the inertness of the electrodes.

Platinum oxidation and reduction peaks could be seen in the cyclic voltammograms of the DLC/Pt electrodes with both coating thicknesses. The coatings were not uniform as could be seen by the SEM images that presented several surface defects and delamination. In part this was caused by the uneven coating process and in part by the delamination that occurred during cyclic voltammetric experiments. One probable cause for the delamination is the formation of oxygen and hydrogen gas at the edges of the potential window. The gas formation is accompanied by bubbles that penetrate under the coating and weaken its adhesion.

The peak potential separation ΔE_p of the oxidation and reduction of dopamine indicated that the heterogeneous electron transfer kinetics were very slow for the DLC/Pt electrodes. Although the transfer kinetics were faster for the 7.5 nm DLC coating, they were still considerably slower than those of the platinum electrode. Therefore the dopamine redox reaction was irreversible at the DLC/Pt electrodes.

The oxidation peak current $I_{p\,ox}$ of both types of DLC/Pt electrodes was higher than that of platinum, which is explained by the low capacitive current that allows an improved signal-to-noise ratio.

Any reliable conclusions could not be made directly from the anodic and cathodic peak ratio i_{pa}/i_{pc}, because the DA redox reaction was irreversible and platinum reduction contributed to the dopamine reduction current. However, the more detailed experiments made for electrode 1-6 (30 nm thick DLC coating) showed that i_{pa}/i_{pc} increases with a decreasing scan rate. This implies that a coupled homogeneous reaction occurs after the oxidation of dopamine into DAQ and that this reaction is emphasized at lower scan rates. Thus, the stability of the redox reaction of dopamine depends on the scan rate used in the experiments.

The electrochemical behavior of electrode 1-6 also displayed a linearity between peak oxidation and reduction currents and scan rate. This suggests that the redox reaction of dopamine is adsorption-controlled, which is in agreement with literature.

Dopamine detection was 100 μM for platinum and the DLC coating made on a silicon substrate, while it was an order of magnitude better for both types of DLC/Pt composite electrodes. Since the enhanced detection could not be attributed specifically to either DLC or platinum, it was deduced that it must arise from the combination of these electrode materials. By combining the inertness and low capacitive current attributed to DLC with the faster heterogeneous electron transfer rate of platinum that acts as a catalyst in the delaminated areas, an improvement in the DA detection of the materials was achieved.

DLC displayed very attractive properties for the electrochemical measurement of dopamine, among which are the very wide potential window observed at the Si+DLC electrode and the low capacitive current. For future applications, the delamination problem could be solved by simply using a different substrate material. Yet, to improve the heterogeneous electron transfer rate of the inert DLC coating, a catalytic material must be used. Other carbon allotropes such as graphene or carbon nanotubes, with established catalytic properties and fast electron transfer kinetics, could be an attractive alternative in this regard.

12. References

[1] Bear, M.F., Connors, B.W. and Paradiso, M.A. *Neuroscience : Exploring the Brain.* Philadelphia, PA, Lippincott Williams & Wilkins, cop. 2007.

[2] Jackowska, K. and Krysinski, P. New trends in the electrochemical sensing of dopamine. *Analytical and Bioanalytical Chemistry,* 2013, vol. 405, pp. 3753-3771.

[3] Robinson, D.L., Hermans, A., Seipel, A.T. and Wightman, R.M. Monitoring Rapid Chemical Communication in the Brain. *Chemical Reviews,* 2008, vol. 108, pp. 2554-2584.

[4] Hurley, M.J. and Jenner, P. What has been learnt from study of dopamine receptors in Parkinson's disease? *Pharmacology & Therapeutics,* 2006, vol. 111, pp. 715-728.

[5] Jaber, M., Robinson, S.W., Missale, C. and Caron, M.G. Dopamine receptors and brain function. *Neuropharmacology,* 1997, vol. 35, pp. 1503-1519.

[6] Tritsch, N. and Sabatini, B. Dopaminergic Modulation of Synaptic Transmission in Cortex and Striatum. *Neuron,* 2012, vol. 76, pp. 33-50.

[7] EPDA, European Parkinson's Disease Association. *Guide to Parkinson's Disease.* Date cited: 30.08.2013. Available: http://www.epda.eu.com.

[8] W.H.O. *Neurological Disorders: Public Health Challenges.* Date cited: 30.08.2013. Available: http://www.who.int/mental_health/neurology/neurodiso/en/.

[9] Venton, B.J. and Wightman, R.M. Psychoanalytical Electrochemistry: Dopamine and Behavior. *Analytical Chemistry,* 2003, vol. 75, pp. 414 A-421 A.

[10] Bard, A.J., Bard, A.J. and Faulkner, L.R. *Electrochemical Methods : Fundamentals and Applications.* New York (N.Y.), Wiley, 2000.

[11] Robinson, D.L., Venton, B.J., Heien, M.L.A.V. and Wightman, R.M. Detecting Subsecond Dopamine Release with Fast-Scan Cyclic Voltammetry in Vivo. *Clinical Chemistry,* 2003, vol. 49, pp. 1763-1773.

[12] Adams, R.N. Probing brain chemistry with electroanalytical techniques. *Analytical Chemistry,* 1976, vol. 48, pp. 1126A-1138A.

[13] Wightman, R.M., May, L.J. and Michael, A.C. Detection of Dopamine Dynamics in the Brain. *Analytical Chemistry,* 1988, vol. 60, pp. 769A-793A.

[14] McCreery, R.L. Advanced Carbon Electrode Materials for Molecular Electrochemistry. *Chemical Reviews,* 2008, vol. 108, pp. 2646-2687.

[15] Qureshi, A., Kang, W.P., Davidson, J.L. and Gurbuz, Y. Review on carbon-derived, solid-state, micro and nano sensors for electrochemical sensing applications. *Diamond and Related Materials,* 2009, vol. 18, pp. 1401-1420.

[16] Higson, S.P.J. and Vadgama, P.M. Diamond like carbon coated films for enzyme electrodes; characterization of biocompatibility and substrate diffusion limiting properties. *Analytica Chimica Acta,* 1995, vol. 300, pp. 77-83.

[17] Falcao Eduardo, H.L. Carbon allotropes. *Journal of Chemical Technology and Biotechnology,* 2007, vol. 82, pp. 524-06-01),.

[18] Robertson, J. Diamond-like amorphous carbon. *Materials Science and Engineering: R: Reports,* 2002, vol. 37, pp. 129-281.

[19] Pleskov, Y.V. New Corrosion-Resistant Electrodes: Synthetic Diamond and Diamond-Based Materials. The Semiconductor and Structure Aspects - a Review. *Protection of Metals,* 2006, vol. 42, pp. - 103-118.

[20] Iuga, C., Alvarez-Idaboy, J. and Vivier-Bunge, A. ROS Initiated Oxidation of Dopamine under Oxidative Stress Conditions in Aqueous and Lipidic Environments. *The Journal of Physical Chemistry B,* 2011, vol. 115, pp. 12234-12246.

[21] Corona-Avendaño, S., Alarcón-Angeles, G., Ramírez-Silva, M.T., Rosquete-Pina, G., Romero-Romo, M. and Palomar-Pardavé, M. On the electrochemistry of dopamine in aqueous solution. Part I: The role of [SDS] on the voltammetric behavior of dopamine on a carbon paste electrode. *Journal of Electroanalytical Chemistry,* 2007, vol. 609, pp. 17-26.

[22] Wen, X., Jia, Y. and Liu, Z. Micellar effects on the electrochemistry of dopamine and its selective detection in the presence of ascorbic acid. *Talanta,* 1999, vol. 50, pp. 1027-1033.

[23] Tse, D.C.S., McCreery, R.L. and Adams, R.N. Potential oxidative pathways of brain catecholamines. *Journal of Medicinal Chemistry,* 1976, vol. 19, pp. 37-40.

[24] Domenech, A., Garcia, H., Domenech-Carbo, M.T. and Galletero, M.S. 2,4,6-Triphenylpyrylium Ion Encapsulated into Zeolite Y as a Selective Electrode for the Electrochemical Determination of Dopamine in the Presence of Ascorbic Acid. *Analytical Chemistry,* 2002, vol. 74, pp. 562-569.

[25] Li, Y., Liu, M., Xiang, C., Xie, Q. and Yao, S. Electrochemical quartz crystal microbalance study on growth and property of the polymer deposit at gold electrodes during oxidation of dopamine in aqueous solutions. *Thin Solid Films,* 2006, vol. 497, pp. 270-278.

[26] Corona-Avendano, S., Alarcon-Angeles, G., Rosquete-Pina, G., Rojas-Hernandez, A., Gutierrez, A., Ramirez-Silva, M.T., Romero-Romo, M. and Palomar-Pardave, M. New Insights on the Nature of the Chemical Species Involved during the Process of Dopamine Deprotonation in Aqueous Solution: Theoretical and Experimental Study. *The Journal of Physical Chemistry B,* 2007, vol. 111, pp. 1640-1647.

[27] WANG, Q., LI, N. and WANG, W. Electrocatalytic Response of Dopamine at a Metallothioneins Self-Assembled Gold Electrode. *Analytical Sciences,* 2002, vol. 18, pp. 635-639.

[28] Kiss, T., Sovago, I. and Martin, R.B. Complexes of 3,4-dihydroxyphenyl derivatives. 9. Aluminum(3+) binding to catecholamines and tiron. *Journal of the American Chemical Society,* 1989, vol. 111, pp. 3611-3614.

[29] Sánchez-Rivera, A.E., Corona-Avendaño, S., Alarcón-Angeles, G., Rojas-Hernández, A., Ramírez-Silva, M.T. and Romero-Romo, M.A. Spectrophotometric study on the stability of dopamine and the determination of its acidity constants. *Spectrochimica Acta Part A: Molecular and Biomolecular Spectroscopy,* 2003, vol. 59, pp. 3193-3203.

[30] Iuga, C., Alvarez-Idaboy, J. and Vivier-Bunge, A. ROS Initiated Oxidation of Dopamine under Oxidative Stress Conditions in Aqueous and Lipidic Environments. *The Journal of Physical Chemistry B,* 2011, vol. 115, pp. 12234-12246.

[31] Schüsler-Van Hees, M.T.I.W., Henegouwen, G.M.J.B. and Driever, M.F.J. Ionization constants of catechols and catecholamines. *Pharmaceutisch Weekblad,* 1983, vol. 5, pp. 102-108.

[32] Aldana-González, J., Palomar-Pardavé, M., Corona-Avendaño, S., Montes de Oca, M.G., Ramírez-Silva, M.T. and Romero-Romo, M. Gold nanoparticles modified-ITO electrode for the selective electrochemical quantification of dopamine in the presence of uric and ascorbic acids. *Journal of Electroanalytical Chemistry,* 2013, vol. 706, pp. 69-75.

[33] Bath, B.D., Michael, D.J., Trafton, B.J., Joseph, J.D., Runnels, P.L. and Wightman, R.M. Subsecond Adsorption and Desorption of Dopamine at Carbon-Fiber Microelectrodes. *Analytical Chemistry,* 2000, vol. 72, pp. 5994-6002.

[34] DuVall, S.H. and McCreery, R.L. Self-catalysis by Catechols and Quinones during Heterogeneous Electron Transfer at Carbon Electrodes. *Journal of the American Chemical Society,* 2000, vol. 122, pp. 6759-6764.

[35] DuVall, S.H. and McCreery, R.L. Control of Catechol and Hydroquinone Electron-Transfer Kinetics on Native and Modified Glassy Carbon Electrodes. *Analytical Chemistry,* 1999, vol. 71, pp. 4594-4602.

[36] Cheer, J.F., Wassum, K.M., Heien, M.L., Phillips, P.E. and Wightman, R.M. Cannabinoids enhance subsecond dopamine release in the nucleus accumbens of awake rats. *The Journal of Neuroscience : The Official Journal of the Society for Neuroscience,* 2004, vol. 24, pp. 4393-4400.

[37] Marsden, C.A., Joseph, M.H., Kruk, Z.L., Maidment, N.T., O'Neill, R.D., Schenk, J.O. and Stamford, J.A. *In vivo* voltammetry—Present electrodes and methods. *Neuroscience,* 1988, vol. 25, pp. 389-400.

[38] Laurila,T., Ed., *Sähkökemian Perusteet (Opetusmoniste).* Aalto University, 2006.

[39] Bockris, J.O. and Drazic, D.M. *Electro-Chemical Science.* London, 1972.

[40] Compton, R.G. and Banks, C.E. *Understanding Voltammetry*. London, Imperial College Press, 2010.

[41] Banks, C.E., Davies, T.J., Wildgoose, G.G. and Compton, R.G. Electrocatalysis at graphite and carbon nanotube modified electrodes: edge-plane sites and tube ends are the reactive sites. *Chemical Communications (Cambridge, England)*, 2005, vol. (7), pp. 829-841.

[42] Pumera, M. Graphene for electrochemical sensing and biosensing. *Trends in Analytical Chemistry*, 2010, vol. 29, pp. 954-965.

[43] Ang, P.K., Wang, S., Bao, Q., Thong, J.T.L. and Loh, K.P. High-Throughput Synthesis of Graphene by Intercalationâˆ'Exfoliation of Graphite Oxide and Study of Ionic Screening in Graphene Transistor. *ACS Nano*, 2009, vol. 3, pp. 3587-3594.

[44] Ambrosi, A. and Pumera, M. Nanographite Impurities Dominate Electrochemistry of Carbon Nanotubes. *Chemistry - A European Journal*, 2010, vol. 16, pp. 10946-10949.

[45] Kim, Y., Bong, S., Kang, Y., Yang, Y., Mahajan, R.K., Kim, J.S. and Kim, H. Electrochemical detection of dopamine in the presence of ascorbic acid using graphene modified electrodes. *Biosensors and Bioelectronics*, 2010, vol. 25, pp. 2366-2369.

[46] Shang, N.G., Papakonstantinou, P., McMullan, M., Chu, M., Stamboulis, A., Potenza, A., Dhesi, S.S. and Marchetto, H. Catalyst-Free Efficient Growth, Orientation and Biosensing Properties of Multilayer Graphene Nanoflake Films with Sharp Edge Planes. *Advanced Functional Materials*, 2008, vol. 18, pp. 3506-3514.

[47] Mark Wightman, R. Detection of dopamine dynamics in the brain. *Analytical® Chemistry*, 1988, vol. 60, pp. 769A-779A.

[48] Rao, T.N. and Fujishima, A. Recent advances in electrochemistry of diamond. *Diamond and Related Materials*, 2000, vol. 9, pp. 384-389.

[49] Yang, X., Haubold, L., DeVivo, G. and Swain, G.M. Electroanalytical Performance of Nitrogen-Containing Tetrahedral Amorphous Carbon Thin-Film Electrodes. *Analytical Chemistry*, 2012, vol. 84, pp. 6240-6248.

[50] Tanaka, Y., Naragino, H., Yoshinaga, K., Nakahara, A., Kondo, T., Fujishima, A. and Honda, K. Controllable Electrochemical Activities by Oxidative Treatment toward Inner-Sphere Redox Systems at N-Doped Hydrogenated Amorphous Carbon Films. *International Journal of Electrochemistry*, 2011, vol. 2012, .

[51] Naragino, H., Yoshinaga, K., Tatsuta, S. and Honda, K. Improvement of Conductivity by Incorporation of Boron Atoms in Hydrogenated Amorphous Carbon Films Fabricated by Plasma CVD Methods and its Electrochemical Properties. *ECS Transactions*, 2012, vol. 41, pp. 59-68.

[52] Maalouf, R., Soldatkin, A., Vittori, O., Sigaud, M., Saikali, Y., Chebib, H., Loir, A.S., Garrelie, F., Donnet, C. and Jaffrezic-Renault, N. Study of different carbon

materials for amperometric enzyme biosensor development. *Materials Science and Engineering: C,* 2006, vol. 26, pp. 564-567.

[53] Yang, G., Liu, E., Khun, N.W. and Jiang, S.P. Direct electrochemical response of glucose at nickel-doped diamond like carbon thin film electrodes. *Journal of Electroanalytical Chemistry,* 2009, vol. 627, pp. 51-57.

[54] Tanaka, Y., Furuta, M., Kuriyama, K., Kuwabara, R., Katsuki, Y., Kondo, T., Fujishima, A. and Honda, K. Electrochemical properties of N-doped hydrogenated amorphous carbon films fabricated by plasma-enhanced chemical vapor deposition methods. *Electrochimica Acta,* 2011, vol. 56, pp. 1172-1181.

[55] Pleskov, Y.V., Evstefeeva, Y.E. and Baranov, A.M. Amorphous Diamond-like Carbon Electrodes: The Catalytic Effect of Platinum Admixture. *Russian Journal of Electrochemistry,* 2001, vol. 37, pp. 644-646.

[56] Liu, L.X. and Liu, E. Nitrogenated diamond-like carbon films for metal tracing. *Surface and Coatings Technology,* 2005, vol. 198, pp. 189-193.

[57] Kim, J., Bordeanu, A. and Pyun, J. Diamond-like carbon (DLC) microelectrode for electrochemical ELISA. *Biosensors and Bioelectronics,* 2009, vol. 24, pp. 1394-1398.

[58] Gao, C., Guo, Z., Liu, J.H. and Huang, X.J. The new age of carbon nanotubes: an updated review of functionalized carbon nanotubes in electrochemical sensors. *Nanoscale,* 2012, vol. 4, pp. 1948-1963.

[59] Jiao, S., Li, M., Wang, C., Chen, D. and Fang, B. Fabrication of Fc-SWNTs modified glassy carbon electrode for selective and sensitive determination of dopamine in the presence of AA and UA. *Electrochimica Acta,* 2007, vol. 52, pp. 5939-5944.

[60] Shahrokhian, S. and Zare-Mehrjardi, H.R. Application of thionine-nafion supported on multi-walled carbon nanotube for preparation of a modified electrode in simultaneous voltammetric detection of dopamine and ascorbic acid. *Electrochimica Acta,* 2007, vol. 52, pp. 6310-6317.

[61] Rautiainen, A.Timantinkaltaisen hiilen adheesio bioelektrodille (eng. Adhesion of diamond-like carbon on bioelectrode).*Aalto University, School of Electrical Engineering,* 2013, .

[62] Millar, J. and Pelling, C.W.A. Improved methods for construction of carbon fibre electrodes for extracellular spike recording. *Journal of Neuroscience Methods,* 2001, vol. 110, pp. 1-8.

[63] E M Hudak and J T Mortimer and,H.B.Martin. Platinum for neural stimulation: voltammetry considerations. *Journal of Neural Engineering,* 2010, vol. 7, pp. 026005.

[64] Cogan, S.F. Neural stimulation and recording electrodes. *Annual Review of Biomedical Engineering,* 2008, vol. 10, pp. 275-309.

[65] Hudak, E.M., Mortimer, J.T. and Martin, H.B. Platinum for neural stimulation: voltammetry considerations. *Journal of Neural Engineering,* 2010, vol. 7, pp. 26005-2560/7/2/026005. Epub 2010 Mar 8.